Muscle to epidermis mechanotransduction' pathways involved in C. elegans embryonic elongation

Saurabh Tak

▶ **To cite this version:**

Saurabh Tak. Muscle to epidermis mechanotransduction' pathways involved in C. elegans embryonic elongation. Development Biology. Université de Strasbourg, 2017. English. NNT : 2017STRAJ054 . tel-01967617

HAL Id: tel-01967617
https://theses.hal.science/tel-01967617v1

Submitted on 1 Jan 2019

HAL is a multi-disciplinary open access archive for the deposit and dissemination of scientific research documents, whether they are published or not. The documents may come from teaching and research institutions in France or abroad, or from public or private research centers.

L'archive ouverte pluridisciplinaire **HAL**, est destinée au dépôt et à la diffusion de documents scientifiques de niveau recherche, publiés ou non, émanant des établissements d'enseignement et de recherche français ou étrangers, des laboratoires publics ou privés.

UNIVERSITÉ DE STRASBOURG

ÉCOLE DOCTORALE des Sciences de la Vie et de la Santé

IGBMC/CNRS UMR 7104/INSERM U964/UniStra
IBPS UMR 7622/UPMC

THÈSE présente par :

Saurabh TAK

Soutenue le : 21 Septembre 2017

Pour obtenir le grade de : **Docteur de l'université de Strasbourg**
Discipline/ Spécialité : Biologie du développement

Les voies de mécanotransduction entre muscles et épiderme impliquées dans l'élongation embryonnaire de *C. elegans*

THÉSE dirigée par :
Dr. LABOUESSE Michel — Directeur de Recherche, Université Pierre et Marie Curie, IBPS

Rapporteur INTERNE :
Dr. REICHHART Jean-Marc — Professeur Emérite, University of Strasbourg, IBMC

Rapporteur EXTERNES :
Dr. GUICHET Antoine — Institut Jacques Monod
Dr. GOTTA Monica — Professeur, University of Geneva Medical School

Acknowledgements

It had been, quite some journey for me. Science had influenced my whole career and every aspect of my life till now, building up to this point today. I am grateful to the spirit of science for letting me, be a part of it.

Being a part of Michel's team gave me a broad overview of development biology, biophysics, genetics and microscopy, besides some of the finer aspects from my own project. I am thankful to my lab-mates Alicia, Flora, Shashi, Thanh, Teresa, Loan, David, Christelle, Sophie, Vincent, Gabi, Sara and Xinyi for such a gala time together and fabulous company all along. Members of Dr. Sophie Jarriault's lab, next door in IGBMC were of great help, numerous times and I am thankful to Arnaud, Steve, Eria and Nadine for this.

Cecil'l'e, Vincent, Jack, Nelly and Augusto came to Michel's or Sophie's lab as interns and I became very good friends with them. Without them, my stay in France till now, would not have been so lively.

I am grateful to Shashi for all those wonderful advices and discussions, whether it was about CRISPR or simply brainstorming about a new experiment. My experience with Shashi provided me with an example of how to nurture a new person in the lab. I had a similar experience with Sunil sir, during my master and I thank him again here. Special regards to Michel, Christelle and Flora, for editing my thesis and helping me, make it a little presentable. I am thankful to Christelle for handing me over such a wonderful and challenging project. Science is a field with a lot of failures, before arriving to a nice result and I express my gratitude to Flora, for encouraging me all the way, to keep me going, besides helping me with the microscope several times. Since I mentioned microscopy, I acknowledge the IBPS microscopy platform and its members Susanne and France for their guidance and help for microscopy. Whether it was simply Confocal microscopy or sophisticated TIRF experiments, France and Susanne were always there to help.

'Captain Cool – Loan' deserves a special mention here. Although he did and keeps doing a lot of mistakes while working, it is his attitude which sets him apart. Always ready to acknowledge his mistakes and trying to make it better immediately made him a very good support for this project. Clara, my intern student helped us with some experiments and I am thankful for her contribution.

To some extent, I am also thankful to people, who provided me wrong strains or wrong protocols, as after losing a lot of time, I understood the value of checking and questioning everything in science. Only experiments done with proper controls are trustworthy, ☺. These incidents instilled, only a better scientific mind-set in me and

taught me how to fight my way back, out of a disaster. At the same time, I am thankful to all those, who helped me - move from Strasbourg to Paris and during my appendicitis surgery. Thanks to Michel and Francois, who helped me move. Nobody knew me in the new city, but it was Jonathan, Tuyet and Neetu, who took care of me, after the surgery. Without Thanh and Pierre, I would never have got an apartment to live in. I am forever grateful to all of them.

Of course, I had my ups and downs. My Parents and sister-Surbhi, stood by me during all my downs, all my failures. My grandma's love and confidence in me, kept me going. I would not insult them, by trying to put it in words here, for how thankful, I am to them.

Swati, whom I met accidentally (I guess she still regrets meeting me, ;)), thank you! Thank you for being there when I needed support. Of course, thank you for having this cleanest and infectious spirit of science. You have been a personal inspiration. Roli, Ankita and Rawat, my craziest friends, PhD and life in general would not have been so funny and light, without you three. Sonal, a beautiful poet and teacher; and Dibesh - vibrant individual and thinker, thank you both, for showing me how not to be scared for following my dreams. Thank you - Javier, Laura, Evry, Anupam, Rajaswi and Priyanka for your unconditional support and just being there. Thank you, Sara A, for helping us in IBPS, when we were new here.

I am extremely thankful to *Alicia*, without her, I would not have - my social security (I would be bankrupt), my visa to work in France and most importantly, my smile. Of course, I am thankful to her about our amazing discussions on cytoskeleton functions in *C. elegans*.

Every new journey is an answer to a previous journey. Therefore, I pay my regards to all my teachers till now, with special mentions of Dr. Placheril John, Dr. NS Punekar and late Dr. O Siddiqi, all of whom nurtured my interest in science and logic, broadened my horizon of science and helped me overcome many of my short-comings.

I am thankful to IBPS administration, mostly Isabelle and Maite for all the help with the documents and moving around in UPMC.

I acknowledge European research council grant for their support to our lab and to the project, I worked on.

Lastly, I express huge gratitude to Dr. Michel Labouesse, my mentor for lending me a part of his long and rich experience in Science. Without his trust, I would never have had this thesis. Thank you, Michel!

To the man,
who had everything, lost everything to destiny
& who made everything,
By himself,

Dedicated to my grandfather
Late Shri Panna Lal Tak

Index – table of contents

II. Methods and Materials/Experimental Procedures

III. Results - Table of contents

Muscle to epidermis mechanotransduction' pathways involved in *C. elegans* embryonic elongation

Force driven biological processes have long puzzled biologists. The evolution of chemical systems necessary for the origin of life has been proposed to be the stimulus from the external environmental structure (Kuhn, Naturwissenchaften, 1976). In the last two decades a lot of force driven biological processes were discovered and extensively studied. Some of the well-known examples include turgor pressure change with response to touch in *Mimosa pudica;* variable differentiation of mesenchymal stem cells (MSC's), depending on the stiffness of the underlying growth medium and wound healing. The various mechanisms by which cell/living tissue converts mechanical stimulus into electrochemical or biochemical activity resulting in physiological processes such as touch and hearing are termed as Mechanotransduction.

The nematode *C. elegans* provides an excellent system to study mechanotransduction. It is used as a model organism in developmental biology, genetics and molecular biology because of its large brood size, rapid development, transparent body (ease to do microscopy) and completely sequenced genome. The *C.elegans* epidermis is a single layered epithelium separated from musculature by a thin basement membrane on its basal surface. Four rows of muscles are attached to the ventral and dorsal epidermis by structures known as hemidesmosomes, making the epidermis, susceptible to the mechanical stress originating from contraction and relaxation of the underlying muscles. Thereby *C. elegans* embryonic elongation is a model in vivo system to study mechanical stress dependent changes in cell shape and junctional remodeling or regulation/activation of gene expression.

Two forces drive the embryonic elongation:

- Actomyosin contractility
- Tension provided by muscle contraction (after 1.7 fold)

Actomyosin contraction drives the early phase of elongation and is regulated by the Rho kinase (*let-502*) and the serine/threonine p21 activated kinase *pak-1*.
Tension provided by muscle contraction (external force for epidermis) recruits GIT-1 to hemidesmosomes (HD), which in turn facilitates further elongation by activating proteins such as *pak-1.* The pathway involves the scaffolding protein GIT-1 and its partner PIX-1, Rac GTPase, three signalling proteins found at the hemidesmosome (HD), and PAK-1. The phosphorylation of intermediate filaments is one of the outcomes of this pathway (Nature 471; 99-103, 2011).

Muscle defective mutants with no effective tension on epidermis arrest midway through elongation at the two fold stage known as paralyzed at two-fold stage or Pat phenotype. Though *git-1, pix-1* and *pak-1* mutants are viable, suggesting that another pathway/s act/s in parallel to GIT-1/PAK-1.

To investigate this further, a genome wide synthetic RNAi screen was performed in the *git-1(tm1962)* mutant background looking for enhancers inducing an elongation arrest. The candidates were categorized by observing body morphology defects (BMD) and two-fold arrest in *git-1* mutant background. Knocking down the genes *dlc-1, cap-1* and

cap-2, which encode subunits of Dynein/Dynactin complex showed strong Body Morphology Defects (BMD) (70%- 100%) in association with *git-1* mutant. RNAi of other subunits and associated proteins or *farl-11*, a known inhibitor of dynein heavy chain (*dhc-1*), produced similar results in a *git-1* mutant background, thereby stressing the role of Dynein/Dynactin complex in *C. elegans* embryonic elongation. Mutants of the Dynein/Dynactin complex complex have early maternal effect lethality. Therefore, in order to study this complex, we used *egl-50,* a thermosensitive (ts) allele of *arp-1,* which encodes a subunit of the Dynactin complex. We combined *git-1(tm1962)* with *egl-50(n1086).* An *egl-50(n1086ts); git-1(tm1962)* double mutant is viable at 15°C, but gives 70 % 2-fold arrest, 20% collapsing embryos and 10% retracting embryos. Similar results were found for a *dnc-1(or404ts); git-1(tm1962)* double combination. *Dnc-1(or404)* is a ts allele of the *C. elegans* homologue of the dynactin subunit p150-GLUED. We subsequently used these mutants to address several questions.

Why do *egl-50; git-1* embryos arrest at 2-fold? What structures are affected?

To answer this question, I created a library of markers in *egl-50; git-1* background to look for structural and dynamic defects. We did not observe any major organization defects of the actin cytoskeleton. Immunostaining of Spectraplakin VAB-10a/b, required for mechanical resilience of epidermis under strain and keeping the epidermis and extracelluar matrix together via HDs; Perlecan UNC-52, which plays essential role in muscle structure and development and intermediate filaments (proteins from HD's) did not show any major defect. Fluorescent CRISPR construct markers of *par-3, noah-1, e-cadherin* and *let-805* (basal side marker of HD) did not show any significant changes in intensities. Par-3 is a component of Partioning complex and noah-1, a protein of extracellular matrix (ECM) and is known to distribute mechanical stress during morphogenesis (Vuong et al, Development, 2017). Myotactin, LET-805 is a protein from basal side of HD, whereas e-Cadherin is junctional protein. I prepared a GFP-fused CRISPR construct of *mup-4* (apical side marker of HD) and examined it. The intensity and the organization of MUP-4 were not affected. While examining HDs by observing Myotactin, I found minor defects in HD, though the defects were not striking and not present in all 2-fold arrested embryos. The lab had previously reported depletion of LET-805::GFP from HD in a double microtubule severed (spastin overexpressed); *let-502* (Rho-kinase) mutant (Quintin et al, Development, 2015). We did not observe it in our system, though we suspected dynamic defects for LET-805. . To test the possibility of a defective LET-805 dynamics at HD, I used FRAP analysis of LET-805::GFP, revealing three kinds of Mobile Fractions in *egl-50; git-1* mutants, which could be similar, lower or higher than wild-type.

Elongation – a global view

To further probe the function of this complex during *C. elegans* embryonic elongation and to connect multiple approaches to understand elongation in the lab, I created *vab-10(ΔSH3)::mcherry;egl-50* and performed *spc-1* RNAi in *egl-50(n1086)* background. From one of the studies in lab, *pak-1(RNAi)* in a *vab-10(ΔSH3)* mutant showed a 2-2.5 fold arrest along with a dislocation of apical dislocation of hemidesmosome at the HD turn .. Sh3 is a domain in spectrin repeats 1-6 in plakin domain of vab-10. A deletion mutant of sh3 had been created in the lab using Crispr-cas9 gene editing technique. (Shashi Suman et al, unpublished data)

I observed a 100% hemidesmosome basal detachment on the turn in two-fold arrested *vab-10(ΔSH3)::mcherry;egl-50* embryos at 25.5°C. Furthermore, performing *cap-1(RNAi)* on *vab-10(ΔSH3)::mcherry;let-805::gfp* I also observed 100 % basal detachment of both *vab-10* and *let-805* at the turn. To connect the previous observations of FRAP on LET-805::GFP in *egl-50; git-1* mutant FRAP on LET-805::GFP in this background is ongoing.
Yet from another project in lab, it was observed that *spc-1*;*pak-1* double mutants retract to their initial length once they reach the 1.5-fold stage (Pasti, Lardennois & Labouesse, unpublished data), which single mutants do not show. So it was interesting for me to check an interaction between *spc-1* and *egl-50*. I observed retraction phenotype from *spc-1(RNAi)* in *egl-50(n1086)* background. Currently we are analyzing the actin defects in this background to compare it with actin defects in *pak-1; spc-1* background.
To look more into the interactions of Dynein/Dynactin , I performed *sma-1(RNAi)* in *vab-10(ΔSH3)::mcherry; egl-50* and I noticed partial rescue of the two fold arrest. *Sma-1* is known to rescue *vab-19 mutant* embryonic lethality. Therefore this experiment indicates interaction of Dynein/Dynactin with *vab-19*.

What can be the probable roles of Dynein/Dynactin in Elongation?

Dynein/Dynactin is a minus-end directed microtubule based motor responsible for polarized transport in the cell. Two of the most probable roles that can be attributed to the complex are

- Transport of essential components
- As a cortical anchor responsible for distributing tension all along the embryo (Gonczy et al, Cell reports, 2016)

How to test the function of Dynein/Dynactin during *C. elegans* embryonic elongation?

To demonstrate which function of Dynein/Dynactin is important for elongation, we performed *pak-1(RNAi)* on Spastin-overexpressing animals. Spastin is a microtubule (MT) severing protein. The transport function of Dynein/Dynactin would require MTs as tracks. Therefore by performing *pak-1(RNAi)* in a MT-severed background, we would expect to get a similar phenotype as in *egl-50;git-1* double mutant, i.e. a two-fold arrest. However, I did not observe a two-fold arrest.
Further, I tried to reproduce a retraction phenotype by performing *spc-1(RNAi)* in Spastin overexpressed, MT-severed background, which would mimic *spc-1(RNAi)* in *egl-50* mutant, if transport by Dynein/Dynactin is indeed crucial for embryonic elongation. Once again, embryos showed a two-fold arrest characteristic of *spc-1(RNAi)*.

Hypothesis

Given my observations and the experiments currently ongoing, the transport function by Dynein/Dynactin does not seem crucial for embryonic elongation.
I rather propose a cortical attachment role for Dynein/Dynactin, which helps distribute and maintain a uniform tension all over the embryo. In a dynactin defective scenario this equilibrium is imbalanced, thereby giving a lower and higher recovery rates in ventral and dorsal HD respectively, as compared to uniform recovery of LET-805 of ventral and dorsal HD in wild type scenario.

Since I observe partial rescue of *vab-10(ΔSH3)::mcherry; egl-50* mutants by performing *sma-1(RNAi)*, I suggest that Dynein/Dynactin interacts genetically with *vab-19* and *sma-1.*
Spectrin mutation alone gives a 2-fold arrest, much like *egl-50(n1086ts); git-1(tm1962)*. Therefore I propose that cortical dynactin spectrin interaction is essential to maintain a lock on an elongating embryo.
In absence of this lock, elongating embryo is not able to maintain its new position and ultimately retracts.

Methods : - Following methods were used in the scope of this work
Genetic Analysis, RNA interference based knocking out of genes, Crispr-cas9 mediated gene editing, Spinning Disk microscopy, Immunostaining, Fluorescence recovery after photo bleaching (FRAP), Time-lapse microscopy, microinjection;

Publications and Conferences: –

1. RAL-1 controls multivesicular body biogenesis and exosome secretion. Vincent Hyenne, Ahmet Apaydin, David Rodriguez, Coralie Spiegelhalter, Sarah Hoff-Yoessle, Maxime Diem, **Saurabh Tak**, Olivier Lefebvre, Yannick Schwab, Jacky G. Goetz, Michel Labouesse, Journal of Cell Biology, 2015.
2. Inserm l'atelier - Approches experimentales de la mecanotransduction:de la molecule au tissue et au pathologique, 21-23 mai, 2014, Bordeaux, France.
3. Conference Jacques Monod - Building, repairing and evolving biological tissues, 13-17 September, Roscoff, France
4. European worm meeting, 1-3 June, Berlin, Germany.
5. 21st International C. elegans conference, University of California, Los Angeles, 2017, USA

Resumé

Les voies de mécanotransduction entre muscles et épiderme impliquées dans l'élongation embryonnaire de *C. elegans*

Les processus biologiques impliquant des forces physiques sont longtemps restés incompris. L'évolution des systèmes chimiques nécessaires à l'origine de la vie a été proposée pour stimuler la structure environnementale externe (Kuhn, Naturwissenchaften, 1976). Au cours des deux dernières décennies, de nombreux processus biologiques répondant à des stress mécaniques ont été découverts ; tel que : le changement de pression de turgor dans la réponse au toucher chez *Mimosa pudic ;* la différentiation variable des cellules souches mésenchymateuses (MSC) en fonction de la rigidité du milieu de croissance sous-jacent ou encore la cicatrisation des plaies. Les différents mécanismes par lesquels le tissu cellulaire convertit le stimulus mécanique en une activité électrochimique ou biochimique entraînant des processus physiologiques tels que le toucher et l'ouïe sont appelés Mécanotransduction.

Le nématode *C. elegans* est un excellent système d'étude de la mécanotransduction. Il est utilisé comme organisme modèle dans la biologie du développement, la génétique et la biologie moléculaire en raison de sa progéniture abondante, de son développement rapide, de son corps transparent (simplifie la microscopie) et de son génome complètement séquencé. L'épiderme de *C. elegans* est un épithélium à monocouche séparé des muscles par une mince membrane sur sa surface basale. Quatre rangées de muscles sont attachées à l'épiderme ventral et dorsal par des structures connues sous le nom d'hémidesmosomes, ce qui rend l'épiderme sensible au stress mécanique résultant de la contraction et de la relaxation des muscles sous-jacents. Par ailleurs, l'élongation embryonnaire de *C. elegans* est un processus rapide (3 heures environ) qui a lieu sans réarrangement ni division cellulaire, seulement permis par la déformation des cellules latérales et dorso-ventrales de son épiderme. C'est un système modèle *in vivo* pour étudier les changements mécaniques dépendant du stress ; dans la forme cellulaire et le remodelage des jonctions ou la régulation / activation de l'expression des gènes.
Deux forces sont responsables de l'élongation embryonnaire:

- la contratilité de l'acto-myosine
- la tension musculaire (après le stade « 1,7-fold », figure 1)

Les contractions d'acto-myosine dans les cellules latérales permettent la phase initiale de l'allongement et sont régulées par la Rho kinase (let-502) et la kinase activée par la serine / thréonine p21-pak-1. Durant la seconde phase, la tension fournie par les contractions musculaires (force externe à l'épiderme) permet le recrutement de GIT-1 aux hémidesmosomes, ce qui facilite encore l'allongement en activant des protéines telles que pak-1. La voie implique GIT-1 et ses partenaires PIX-1 et Rac GTPase, trois protéines de signalisation localisées au niveau des hémidesmosomes ainsi que la kinase PAK-1. La phosphorylation des filaments intermédiaires est l'une des conséquences de cette voie (Nature 471; 99-103, 2011).

Lorsque l'activité musculaire est inhibée, il n'y a pas de tension transmise à l'épiderme et les embryons sont paralysés à un stade « 2-fold » . On parle de phénotype Pat. Pourtant les mutants *git-1*, *pix-1* et *pak-1* soient viables, suggérant qu'une autre voie agit en parallèle de GIT-1 / PAK-1.

Pour approfondir cette idée, un crible ARNi sur tout le génome a été réalisé en contexte mutant *git-1 (tm1962)* afin d'identifier d'autres régulateurs induisant un arrêt de l'élongation. Les candidats ont été classés selon leurs défauts morphologiques (DM) et leurs défauts d'élongation. L'inhibition des gènes *dlc-1, cap-1* et *cap-2*, qui codent pour les sous-unités du complexe Dynéine / Dynactine, a conduit à de forts défauts morphologiques (DM) (70% - 100%) en contexte

mutant *git-1*. Un ARNi visant d'autres sous-unités du complexe, des protéines associées ou *farl-11*, un inhibiteur connu de la chaîne lourde de la dynéine (*dhc-1*), a fourni des résultats similaires en contexte mutant *git-1*, soulignant ainsi le rôle du complexe Dynéine / Dynactine dans l'élongation embryonnaire de *C. elegans*. Par ailleurs, les mutants pour le complexe Dynéine / Dynactine montrent une létalité précoce (effet maternel). Par conséquent, pour étudier ce complexe, nous avons utilisé *egl-50*, un allèle thermosensible (ts) d'arp-1, codant pour une sous-unité du complexe Dynactine. Nous avons combiné *git-1 (tm1962)* avec *egl-50 (n1086).* Un double mutant *egl-50 (n1086ts); git-1 (tm1962)* est viable à 15 ° C, mais 70% des embryons s'arrêtent à « 2-fold », 20% d'embryons rétrécissent et 10% des embryons rétractent jusqu'à leur taille initiale. Des résultats similaires ont été trouvés pour le double muant *dnc-1 (ou404ts); git-1 (tm1962)*. Chez *C. elegans dnc-1 (or404)* est un allèle thermosensible de l'homologue de la sous-unité de la dynactine p150-GLUED. Nous avons ensuite utilisé ces mutants pour répondre à plusieurs questions.

1) Pourquoi les mutants *egl-50 ;git-1* sont-ils bloqués à « 2-fold »? Quelles sont les structures affectées?

Pour répondre à cette question, j'ai créé une bibliothèque de marqueurs dans un contexte mutant *egl-50; git-1* afin de rechercher des défauts structurels et de dynamique. Nous n'avons pas observé de défauts majeurs d'organisation du cytosquelette d'actine. Des immunomarquages de la Spectraplakine VAB-10a / b (requise pour la résistance mécanique de l'épiderme lorsque soumis à une contrainte et du maintien de l'épiderme et de la matrice extracellulaire via les hémidesmosomes); de perlecan UNC-52 (joue un rôle essentiel dans la structure musculaire et le développement) ; et des filaments intermédiaires (protéines des hémidesmosomes) n'ont pas non plus montré de défaut majeur. De plus, les marqueurs fluorescents obtenus par CRISPR de *par-3, noah-1, e-cadherine* et *let-805* (marqueur basal des hémidesmosomes) n'ont montré aucun changement significatif d'intensité. Par-3 est une composante de Partioning complex. Noah-1 est une protéine de la matrice extracellulaire (ECM) connue pour répartir le stress mécanique pendant la morphogenèse (Vuong et al, Development, 2017). Myotactine, LET-805 est une protéine localisée au niveau basal des hémidesmosomes, alors que l'e-Cadherine est une protéine située au niveau des jonctions. J'ai réalisée une construction de *mup-4* (localisée au niveau apical des hémidesmosomes) fusionnée à la GFP par CRISPR et j'ai constaté que l'intensité et l'organisation de MUP-4 ne sont pas affectées. En examinant les hémidesmosomes via la Myotactine, j'y ai trouvé des défauts mineurs. Ces défauts n'étaient pas frappants et n'étaient pas présents dans tous les embryons arrêtés à « 2-fold ». L'équipe avait précédemment montré une diminution de l'intensité de LET-805 :: GFP au niveau des hémidesmosomes en contexte double mutant pour les microtubules *(surexpression de spastine); let-502 (Rho-kinase)* (Quintin et al, Développement, 2015). Nous ne l'avons pas observé dans notre système, bien que nous soupçonnions des défauts dynamiques pour LET-805. Pour tester la possibilité d'une dynamique défectueuse de LET-805 au niveau des hémidesmosomes, j'ai réalisé une analyse de FRAP sur LET-805 :: GFP. Cette analyse a révélé deux catégories de fractions mobiles en contexte *egl-50; git-1* mutant, qui pourraient être similaires, plus basses ou plus élevées que le contrôle sauvage.

2) Elongation - une vue globale

Pour mieux comprendre la fonction de ce complexe lors de l'élongation embryonnaire de *C. elegans*, j'ai connecté de multiples approches. J'ai créé un double mutant *vab-10 (ΔSH3) :: mcherry; egl-50* et inhibé *spc-1* par ARNi dans la lignée mutante *egl -50 (n1086)*. En effet un autre projet de l'équipe a montré qu'un ARNi contre *pak-1* en contexte *vab-10 (ΔSH3)* conduit à un arrêt à « 2-2,5 –fold » combiné à une dislocation apicale des hémidesmosome au niveau de la zone de pli de l'embryon. SH3 correspond à une zone située au niveau des répétitions spectrines

du domaine plakine de la protéine vab-10. Une délétion de ce domaine SH3 a été créée dans le laboratoire en utilisant la technique d'édition de gènes Crispr-cas9. (Shashi Suman et al, données non publiées)
J'ai observé un détachement basal à 100% des hémidesmosomes dans la zone de pli des embryons *vab-10 (ΔSH3) :: mcherry, egl-50* arrêtés à « 2-fold » à 25,5 ° C. En outre, en utilisant un ARNi contre *cap-1* sur des vers *vab-10 (ΔSH3) :: mcherry; let-805 :: gfp* ; j'ai également observé ce détachement basal à 100% de *vab-10* et *let-805* dans la même zone. La recherche du lien entre les précédentes observations de FRAP sur LET-805 :: GFP en contexte mutant *egl-50*; *git-1* et celles de FRAP sur LET-805 :: GFP dans ce contexte est en cours.
En parallèle, dans un autre projet de l'équipe, on a observé que les doubles mutants *spc-1 ; pak-1* s'allongent jusqu'à environ un stade « 1,5-fold » avant de se rétracter à leur longueur initiale (Pasti, Lardennois et Labouesse, données non publiées). C'est un phénotype frappant que les simples mutants *pak-1* et *spc-1* ne montrent pas. Il était donc intéressant de vérifier une interaction entre *spc-1* et *egl-50*. J'ai alors observé ce même phénotype de rétraction en utilisant un ARNi contre *spc-1* en contexte *egl-50 (n1086)* muté. Nous analysons actuellement les défauts d'actine dans ces conditions afin de le comparer aux défauts d'actine déjà identifiés chez les doubles mutants *pak-1; spc-1*.
Pour en savoir plus sur les interactions de Dynéine / Dynactine, j'ai inhibé *sma-1* par ARNi chez des mutants *vab-10 (ΔSH3) :: mcherry; egl-50* et j'ai constaté un sauvetage partiel de l'arrêt à « 2-fold ». Dans la littérature, *Sma-1* est connu pour sauver la létalité embryonnaire des mutants *vab-19*. Ce résultat indique une interaction du complexe Dynéine / Dynactine avec vab-19.

3) Quels peuvent être les rôles du complexe Dynéine / Dynactine dans l'élongation?

Dynéine / Dynactine est un moteur moléculaire basé sur les microtubules et interagissant avec l'extrémité de ces derniers. Le complexe est responsable du transport polarisé dans la cellule. Deux des rôles les plus probables qui peuvent être attribués au complexe sont les suivants :

- Transport de composants essentiels
- Attachement cortical distribuant de la tension tout au long de l'embryon (Gonczy et al, Cell reports, 2016)

4) Comment tester la fonction de Dynéine / Dynactine pendant l'élongation embryonnaire de *C. elegans*?

Pour déterminer quelle fonction de Dynéine / Dynactine est importante lors de l'élongation, nous avons utilisé un ARNi contre *pak-1* sur des animaux sur-exprimant la Spastine. La Spastine est une protéine de dissociation des microtubules. La fonction de transport de Dynéine / Dynactine nécessiterait que les microtubules agissent comme des rails. Par conséquent, en inhibant *pak-1* par ARNi dans un contexte où les microtubules sont affectés, on s'attendrait à obtenir un phénotype similaire à celui du double mutant *egl-50 ; git-1*, (i.e . un arrêt à « 2-fold »). Or, je n'ai pas observé ce phénotype.
En outre, j'ai essayé de reproduire un phénotype de rétraction en inhibant *spc-1* par ARNi dans des vers sur-exprimant Spastine (contexte dans lequel les microtubules sont une nouvelle fois affectés. Ces conditions devraient imiter le phénotype obtenu en combinant *spc-1(RNAi) ; egl-50*, si le transport par Dynéine / Dynactine est en effet crucial lors de l'élongation. Encore une fois, les embryons ont montré un arrêt à « 2-fold » caractéristique de *spc-1 (RNAi)* seul.

5) Hypothèse

Compte tenu de mes observations et des expériences actuellement en cours, la fonction de transport de Dynéine / Dynactine ne semble pas cruciale pour l'élongation embryonnaire.

Je propose plutôt un rôle d'attachement cortical du complexe Dynéine / Dynactine, aidant à répartir et à maintenir une tension uniforme dans tout l'embryon. Dans une perte de fonction en Dynactine, cet équilibre est perturbé, conduisant à des taux de récupération inférieurs et supérieurs respectivement dans les hémidesmosomes ventraux et dorsaux.
Puisque j'observe un sauvetage partiel des double mutants *vab-10 (ΔSH3) :: mcherry; egl-50* en utilisant un ARNi contre sma-1, je suggère que Dynéine / Dynactine interagit génétiquement avec *vab-19* et *sma-1*.
La mutation de Spectrin seule conduit à un arrêt à « 2-fold », tout comme *egl-50 (n1086t); git-1 (tm1962).* Par conséquent, je propose que l'interaction corticale de Dynactine et Spectrine soit essentielle pour maintenir un verrou sur un embryon qui s'allonge.
En l'absence de ce verrou, l'embryon en cours d'élongation n'est pas capable de maintenir sa nouvelle longueur et finit par se rétracter.

Méthodes: - Les méthodes suivantes ont été utilisées dans le cadre de ce travail
Analyse génétique, ARN interférent pour inhiber l'expression de gènes, technique d'édition du génome par Crispr-cas9, microscopie à disque rotatif, immunomarquage, redistribution de fluorescence après blanchiment (FRAP), microscopie à lapse de temps, micro-injection;

Publications et Conférences:

1. RAL-1 controls multivesicular body biogenesis and exosome secretion. Vincent Hyenne, Ahmet Apaydin, David Rodriguez, Coralie Spiegelhalter, Sarah Hoff-Yoessle, Maxime Diem, **Saurabh Tak**, Olivier Lefebvre, Yannick Schwab, Jacky G. Goetz, Michel Labouesse, Journal of Cell Biology, 2015.
2. Inserm l'atelier - Approches experimentales de la mecanotransduction:de la molecule au tissue et au pathologique, 21-23 mai, 2014, Bordeaux, France.
3. Conférence Jacques Monod - Building, repairing and evolving biological tissues, 13-17 September, Roscoff, France
4. European Worm Meeting, 1-3 June, Berlin, Germany.
5. 21st International *C. elegans* conference, University of California, Los Angeles, 2017, USA

Abbreviations

Arp-1	Actin Related Protein
BMD	Body Morphology Defect
C. elegans	Caenorhabditis elegans
CeAJ	C. elegans Adherens Junctions
CeHD	C. elegans HemiDesmosome
DIC	Differential Interference Contrast
DHC	Dynein Heavy Chain
DLC	Dynein Light chain
DNA	Deoxyribonucleic Acid
E-Cad	Epithelial Cadherin
EGL	EGg-Laying defective
RNA	Ribonucleic Acid
ECM	Extracellular Matrix
FRAP	Fluorescence Recovery After Photobleaching
GFP	Green Fluorescence Protein
GIT	G protein-coupled receptor kinase InTeractor
IF	Intermediate Filament
L1-L4	Larval stages of C. elegans
MLC	Myosin Light Chain
MT	MicroTubule
MTOC	MicroTubule Organising Centre
NGM	Nematode Growth Medium
PAK	p21-Activated Kinase
PCR	Polymerase Chain Reaction
qPCR	Quantitative Polymerase Chain Reaction
RNAi	RNA interference
ROCK	Rho-associated Kinase
Sg RNA	Single Guide RNA
SH3	Src homology domain
VAB	Variable ABnormal Morphology
WT	Wild Type

Common abbreviations for mutant phenotypes in *C. elegans*

Let	Lethal
Sma	Small size
Unc	Uncoordinated movement
Pat	Paralysed at two-fold
Dpy	Dumpy
VAB	Variable ABnormal Morphology

Introduction

I. Introduction

Index – table of contents

1. **This thesis is about** …

How scientific explanations or theories, once considered to be outrageous, create a niche for themselves and today represent a whole systematic field of study. How two fields which seem totally unrelated to each other can act as model tools to study one another. Biological studies picked up their pace, when it was studied with the vision of the chemists and transformed itself from a science of observation to an experimental science, thereby opening the field of biochemistry. Once again in the 1980's, techniques such as Raman effect, electron diffraction, NMR and X-rays revolutionized biology and opened the gates of Biophysics.

This thesis is about a field, Mechanotransduction, relatively new, which has been slowly picking up its pace for the last two decades. Mechanical forces in biology have been hinted since D'arcy Wentworth Thompson published his book 'On Growth and Form' in 1917. An excerpt from the preface of this book – 'Naturalists are little accustomed to employ the methods of physical science while studying life'.

Today, D'arcy Wentworth Thompson's vision of studying life by all tools available, whether it is mathematics or other streams of science is very much a reality. I have tried to incorporate my knowledge and understanding, benefit of my mentor's experience and the skills and knowledge of my colleagues, while employing the advances of molecular biology, microscopy, programming, microbiology and statistics, for writing this thesis.

In the following pages, there is an introduction to the process of Mechanotransduction, how cells have evolved structures that can, not only sense the external and internal physical cues, but can respond to them efficiently. Such processes have been vital for both at origin and for maintaining the life. The structures required are evolutionary conserved and will be presented in the introduction of this thesis, for, it is these structures, most of my experiments are based on. The thesis will also briefly mention the transport protein complexes as it is, these complexes, which keep the cell dynamic, and should respond to biochemical or mechanical cues. I have tried to incorporate the illustrations and schemes to make it easy to follow the methods and materials, used for my experiments. The experiments have been mentioned in the simplest possible manner, followed by a discussion. We have chosen to work on *C. elegans*, for it is genuinely an elegant organism to study development, genetics and mechanotransduction along with many other fields of study. The thesis is written in an easy format and I welcome the comments of the readers.

2. Mechanotransduction

The origin of life is a complex physico-chemical process. Synthesis of first life forms can be because of an accidental change in environment, though how such life forms manage to turned themselves into first self-reproducing life forms is a puzzling matter even today. Formation of self-replicating life forms required a genetic material, its replication and translation of proteins from this genetic material. How these complex reactions assimilated to form living systems? It has been argued (Kuhn 1976) that the external environment played as a trigger for a certain set of chemical reactions, though it was not the only driving force; the physical forces such as osmotic pressure and viscosity helped shape the first self-replicating living organism. Questions containing the detailed chemical composition and structure are of secondary importance as without the proper physical conditions, the complexes required for life would have not gradually built up as complex aggregates together to initiate a self-sustaining life, as we know it today.

Eons later, after the beginning of life; in twentieth century, a complex life form termed as 'Humans' are systematically studying processes where force affects the biological system. For instance - '*Mimosa pudica'* is a plant which responds to touch, a physical force. Upon touching, the leaves of the plant *Mimosa pudica*, also known as touch-me-not plant, recoil, shrink and go to sleep. Leaves of plants stay upright because of the turgor pressure, which is the pressure applied by the water inside the cells on the cell walls. Seismonastic movements such as touch or shaking trigger a movement of potassium ions, which make water/electrolytes flow out of the cell, resulting in a loss of cell pressure, causing cells to collapse and leaves to get squeezed shut.

Variable differentiation of mesenchymal stem cells is another example where physical forces effect a biological process. Young mesenchymal stem cells (MSC's) differentiate in response to the stiffness of the underlying matrix. Softer matrices lead to the differentiation of MSC's into neuronal cells, i.e. brain, and are neurogenic, stiffer matrices that mimic muscles lead the MSC's to differentiate into muscles and are therefore myogenic, whereas rigid matrices that mimic bones differentiate the MSc's into osteocytes and are eventually osteogenic. (Flanagan, Ju et al. 2002, Neuhuber, Gallo et al. 2004, Garcia and Reyes 2005, Engler, Sen et al. 2006) (Figure 1)

On a cellular level, all cells and organisms have the ability to respond to environmental pressures including diverse sets of mechanical forces such as viscosity and touch. Both unicellular and multicellular complex eukaryotes, all express receptors such as integrins, which transmit forces from the external

environment across the cell membrane. A wide range of forces such as compressive, tensile, fluid shear stress and hydrostatic pressure play an intricate

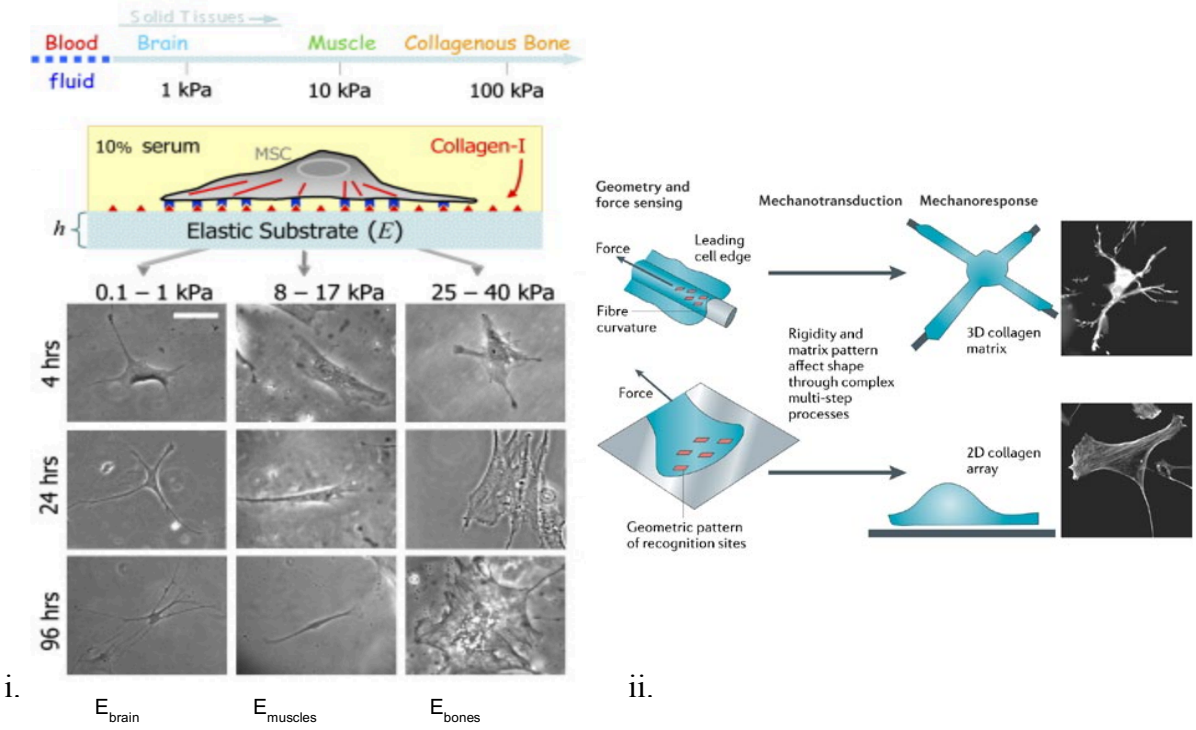

Figure 1. i. - Solid tissues exhibit a range of stiffness, as measured by the elastic modulus, *E.* The in vitro gel system controls *E* through crosslinking, control of cell adhesion by covalent attachment of collagen-I, and control of thickness, *h*. Naive MSCs of a standard expression phenotype are small and round but develop increasingly branched, spindle, or polygonal shapes when grown on matrices respectively in the range typical of ~E_{brain} (0.1–1 kPa), ~E_{muscle} (8–17 kPa), or stiff crosslinked-collagen matrices (25–40 kPa). (Engler, Sen et al. 2006).

ii. - The steps that are involved in the responses of cells to their environment. Force-induced changes in protein conformation and geometry-dependent interactions are transduced into biochemical signals that activate various mechanosensitive signalling pathways, ultimately regulating cellular mechanoresponses. The dramatic difference in morphology of same cells after 4 hours in different matrices. Human fibroblasts project a dendritic network of extensions in collagen matrices but not on collagen-coated coverslips (DuFort, Paszek et al. 2011).

part in the shaping, development and maintenance of the tissue. The manner in which cells interact with these forces and respond to them is dictated by the physical properties of the cells, their adjacent cells and the extracellular matrix (ECM). Biological materials are viscoelastic i.e. they deform upon applying external force and return back very close to their original shape once the external stress is removed. Though the tissue retains some permanent change due to viscous component of viscoelasticity (DuFort, Paszek et al. 2011).

The various mechanisms by which cells/living tissues convert a mechanical stimulus into an electrochemical or biochemical activity resulting in physiological processes such as touch and hearing are termed as '**Mechanotransduction**'.

i. Mechanical cues and their integration in the cell

Survival is based upon the ability of the organism to respond to environmental pressures, including diverse sets of mechanical force. Almost all organisms have evolved specific structures that are tailored to respond to physical force. Single-celled organisms, such as bacteria, and complex multicellular eukaryotes, such as plants and animals, all express stretch-activated ion channels. Cell surface receptors such as integrins, which transmit forces from the external environment across the cell membrane, are also evolutionarily conserved molecules from primitive organisms to complex, more evolved eukaryotes. The complexity of such structures increases both in terms of organization and their regulation, so as to sense the degree of force exerted and respond accordingly to it. A number of diseases such as atherosclerosis, osteoporosis, cancer, deafness and disorders such as 'Hutchinson-Gilford progeria syndrome' have been attributed to either altered tensional homeostasis or perturbed cellular response to mechanical stimuli. The process of mechanotransduction is important for maintaining tensional homeostasis. (DuFort, Paszek et al. 2011).

Mechanoresponsiveness is coordinated to cell shape, tissue architecture and cellular microenvironment. In D'Arcy Wentworth Thompson's 'On Growth and Form', 1917, it has been argued that different biological structures have different mechanical functions or different biological tissues evolve and adapt to the function in terms of their mechanical environment. For instance, small subcutaneous ligaments and hollow bones in the wings of the birds for easy flight and different egg shell shapes in accordance to the habitat, the organism survives in. On a much smaller scale, shapes of eukaryotic cells are defined by cycles of mechanosensing, mechanotransduction and mechanoresponse. Responses from parameters such as substrate rigidity and cell density regulate cell growth, differentiation and cell-level form. Structural motifs containing proteins that can mechanically switch between conformations serve as mechanosensory elements. The physical aspects of the cellular environment are sensed by the cells are force and geometry at the nano-to-micrometer level. Therefore, it is important to identify the primary sensory processes, the transduction processes and the downstream mechanoresponsive pathways.

Cytoskeletal filaments can propagate stresses over long distances, whereas structures such as focal adhesions, desmosomes and junctions provide both tensile strength and effective transmission of stress (Figure 2).

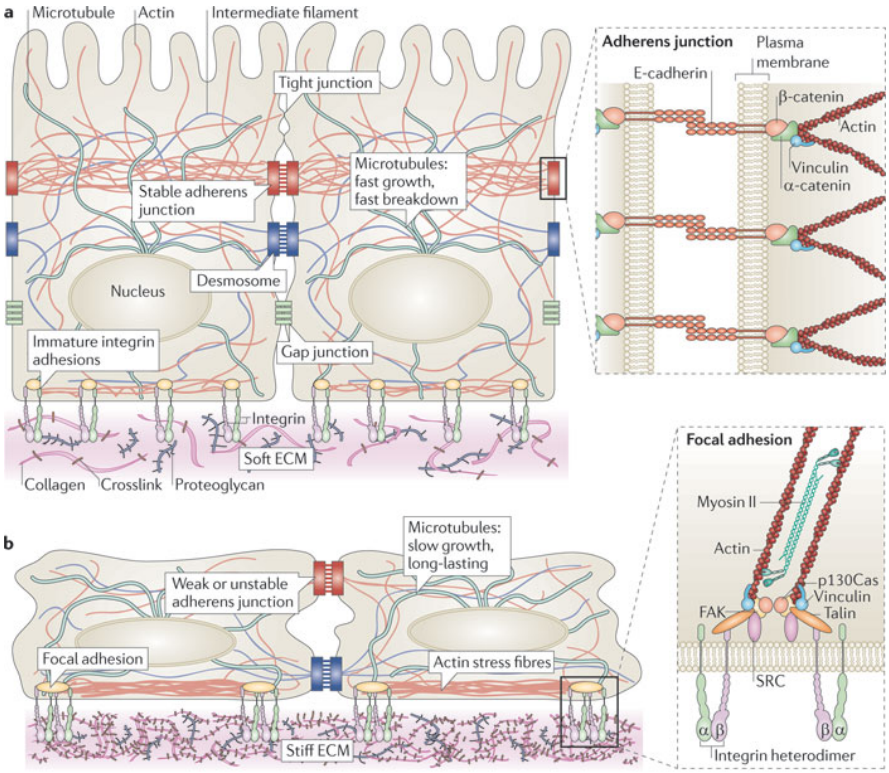

Figure 2. Tissues are mechanically integrated structures, defined by interconnected networks. Cell–matrix adhesion complexes containing integrins can also directly sense the physical properties of the ECM. These complexes contain specialized protein sensors, including talin, p130Cas (also known as BCAR1), and integrins themselves, that undergo force-dependent conformational changes to elicit downstream signalling responses. The physical properties of the ECM are determined by its composition, the organization of its components, and their degree of intramolecular and intermolecular crosslinking. Transcellular tension transmitted across adherens junctions affects ECM remodelling, which in turn regulates cell–matrix and cell–cell adhesions. Increased ECM stiffness owing to remodelling can result in changes in cell and nuclear shape, chromatin organization, assembly of cell–matrix adhesions (called focal adhesions), formation of actin stress fibres, destabilization of cell–cell adhesions, and changes in microtubule dynamics. FAK, focal adhesion kinase. (DuFort, Paszek et al. 2011)

A later chapter in Introduction section will talk more about the structures such as cytoskeleton and focal adhesions.

ii. Mechanisms of force sensing

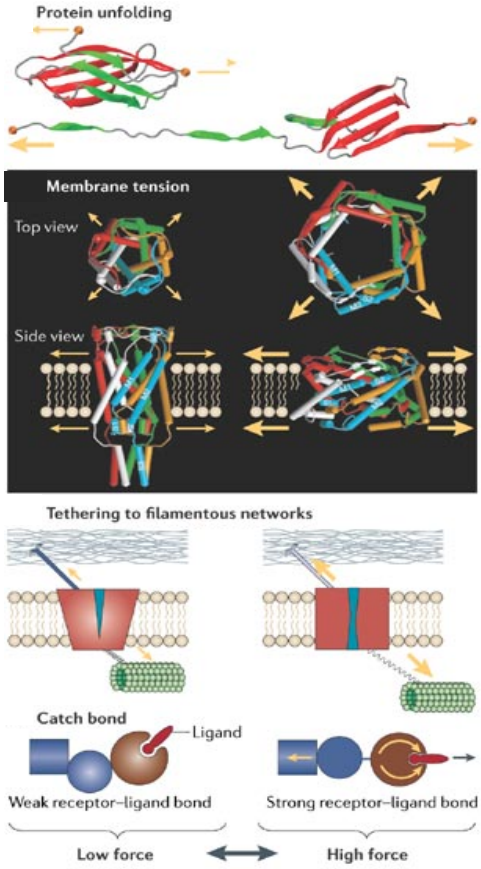

Figure 3. Top. Conversion of force into biochemical signals by partial protein unfolding (as shown for the fibronectin module III). This can result in the gain or loss of binding sites, increased separation between protein domains, or the gain or loss of enzyme function.
Middle. The opening of some mechanosensitive ion channels can be regulated by membrane tension, whereas the opening of others requires that their intra- and/or extracellular domains are physically connected to force-bearing filaments.
Below. Stabilizing receptor–ligand bonds by switching them to a long-lived state by force (catch bonds). Yellow arrows indicate forces. (Vogel and Sheetz 2006)

How the structures mentioned in the previous segment sense the force? Most mechanosensing mechanisms involve proteins that undergo conformational changes in response to a physical force (Figure 3). Such proteins link the integrins or intermediate filaments of the structure to cytoskeleton. These proteins generally consist of tandem-repeat sequences such as spectrin-family members (actinin, dystrophin, talin, titin, fibronectin and cadherins). Forces can either unravel a domain or hinder the movement of a particular domain, both resulting in change of the ligand binding topology. Differences in the elasticity and structure of such repeats would define the order of sequence they reveal in time. The passing of energy barriers to unravel proteins typically coincides with the breakage of force-bearing hydrogen bonds that stabilize their tertiary structure.

The mechanical stability of the modules therefore depends on how frequently the force-bearing hydrogen bonds can be attacked by free water molecules. Amino acid side chains differ in their behaviour of being hydrophilic or hydrophobic and thus can selectively shield the water. An important role of amino-acid side chains in regulating mechanical stability is whether they shield or expose those underlying bonds from electrophilic attack by water molecules. Local charges also affect the shielding efficiency of amino-acid side chains and, consequently, pH and ionic strength can both further tune the mechanical stability of proteins. Finally, many modules are mechanically stabilized by disulphide bonds and their redox state can be force-sensitive if the disulphide bonds are buried deep in the module. Many enzymes or substrates change their conformational state under the stress resulting in change in their enzyme activity. Protein interactions also mediate the cytoskeletal interaction with ECM through weak non-covalent bonds. If breaking one bond requires a force F, breaking N bonds would require NF force, which would be a linear relationship. This relationship can get non-linear, if the rebinding of single broken bands happens (Vogel and Sheetz 2006).

Mechanosensitive ion channels provide, yet another way of force sensing. The bacterial potassium ion channel MscL (15-KDa protein comprising 136 amino acid residues) responds to stress in lipid bilayer. Bacterial channels are relatively force insensitive and respond mostly to high lytic tensions for the lipid bilayer. In *C. elegans* the touch sensor has been identified as a mechanosensitive ion channel. Tensions in plants are usually lower than in bacteria and in animals they are many folds lower from both bacteria and plants. (Vogel and Sheetz 2006)

Thus, in the context of life, there are always structures from nano scale to macro scale, which sense the tension and respond to it.

3. Morphogenesis

Morphogenesis (beginning of the shape) may be defined as the study which attempts to explain the development of the form of the individual (ontogenesis) and of the race (phylogenesis). Morphogenesis is a subdivision of general physiology, in as much as it deals with activities – processes, development and evolution. (Davenport 1898). Enzmann and Haskins studied morphogenesis by means of x-rays for inherited cuticular tumour in *Drosophila* in 1936.

How all living things do not have the same shape? Conserved mechanisms govern the development of all living beings. These conserved mechanisms can act at the level of morphology, anatomy and more peculiarly at cellular and molecular levels. Plant models such as Arabidopsis and animal models such as *Dictyostelium*, *Drosophila*, echinoderms (Sea urchin) and nematodes (*C. elegans*) have provided continuous and extensive insights into cellular and molecular aspects of morphogenesis. Morphogenesis requires the formation of a body plan or axis, for which different animals deploy different mechanisms. The initial asymmetry in *Drosophila* is established in the oocyte, and development is initiated by fertilisation. Similarly, in *C. elegans* the initial asymmetry is established before the first cell division by the sperm, which results in asymmetric division of polarity proteins anterio-posteriorly in the fertilized embryo, leading to asymmetric division into two cells, having two distinct development potentials. But in mammals, asymmetry is established after several cell divisions (Chisholm and Firtel 2004). The steps of morphogenesis in eukaryotes involve steps such as formation of blastomeres, gastrulation and subsequent formation of organs. Expression of genes responsible for embryogenesis and differentiation of cells leads to differentiation of cells. Different organisms follow different processes such as epiboly, ingression, invagination, delamination and involution to place the cells in the interior of the embryo. All these processes involve shape and size change.

i. Forces in Tissue morphogenesis

The processes by which multicellular organisms take shape are driven by forces that are typically generated by molecular motors and transmitted via cytoskeletal elements within the cell and adhesion molecules between cells. Early embryologists analysed morphogenesis as a physical, mechanical problem of how forces generated by oriented cell division, directed cell crawling and bending of cell sheets by the integration of local cell shape, reshape the embryo as a whole. Holtfreter provided the concepts of recognition and selective affinity and the concept of mechanically integrated cell motile behaviour. He studied different

types of cells in vitro, as individuals, groups or large aggregates and combined tissues of the three primary germ layers – ectoderm, mesoderm and endoderm. They showed either positive or negative affinities with each other. Endoderm and ectoderm develop a negative affinity and isolate from one another, whereas mesoderm has a positive affinity for both, which represents their rearrangements during gastrulation, where the three germ layers rearrange into formation of epidermis, gut and muscles. Cell behaviour is integrated at the tissue level. He observed that the outer cells of the amphibian embryo were mechanically linked into a sheet and that a subset of these cells became bottle-shaped ("bottle cells"), bending the outer layer inward to form the blastopore. Holtfreter cultured these cells in clusters and observed protrusive activity—extensions of their margins that attach to and exert traction on the substratum—and directional crawling. He postulated that in the embryo, these cells migrate directionally inward, and because of their mechanical linkage to the rest of the outer layer of the embryo, they "tow" it into the embryo, forming the precursor to the gut (Holtfreter 1943, (Keller 2012).

Nowadays, numerous tools such as laser cutting devices, micropipettes and atomic force microscopy are used to analyse the mechanical properties of the cells and tissues. Changes in cell number, size, shape and position drive the forces in a tissue. Cell proliferation is driven by cell division and giving rise to two daughter cells, whereas cell death results in the disappearance of the dying cell. Cell shape change can happen by cell elongation, formation of cell protrusions, cell growth and osmotic swelling. Changes in cell position are brought about by either cell migration or cellular rearrangements, such as cell intercalations and neighbour exchanges. Cell-cell adhesion mediates the force transmission between the individual cells and allows the individual cell changes into more global alterations in tissue morphology. Coordinated changes in position of individual cells can trigger tissue rotations, spatially controlled cell proliferation, cell division orientation and cell death within multicellular tissues can give rise to global changes in tissue shape (Heisenberg and Bellaiche 2013).

Cells can generate forces via actin or microtubule polymerization and osmotic pressure, though cellular force generation mostly relies on motor proteins such as myosin and Dynein. These proteins interact with cytoskeletal filaments such as actin and microtubules to change the organization of cellular organelles. Cytoskeletal filaments are connected to the structures as cell-cell adhesions and cell-matrix adhesions through transmembrane molecules such as cadherins and integrins. These structures transmit the force further. Actomyosin contractility and cadherin mediated cell adhesion are one of the most studied force generating and force-transmitting structures. Mesoderm invagination during gastrulation in *Drosophila* is driven by the coordinated apical constriction of mesodermal cells. MyoII spots and fibres are formed at the apical cortex of invaginating mesodermal

cells, which results in apical constriction. The MyoII structures increase in intensity and move towards the centre of cell apex, resulting in pulsatile centripetal actin-myosin flows. Actin-myosin network coupling to apical junctions leads to MyoII organizing into a supracellular network that connects each cell to transmit forces across the tissue (Figure 4) (Bosveld, Bonnet et al. 2012) (Martin, Gelbart et al. 2010) (Heisenberg and Bellaiche 2013).

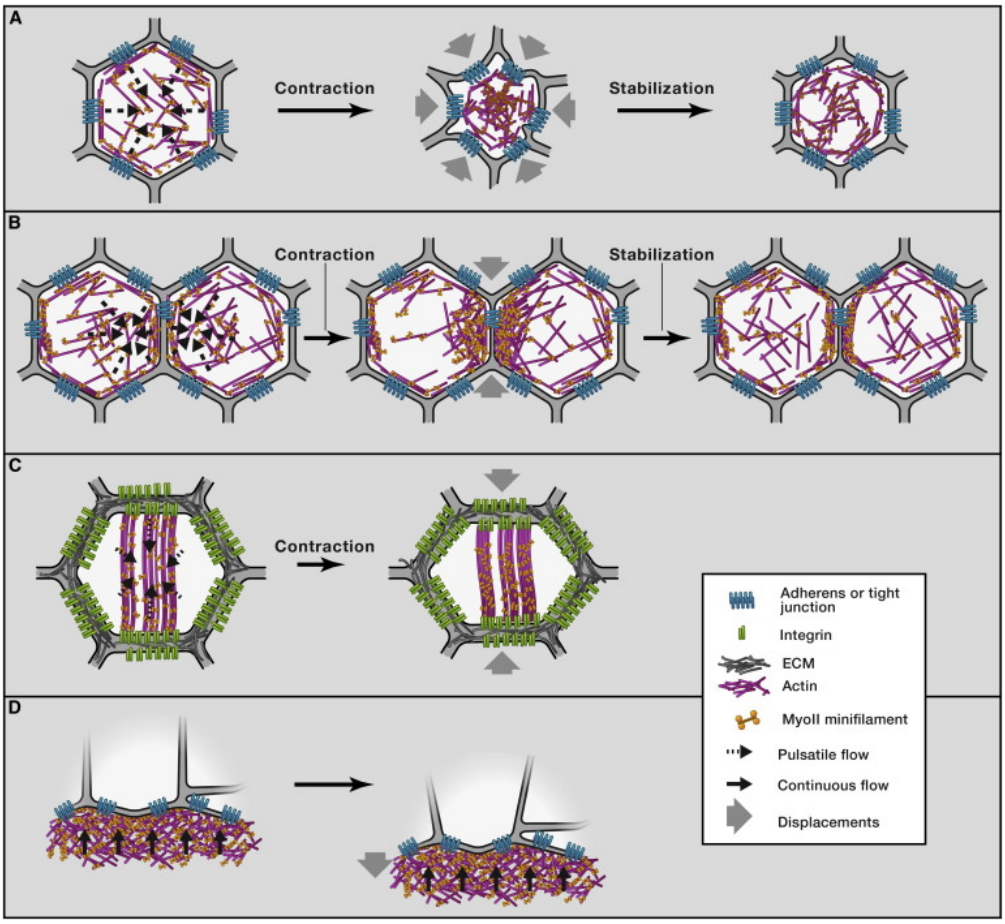

Figure 4. Actin-Myosin Network Dynamics and Force Generation

(A) Pulsatile and centripetal flow of the apical actin-myosin network promotes apical cell constriction. In *Drosophila,* mesodermal cells, the accumulation of apical actin-myosin stabilize cell shape changes between each pulse, leading to incremental reductions of the cell apex area. (B) Pulsatile anisotropic flow induces junction shortening during cell intercalation. Resulting enrichment of actin-myosin at the junction stabilizes junction length reduction. (C) Basal myosin flow on a static-oriented actin network produces anisotropic deformation of the base of the *Drosophila* follicular cells.(D) Continuous actin-myosin flow in the zebrafish yolk cell produces the mechanical force necessary for EVL spreading over the yolk cell during early zebrafish development (Heisenberg and Bellaiche 2013).

4. Cell boundaries

i. Adherens Junctions and their components – cadherins and catenins

Junctions connect cells to one another. The primary function of cell-cell junctions is to resist the external forces that pull cells apart. For instance, epithelial cells must remain tightly linked when they are stretched and pinched. These junctions are dynamic to accommodate the changes in cellular environment such as growth and remodelling. These junctions employ cadherins and catenins to link the cytoskeleton of one cell to that of its neighbour. Cadherins are present ubiquitously all across animal kingdom, but are absent from plants, fungi, archaea and bacteria. Cadherins derive their names from their calcium dependence. Removal of Ca^{+2} ions lead to the rupture of cadherin dependent junctions. Cadherins were classified according to the tissue types they were first discovered in. For example, *E-cadherin (**hmr-1*** in *C. elegans)* in epidermis, *N-cadherin* in nerve cells and *P-cadherin* in placenta. The cadherins are closely related in sequence and thereby constitute a cadherin superfamily (Hinck, Nathke et al. 1994, Costa, Raich et al. 1998, Ichii and Takeichi 2007, Harris and Tepass 2010).

Cadherins molecules consist of extracellular (EC) domains, membrane domains and intracellular domains. Cadherin molecules from neighbouring cells bind to each other from N-terminal tips, the domain farthest from the membrane. Unlike most other cell-cell adhesion proteins, cadherins bind to their partners with low affinity. It is the number of these weak bonds which result in formation of strong attachments. Cadherin molecules regulate the epidermal-mesenchymal transition. Switching on the expression of cadherin genes, unattached mesenchymal cells arrange themselves to form an epithelium, whereas by downregulating the cadherin expression, the epithelium falls apart to mesenchymal cells. These transitions form the basis of cancer. Cancer starts in epithelium, but it is when the cells fall apart and invade other tissues, it becomes malignant (Lecuit, Lenne et al. 2011).

Cadherins interact with the cytoskeleton through their intracellular domains indirectly, via interactions through other proteins. Cytoplasmic tails of cadherin binds to *ß-catenin* and *p120-catenin*. *ß-catenin (**hmp-2*** in *C. elegans)* interacts with *α-catenin (**hmp-1*** in *C. elegans)*, which in turn recruit other proteins, which provide a dynamic linkage to actin cytoskeleton (Nathke, Hinck et al. 1994).

Mature adherens junctions are dense regular arrays of huge protein complexes containing thousands of cadherin molecules, a complex network of catenins,

actin regulators. Actin bundles are linked to these structures. The junctions experience pulling forces generated by the attached actin. The contractile forces acting on a junction in one cell are balanced by contractile forces at the junction of the opposite cell, thereby maintaining a uniform tension in the tissue. Junctions are not just passive sites of protein-cytoskeletal interaction, but are dynamic tension sensors, that change and modify in response to changing mechanical landscape. The protein *α-catenin* has been proposed to sense the increased tension along the junction, by stretching into an extended conformation from a folded structure. This exposes the binding site for vinculin, which increases actin attachment to the junction. Vinculin binding sites are absent in nematode *C. elegans*. Coordinated contraction of the attached actin network provides the motile force for the folding of epithelial cell sheets into tubes, vesicles and other structures (Leckband, le Duc et al. 2011).

Another kind of junctional complex consisting of a membrane bound guanylate kinase disc large DLG-1 and a nematode specific coiled coil protein AJM-1 is found in *C. elegans* (Pasti and Labouesse 2014).

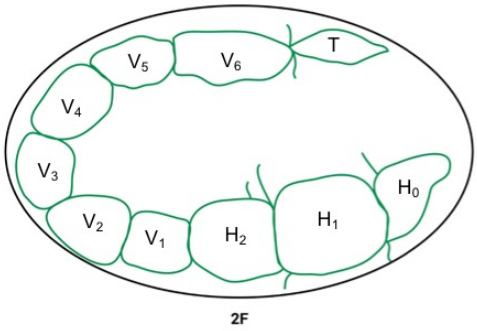

Figure 5. Lateral cells and their junctions in *C. elegans* 2-fold embryo stage. The cells are labelled.

ii. Desmosomes

Essentially all epithelia are anchored to other tissue on one side – the basal side and free of such attachment on their opposite side – the apical side. Desmosomes are specialized cell to cell junctions that bind epidermis to underlying basement membrane. Thus, desmosomes provide polarity to epithelial tissue. Desmosomes are plentiful in structures that are subjected to high levels of mechanical stress such as heart muscle. Desmosomes consists of intracellular adaptor proteins, intermediate filaments and integrins. In the intestines of mammals, the apical sides of desmosomes actively take the nutrients while the basal side passively diffuse the same nutrients into the blood stream of small blood vessels. To maintain the correct desmosome structure, apical transporters must be rightly sorted to apical side, whereas the ones at the basal side to the basal side.

iii. Extracellular Matrix (ECM)

The extracellular matrix is an evolutionary conserved, ancient structure present in all the metazoans. Tissues are not solely made up of cells. The ECM are a complex network of macromolecules (polysaccharides and proteins), which are secreted locally and organized closely with the surface of the cells producing them. The matrix can become calcified and hard as rock in case of bones and teeth or produce carapace as in turtles. The cells which produce the matrix also control the organization of the matrix through controlling the orientation of the cytoskeleton inside the cell. Major constituents identified initially in extracellular matrices included collagens, non-collagenous glycoproteins and proteoglycans. Different organisms have evolved different macromolecules for ECM, yet they are not so different in their functions. For instance, specialized collagens are secreted in nematodes and mussels for formation of cuticle and for attachment respectively. In *C. elegans* apical ECM promote elongation. Zona pellucida domain proteins NOAH-1 and NOAH-2 are important for muscle anchoring and mechanical input from muscle contractions, which are essential for elongation. (Vuong-Brender, Suman et al. 2017). ECM related integrins have roles during neural development of *drosophila* such as axonal growth and synapse formation (Broadie, Baumgartner et al. 2011).

Cell adhesions represent the interaction interfaces between cells and the extracellular matrix. Extracellular matrix proteins provide rigid mechanical anchor that supports and guides migrating cells. The ECM protein tenascin is an elastic protein and can stretch several times its length. The extensibility of tenascin is due to stretch-induced unfolding of its 15-fibronectin type III domains. Proteins like tenascin provide the necessary mechanical resilience to the ECM (Oberhauser and Marszalek et al, 1998). Extracellular matrix serves as a bridge between external and internal environment. Cells use the connection between cytoskeleton and ECM as mechanosensors to probe the external environment. For instance, actin-integrin adhesion complexes have been shown to probe the rigidity of the extracellular environment, mediates adhesion, trigger signalling and remodel the extracellular matrix (ECM). The physical forces induce transitions in the types and functions of these cell-matrix adhesions. Cells in turn probe, respond to and remodel the extracellular matrix (ECM) using the ECM/integrin - actin cytoskeleton adhesion complexes (Geiger and Yamada et al, 2001).

5. Cytoskeleton in Cell

i. Introduction

Three aspects which define life are reproduction, response to stimuli and locomotion (polarised growth in plants). All these three defining features of life require the organism to interact with the environment and organize itself in space accordingly. The organisms have to become correctly shaped, and grow in a predefined controlled manner. The cells have to rearrange the internal components, to grow, divide and respond to the environment. These mechanically robust actions are performed by filaments acting as tracks, anchors and interlinking threads and tubules present in all walks of life (from archea to eukaryotes), from nucleus to cytoplasm, known as Cytoskeleton.

The three widely known cytoskeletal filaments are actin filaments, microtubules and intermediate filaments. Each type differs in their composition, biological role, dynamics and mechanical properties. Actin filaments determine the shape of the cell's surface and are necessary for whole-cell locomotion and cell membrane pinching during cell division. Microtubules determine the positions of the membrane bound organelles, direct intracellular transport, form and orient the mitotic spindle that segregates the chromosomes. Intermediate filaments provide the mechanical strength. A network of proteins regulates the cytoskeleton. Accessory proteins, which include a variety of motor proteins such as Myosins, Kinesins and Dynein control the assembly of cytoskeletal filaments in particular locations. The motor proteins use the energy of ATP hydrolysis to move organelles or filaments itself (Howard 1997, Fehon, McClatchey et al. 2010).

ii. Actin

Actin filaments or microfilaments are right handed helical polymers of the protein G-actin. They are flexible structures of diameter 4-7nm, that have the capacity to organize into anything from a simple filament to a 3-dimensional sheet are called F-actin or Filamentous actin. The cortex of cells underlying the plasma membrane is rich in actin filaments and providing strength and shape. Actin filament polymerization generate force by pushing the growing plus end against membrane barriers such as organelles and cell membrane itself. Actin filaments, help forming cell projections such as filopodia to explore the territory around and form bundles to form sound sensing rigid rods of stereocilia on hairs cells in the inner ear. Bundles of actin also form microvilli to increase the area of absorption in intestine.

The actin molecule, which is known as G-actin or globular actin is a 375-amino acid polypeptide carrying a tightly associated ATP/ADP molecule. Actin is well conserved among different eukaryotes. Minor differences in the sequence of actin isoforms results in change in their function. For instance – in mammals there are three isoforms of actin α-actin, β-actin and γ-actin, which differ slightly in their sequences but display tissue specific expression: α-actin in muscles, while the other two in non-muscle tissues. Actin filaments have two ends: the plus end – that grows faster and the minus end – that grows slower, thereby making the actin filaments polarised. Actin dynamics are influenced by the availability of actin monomers, nucleating factors which accelerate actin polymerization and are responsible for branched filaments, filament stabilizing proteins such as capping proteins, severing proteins such as gelsolin and depolymerisation factors as cofilin. Therefore, the structural organization of different actin networks such as bundles, dendritic networks and web-like structures depends on specialized accessory proteins. These proteins also control the interactions of other proteins such as Myosin with actin filaments. For example – fimbrin binds the actin filaments closely and thus myosin binding is excluded. The fimbrin bound fibres are thus non-contractile. In contrast α-actinin cross links actin filaments into loose bundles, eventually allowing myosin recruitment, resulting in contractile actin bundles (Mullins, Heuser et al. 1998, Cooke 2004, Zigmond 2004).

Myosin motors use actin filaments/bundles as tracks to move along them, which generates contractile forces along Actomyosin fibres in both muscle and non-muscle cells. Actomyosin structures and contractility are controlled by Rho family of proteins (De La Cruz, Wells et al. 1999, Wells, Lin et al. 1999, Yildiz, Forkey et al. 2003, Cooke 2004) .

iii. Spectrin

Spectrin denotes the family of α-helical, high molecular weight, multifunctional actin binding proteins, usually found in association with the plasma membrane of mature cells. Spectrins were first identified in the mammalian erythrocytes. All spectrins share a repetitive 106 amino acid motifs, with non-homologous sequences at each terminus. The individual 106 residue spectrin repeat consists of a triple helical coiled coil. Individual spectrin repeats unfold independently under tension, in an all-or-none process. The force required to mechanically unfold these repeats is approximately 25-35 pN. Spectrins occur as diverse polymeric forms such as homo-polymers of ß-spectrin, or heteropolymers of α-spectrin and ß-spectrin in stoichiometric quantities. The heteropolymer of $(\alpha\ ß)_2$ is long, flexible protein, with two actin filament binding sites that are approximately 200nm apart.

A lot of diverse spectrins have been since discovered. Functional specialization in spectrin are result of non-homologous sequences inserted either between repeat units or within one of the helices of the repeat unit. Spectrin is concentrated just beneath the plasma membrane of red blood cells, where it forms a 2-dimensional structure hold together by short actin filaments of 12 monomeric subunits. Spectrin is associated with the cytoplasmic surface of the membrane by attachment to ankyrin. Ankyrin, which is a peripheral membrane protein, is linked to the membrane by association with the cytoplasmic domain of band 3, a major membrane-spanning integral protein. This network provides elasticity to the cell cortex and red blood cells can spring back to their original size after passing through a capillary. Thus, spectrins bestow the mechanical stability and resilience.

Spectrins have no intrinsic enzymatic activity. They have been shown to associate in vitro with itself, ankyrins, F-actin, dynamin and membrane proteins (Bennett and Gilligan 1993, Yan, Winograd et al. 1993, Beck, Buchanan et al. 1994, Rief and Gaub et al, 1998).

iv. Tubulin

Microtubules are known to form structures such as cilia and flagella, the motile and sensory whips or sensory devices on the surface of the cell. Microtubules can organize themselves as tracks for the transport of materials in the cell. Microtubules are long hollow cylinders made of protein tubulin. The outer diameter is 25 nm and these structures are rigid as compared to actin microfilaments and are more complex than actin. Microtubules are long with frequently one end attached to a microtubule-organizing centre called centrosome. Although non-centrosomal microtubule arrays have also been

shown to assemble in differentiated tissues to perform mechanical and transport-based functions. NOCA-1 is a *C. elegans* protein homologous to the vertebrate nenein, which functions redundantly with the minus end protection factor Patronin/PTRN-1 to assemble a non-centrosomal circumferential microtubule array in *C. elegans*. The roles of microtubules are diverse and comparatively more dynamic than actin. The two monomeric globular proteins which polymerise to form 13 protofilaments which fold into a tubular hollow cylindrical microtubule heteropolymers are α-tubulin and ß-tubulin. Each globular monomer comprises of 445-450 amino acids. Both α- and ß-tubulin bind to a GTP molecule, though the hydrolysis of GTP occurs only at the ß-tubulin. Two different forms of tubulin, that is GTP bound (T form) and after hydrolysis, GDP bound (D form) one, are found in the heterodimer. Under physiological conditions GTP-tubulin polymerises, while GDP-tubulin depolymerises. This leads to dynamic instability in microtubules. Microtubules emanate from microtubules organising centres (MTOC), where another isoform of tubulin: - γ-tubulin is most enriched. The ends of the microtubule bound to the MTOC are minus ends, whereas the ends free in cytoplasm are plus ends (Burns and Starling 1974, Petzelt 1979, Aldaz, Rice et al. 2005, Doxsey, McCollum et al. 2005, Hachet, Canard et al. 2007, Wang, Oegema et al, 2007).

Chemical compounds such as colchicine and nocodazole depolymerise microtubules, while Taxol stabilizes microtubules and leads to increase in polymerisation. These compounds are therefore used extensively to study the role of microtubules. Both polymerising and de-polymerising agents kill the dividing cells; as proper microtubules organisation is important for spindle formation in dividing cells. Therefore, agents such as Taxol are used as drugs to treat rapidly dividing cancerous tumours.

Several microtubules stabilizing and destabilizing proteins help control the dynamics in the cell. Proteins like stathmins don't allow tubulin monomers to polymerise. Some proteins like katanin and 'Spastin' do the task of severing the microtubule and contribute to the rapid depolymerisation observed at the poles of the spindle during mitosis. Two kinds of motor proteins bind and use microtubules as tracks or pulling cables i.e. kinesins and dyneins. Kinesins are similar in structure to Myosin II, having two heavy chains (Vale, Reese et al. 1985, Vale and Goldstein 1990). The nematode *C. elegans* has 20 kinesins. Most kinesins walk towards the plus end of the microtubules. Some isoforms of kinesins walk towards minus end, while some don't move and depolymerize microtubules (Vale, Reese et al. 1985). *The dyneins are minus end directed proteins. There is a separate section devoted to them, later*.

v. Intermediate Filaments

Intermediate filaments are rope like fibres with a diameter of about 10nm, constituted of many variants of a vast family of intermediate filament proteins. Eukaryotes such as nematodes, molluscs and vertebrates use intermediate filaments as cytoskeleton. Intermediate filaments provide extra strength to cells which experience a lot of tension. Therefore, animals such as arthropods and echinoderms, with hard exoskeleton on them, do not have intermediate filaments. They span through epithelial tissues in junctions and desmosomes, thereby strengthening the structures against mechanical stress. The members of intermediate filament family contain a conserved central α-helical domain containing approximately 40 heptad-repeat motifs that form an extended coiled-coil structure with another monomer. Intermediate filament subunits do not bind a nucleotide like actin and tubulin subunits. Assemblies of intermediate filaments can be very stable, but some filaments such as vimentin can form dynamic structures as in fibroblasts. Nuclear lamina is underlined by intermediate filaments to provide it stability (Helfand, Chang et al. 2003, Isermann and Lammerding 2013).

Keratins are the most diverse intermediate filament family in vertebrates. Multiple isoforms of keratins can be produced by epithelial cells and tissues and heteropolymers can be formed. Several diseases are caused by defective keratin genes such as a disorder called epidermolysis bullosa simplex which affects the keratin genes KRT5 and KRT14, in which skin blisters to even very slight mechanical stress (Coulombe, Hutton et al. 1991, Schweizer, Bowden et al. 2006).

Proteins such as plectins, plakins and spertraplakins link various cytoskeletal elements to allow the communication between the three major cytoskeletal elements.

vi. Cytoskeleton and ECM in *C. elegans*

All three cytoskeletal elements are found in C. elegans as compared to Drosophila, only actin and microtubules found in *Drosophila* (Cytoplasmic IF are absent in *drosophila,* but they have nuclear lamins). *C. elegans* have 5 isoforms of actin (ACT-1-5)(Fyrberg, Ryan et al. 1994). The non-muscle myosin II subunits include the heavy chains NMY-1 and NMY-2 (the latter is mostly required in early embryos), the regulatory light chain MLC-4 and the essential light chain MLC-5 (Fyrberg, Ryan et al. 1994, Shelton, Carter et al. 1999, Piekny, Johnson et al. 2003, Gally, Wissler et al. 2009).The phosphorylation of MLC-4^{S18} and MLC-4^{T19} control the activity of myosin II in epidermal cells of *C. elegans* (Gally, Wissler et al. 2009). In the epidermis, actin filaments display mostly circumferentially

oriented anisotropic organization. Starting at the 1.5-fold stage in dorsal and ventral epidermal cells, they form parallel bundles of 5-10 individual filaments which are anchored to *C. elegans* adherens junctions (CeAJs) and associated with non-muscle myosin below the furrows of the embryonic sheath. In lateral seam cells, actin filaments are associated with high levels of non-muscle myosin II foci, but do not tightly anchor to junctions as in dorsal/ventral cells (Costa, Raich et al. 1998, Gally, Wissler et al. 2009). Within the dorsal and ventral epidermal cells, the specific molecular composition, the organization, and the polarity of filaments within bundles has not been established. In particular, it is not known whether actin polymerizes as long filaments running from one dorsal-seam CeAJ to the other, whether they run from one CeAJ to a hemidesmosome, or whether they make several short-intermingled filaments of similar or opposite polarity. The occurrence of apparent actin bundle discontinuities at the level of hemidesmosomes in some backgrounds could indicate that hemidesmosomes represent an intermediate anchoring structure between CeAJs. Actomyosin in seam cells represents the important driving force until the embryos reach the two-fold stage (Bonfanti, Colombo et al. 1992, Cheney and Mooseker 1992, Satterwhite and Pollard 1992, Shelton, Carter et al. 1999, Piekny, Johnson et al. 2003, Gally, Wissler et al. 2009).

Microtubules are circumferentially oriented in dorso-ventral (DV) cells in epidermis. Before elongation, microtubules are found in complex cytoplasmic networks in interphase cells, or associated with the spindle apparatus in mitotic cells. The microtubules in the dorsal and ventral cells undergo a remarkable transition in pattern at the start of elongation in *C. elegans* embryo and become circumferentially oriented. The intensity of the microtubules is strongest during the early phases of elongation and fades as the elongation proceeds. Microtubules of other orientations also appear in DV cells later in elongation phase. The microtubules in the lateral epidermis or seam cells remain like a network both during embryogenesis and elongation. Microtubules in DV cells appear to be attached to membranes whereas the ones in seam cells are distributed throughout their cytoplasm (Figure 6).

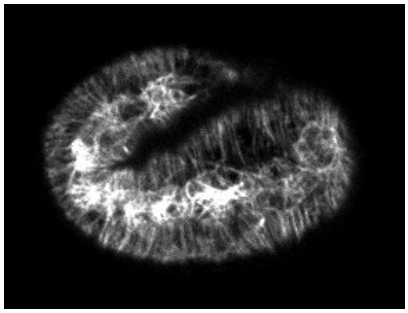

Figure 6. Microtubules are circumferentially oriented in DV cells, whereas they remain like a network in seam cells at the 2-fold stage of *C. elegans* embryo.

Microtubules function during embryogenesis and elongation has been tested by the use of drugs colcemid and griseofulvin. These drugs prevent mitosis. Use of microtubule inhibitors did not block elongation immediately, when embryos were exposed to them before, during or after elongation. These embryos developed abnormalities such as depressions and constrictions and could not elongate fully. The microfilament pattern was not affected, in microtubules inhibited embryos except at the bulges (Priess and Hirsh 1986).

One of the major pitfall of using drugs in an organism is that the resulting defect (halt in elongation in embryos of *C. elegans*) might arise from defects in multiple tissues. To avoid the effect on multiple tissues, microtubules could be specifically disrupted in the epidermis of *C. elegans* embryos using two approaches, either by expressing the microtubule-severing protein Spastin or by inhibiting the function of NOCA-1, which is required for the assembly of non-centrosomal microtubules in the epidermis. Expressing spastin before the lima-bean stage suppresses elongation, however expression of spastin midway through elongation does not affect the elongation. Epidermal microtubules are dispensable, once the elongation has started. The spastin is expressed under the epidermal promotor *dpy-7*. Spastin expression, coupled to that an mCherry via an operon linker to not affect the spastin function. Expressing under *dpy-7* slowly builds up, as there is no expression before the start of elongation, a little expression at the start and a complete full expression at 1.6-fold embryos. The microtubule depletion follows a similar pattern as the expression of mCherry. Degraded microtubules appear dotty rather than linear. The continuum mechanics model suggests that microtubules might be important for elongation but not necessary for it. Therefore, in the absence of microtubules, elongation is further more dependent on the balance of actomyosin forces between dorso-ventral and seam cells, by lowering the myosin II activity, by introducing a temperature sensitive mutant of LET-502/ROCK i.e. *let-502(sb118ts)* in the spastin background. Almost 93% embryos develop normally at the semi-permissive temperature of 23 °C for *let-502(sb118ts),* though for *let-502(sb118ts)* in the spastin background, the percentage of embryos arrested at 2-fold increases significantly (Quintin, Wang et al. 2016).

In *C. elegans*, the α-spectrin/SPC-1 and its binding partner ß-spectrin/SMA-1 form an actin-binding hetero-tetramer, which colocalizes with actin (Praitis, Ciccone et al. 2005). Loss of function of ß-spectrin/SMA-1 partly bypasses the requirement for VAB-19, an ankyrin repeat containing protein and a component of hemidesmosomes in *C. elegans* (Ding, Goncharov et al. 2003). The hemidesmosomes contain multiple proteins that can facilitate the attachment between cytoskeleton and itself, thereby holding the cytoskeleton. A detailed section on hemidesmosomes is provided later.

The *C. elegans ifb-1* locus encodes two cytoplasmic intermediate filament (cIFs) isoforms, IFB-1A and IFB-1B, that differ in their head domains. Both IFB-1 isoforms are expressed in epidermal cells, within which they are localized to muscle-epidermal attachment structures. Reduction in IFB-1A function by mutation or RNA interference (RNAi) causes epidermal fragility, abnormal epidermal morphogenesis, and muscle detachment, consistent with IFB-1A providing mechanical strength to epidermal attachment structures. Reduction in IFB-1B function causes morphogenetic defects and defective outgrowth of the excretory cell. Reduction in function of both IFB-1 isoforms results in embryonic arrest due to muscle detachment and failure in epidermal cell elongation at the 2-fold stage (Ding, Woo et al. 2004, Woo, Goncharov et al. 2004)

The embryonic sheath in *C. elegans* is an extracellular layer, secreted over the surface of the embryo before the elongation starts to provide the mechanical support for tissue assembly and organ shape. The embryonic sheath is attached to the epidermis directly above the actin cytoskeleton. The embryonic sheath maintains the shape of embryo after elongation. In absence of actin microfilaments (by adding cytohalasin D), embryos change shape. Nevertheless, after the elongation is over microfilaments lose their arrangement and it is the extracellular matrix (ECM), which holds the shape (Priess and Hirsh 1986).

The zona pellucida domain containing proteins NOAH-1 and NOAH-2 act in parallel with leucine rich repeat proteins LET-4, FBN-1 and SYM-1 to ensure embryonic integrity and elongation. Embryos lacking sheath proteins rupture sometime after elongation arrest. Twitching became less pronounced and embryos rolled less when *noah-1* was depleted in *fbn-1(ns283)* background, suggesting that muscle function was indeed affected. It has been suggested that embryonic sheath might anchor muscles through hemidesmosomes and thereby transmit muscle tension to whole body. Indeed, muscles are displaced in the *fbn-1 (ns283); noah-1(RNAi)* (Vuong-Brender, Suman et al. 2017).

Laser nano-ablation experiments to cut sheath layers, comparing the recoil dynamics and opening shape of the cut gives the information about the stiffness and mechanical stress. These experiments proved that the embryonic sheath can relay the mechanical stress provided by the actomyosin and the muscles (Vuong-Brender, Suman et al. 2017).

6. Dynein/dynactin complex

i. Introduction

The cytoplasmic dynein/dynactin complex is one of the two major motor protein complexes in the cell, the other one being kinesin. In the scope of this thesis, we shall discuss a bit more about the dynein, its interaction with dynactin and their assembly and functions. Dynein is a polarized minus end motor as it moves towards the minus end of the microtubules, while using microtubules as tracks or pulling cables. Dynein motors power ciliary beating, transport intracellular cargos and help construct the mitotic spindle (Kikkawa 2013).

Dynein was first described in 1965, when Gibbons JR isolated 14S and 30S (polymeric) fractions of protein having an adenosine triphosphatase activity, purified from cilia of *Tetrahymena pyriformis*. The term dynein is constituted of dyne, force; in, protein. The ATPase activity can be activated by Ca^{+2} or Mg^{+2} and inhibited by EDTA (Gibbons and Rowe 1965). Dynein complex was purified and its enzymatic properties were described such as its specificity for certain divalent ions such as Ca^{+2}, Mg^{+2}, Mn^{+2} and ATP among several nucleoside triphosphates (Gibbons 1966). First axonemal dynein was isolated, purified and characterised from sperm of sea urchin *Colobocentrotus*. The bound dynein and the soluble dynein did not have the same enzymatic properties and it was predicted that it was because of the interactions of dynein with microtubules and other axonemal proteins (Gibbons and Fronk 1972). Minoru Otokawa gave the first biochemical evidence that microtubule binding increases the ATPase activity of dynein (Otokawa 1972). This was the first observation in support of models involving interaction between tubules and dynein in ciliary movement. ATPase activity of bound and extracted dynein was further characterised in various tissues such as cilia of *Tetrahymena,* sperm of sea urchin, neurotubules and brain, suggesting that dynein is a ubiquitous protein (Blum 1973, Summers and Gibbons 1973, Burns and Pollard 1974, Gaskin, Kramer et al. 1974). Dynein was also found to be important for sperm motility and fertility, sinusitis and mitosis (Afzelius, Eliasson et al. 1975, Afzelius 1976, Afzelius 1976, Petzelt 1979).

All motor proteins use a common principle to generate movement in which they bind to the track, undergo a force-producing conformational change, release for the track and return to their original conformation. These conformational changes are result of chemical alterations in the motor's adenosine triphosphatase (ATPase) cycle [adenosine triphosphate (ATP) binding, hydrolysis and product release] (Astumian 2017). Kinesins and myosins have a common evolutionary origin and share a protein fold. Dyneins are unrelated to them and instead belong to AAA ATPases (ATPases associated with diverse cellular activities) family.

Some of the AAA ATPases participate in protein unfolding, disassembly of stable protein complexes and helicase activities. The AAA ATPases self-assemble into hexameric rings to function as the active site (Ogawa, Okuno et al. 1975, Tucker and Sallai 2007, Carter, Cho et al. 2011).

ii. Structural-functional overview of dynein

Dyneins can be classified into three types on the basis of their spatial functioning: **axonemal dyneins** – which power the ciliary and flagellar beating, **intraflagellar transport (IFT) dyneins**, which transport proteins in the axoneme and **cytoplasmic dyneins** which perform the cargo transport of membranes, mRNA, nuclei and viruses along eukaryotic cells. The N-terminal third of dynein heavy chain differs among the various types of dyneins and lead to their specification. The N terminus serves as the mechanical linker for the C-terminal motor domain head, which is conserved across dyneins. The linker is followed by four AAA domains (AAA1 to 4) that contain functional nucleotide binding sites and two structural AAA domains with no activity. ATP hydrolysis is essential at AAA1 for motor domain movement. Unlike myosin and kinesin, binding site of the polymer (microtubule in this case) is not close to the binding site of the nucleotide. Cryo-EM and X-ray crystallography showed that dynein binds to the microtubules through a small globular domain at the end of a 15 nm-long antiparallel coiled-coil stalk. The six dynein AAA small domains (AAAs), which form the C-terminal face of the ring are connected by well-ordered loops in five helices. All the AAA domains take distinct conformations and produce asymmetry of the ring (Vale and Goldstein 1990, Samso and Koonce 2004, Roberts, Numata et al. 2009, Carter, Cho et al. 2011).

For dynein to function as a motor protein, nucleotide transitions at AAA1 (the main ATP hydrolytic site) are conveyed to the linker and distant microtubule binding site MTBD. ATP binding closes the large gap between AAA1 and AAA2, which is required for ATP hydrolysis. How does dynein dimer interact with microtubules? To move along the tracks, both myosin and kinesin bind with both their motor domains to their tracks. To enable simultaneous binding of both MTBDs, the two dynein motor domains must rearrange substantially (Kon, Mogami et al. 2005, Roberts, Nagle et al. 2009, Carter, Cho et al. 2011).

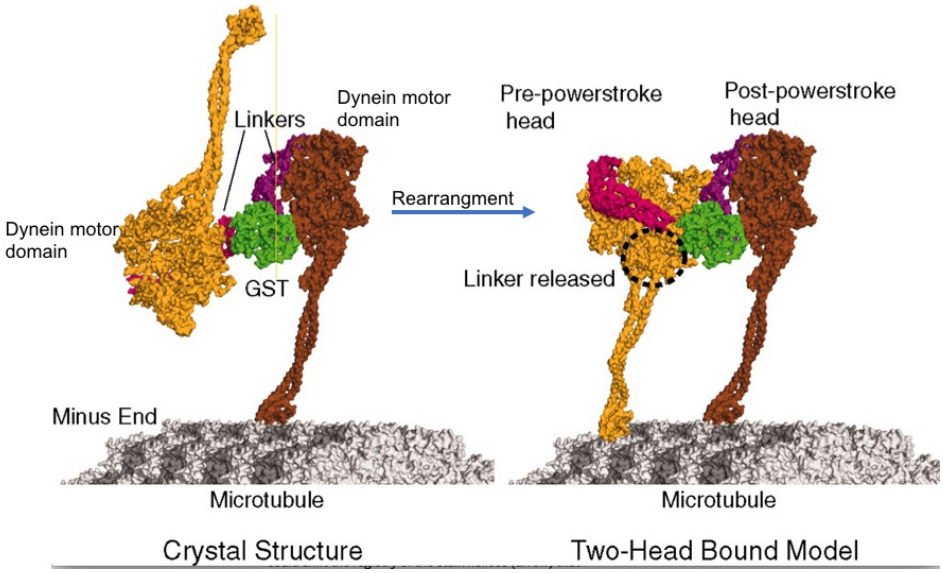

Figure 7. Two dynein motor domain are linked to microtubules with the help of a stalk or microtubule binding domain (MTBD). The simultaneous binding of both MTBDs is required for dynein to effectively slide along microtubules which requires a rearrangement (Carter, Cho et al. 2011).

iii. Necessity of dynactin

As seen before cytoplasmic dynein is an oligomeric complex of two catalytic heavy chains and a number of accessory subunits. Vesicle motility assays to observe dynein's motility in vitro revealed dynein's ability to serve as a minus–end directed transporter of membranous organelles depends on a lot of adaptor proteins. The dynein motor activity is controlled by dynactin and the Lis1-NuDEL complex. The latter acts as a clutch and binds it strongly to microtubules to suppress the motility. Single molecule motility TIRF experiments on mammalian dynein purified from rat brains showed poor motility. It was because of the absence of activator cofactors such as BicD2 and dynactin. BicD2 is a conserved, dimeric adapter protein, its N terminus facilitates a stable dynein-dynactin-BicD2 (DDB) ternary complex. The DDB complex is highly flexible, because of the variable orientations adopted by dynactin's ARP-1 filament and the variable separation of the two motor domains. DDB complexes move robustly and processively along MTs as compared to only dynein as studied by using the GFP-tag on BicD2. DDB complexes also show diffusive motion and accumulated on minus ends of MTs. Addition of BicD2 alone does not increase the processivity of dynein, thereby indicating the presence of both dynactin and BicD2 is essential. When measured at physiological temperature (37°C), the velocity is 892 nm/s, very close to speeds of retrograde transport in vivo. Processive motility is completely abolished by the ATPase inhibitor vanadate. To further confirm that motile DDB complexes contain single BicD2 and not oligomers or aggregates,

two fluorescently labeled BicD2 preparations (TMR- and 505-Star–labelled) were added to pig brain lysates followed by DDB complex purification. Two-color kymographs revealed that moving DDB complexes contain either TMR- or 505-Star-BicD2 but not a mixture, confirming that each DDB complex contains only a single BicD2 molecule. The binding of BicD2 increases the processivity of dynein/dynactin complex (Gill, Schroer et al. 1991, Holzbaur, Hammarback et al. 1991, Reck-Peterson, Yildiz et al. 2006, McKenney, Huynh et al. 2014).

iv. Structure of dynactin

The cytoplasmic dynein without attachment to a cargo, adopts an inactive conformation that cannot undergo processive motion. Activation of motility requires the simultaneous binding of dynein to an adaptor protein and dynactin, a universal activator involved in the transport of many dynein cargos (Gill, Schroer et al. 1991, Holzbaur, Hammarback et al. 1991, Urnavicius, Zhang et al. 2015). The term dynactin means activator of dynein. It was discovered as a 20S polypeptide complex which stimulates dynein-mediated vesicle transport. Dynactin has 23-subunits. Its components involve a drosophila homologue of Glued, which is a 1053 amino acid polypeptide composed of two coiled coil α-helical domains interrupted by a spacer. Actin is highly conserved protein involved in vesicle transport, cell locomotion and cytokinesis in association with

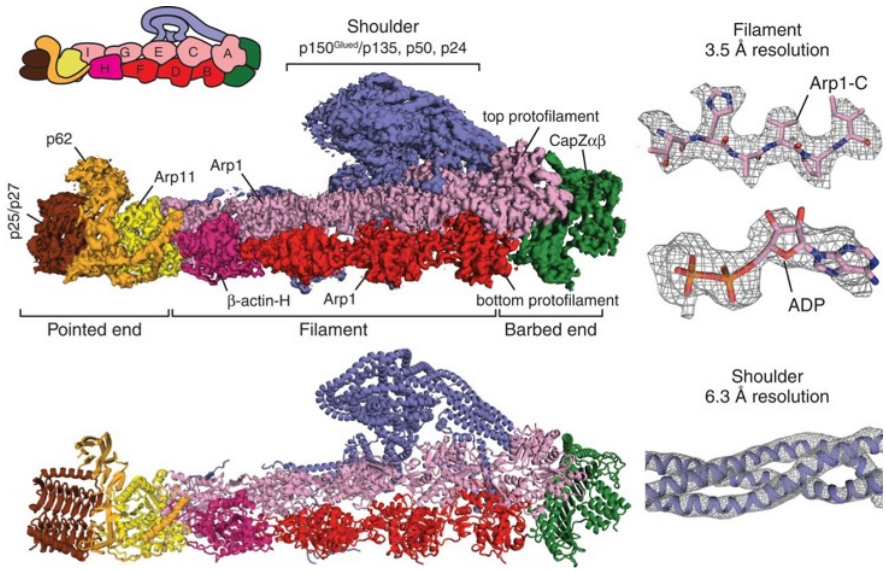

Figure 8. Structure of mammalian (pig) dynactin. The dynactin complex is built around two protofilaments *of arp-1* each containing 4 & 5 subunits of *arp-1* (Urnavicius, Zhang et al. 2015).

myosin motor protein. Several organisms have closely related actin isoforms. Yeast have been shown to contain actin related proteins essential for viability. Actin RPV (actin related protein in vertebrates), which is now known as ARP-1 was recognised as an activator of dynactin as shown by minus end directed vesicle motility assays. It co-sediments at 20S when purified dynactin is sedimented into sucrose gradient and co-precipitates with antibodies of 150k dynactin subunit Glued. Sequencing of the actin isoforms from human brain revealed a new actin related protein with 374 amino acids (376 in *C. elegans*) which shared 54% amino acid identity and 69% similarity to actin. Similar to actin, *arp-1* filament has a barbed end and a pointed end. X-ray crystallography confirmed the presence of actin domain structure, but unlike conventional actins, which work in association with myosin motors, Arp-1 is involved with microtubule

associated motor. Actin binding proteins which bind to actin to regulate its polymerisation can also bind and regulate Arp-1 polymerisation. Electron microscopy showed dynactin as short laterally oriented 37 nm long filament with globular heads. Locations of constituent polypeptides were identified by applying antibodies to decorate dynactin complex before electron microscopy. ARP-1 is predominant polypeptide in dynactin. Densitometry analysis of 2-D gels showed the stoichiometry of Arp-1 as 9 moles per mole of dynactin and conventional actin to be 0.5-1 mole per mole of dynactin. Stoichiometry of p150, p62, p50, p37, p32, p27 and p24 were shown to be 2:1:5:1:1:1:1. Recent cryo-electron microscopy improved all these almost perfect findings and state that dynactin is built around a filament containing eight (instead of 9) copies of the actin related protein Arp-1, one of ß-actin and ARP-11 and one dimer of capping proteins. The two protofilaments of ARP-1 are wrapped around each other. The ratio of Arp-1 to ß-actin is 8:1 as confirmed again by mass spectrometry. At the barbed end of the dynactin, a *capZαß* heterodimer binds across both protofilaments. The C-terminal helices of capping protein dimer fits between the first two Arp-*1* subunits. The tight bundling of capping proteins stabilizes dynactin structure. At the pointed end, the bottom protofilament ends with ß-actin, whereas the top ends in ARP-1, creating a binding site for Arp-11. Arp-11 binds other subunits such as p25, p27 and p62 to form the pointed end. Another subunit $p150^{glued}$ forms dynactin shoulder projection. Its C-terminal sticks the two arms made by p50-p24 interaction together (Gill, Schroer et al. 1991, Clark and Meyer 1992, Hug, Miller et al. 1992, Lees-Miller, Helfman et al. 1992, Frankel, Heintzelman et al. 1994, Fyrberg, Ryan et al. 1994, Schafer, Gill et al. 1994, Schroer, Fyrberg et al. 1994, Cheong, Feng et al. 2014, Urnavicius, Zhang et al. 2015).

v. Structural-functional overview of the DDB complex

Dynein, dynactin and BicD2 form a stable complex only when all three components are present. The dynein tail binds directly to the Arp-1 filament stretching from ß-actin to the barbed end. This interaction is stabilized by a 270-residue coiled coil of BICD2N that runs the length of the filament. The N terminus of BICD2N lies close to the barbed end and its C terminus emerges from the pointed end. The C-terminus of the BICD2 and the pointed end complex of dynactin, which are implicated in cargo binding and thus diametrically opposed to the dynein motor domain. The dynein tail consists of two copies of the dynein heavy chain (DHC), intermediate chain (DIC2), light intermediate chain (DLIC1) and light chains (Urnavicius, Zhang et al. 2015).

The motor domains of dynein self-dimerise and are locked in a conformation with weak affinity for microtubules. Disrupting the motor dimer by structure-based mutagenesis drives dynein into an open form with increased affinity for microtubules and dynactin. Surprisingly, the open form of dynein is also inhibited. Combination of 2D analysis of EM images and a 3D cryo-EM structure of the whole dynein/dynactin machinery explains how dynactin overcomes this inhibition and directly reorients the motor domains to make dynein processive.

Isolated dynein exists in two forms – phi dynein and open dynein and both are autoinhibited without dynactin. A transition between them is important part of the regulation. The motor domains are held together by interactions between their linker, AAA4, AAA5, stalk domains and a contact between heavy chains in the tail. The motor domains are locked with low affinity for microtubules. Phi-dynein is also inhibited from binding dynactin because motor self-dimerization prevents it from undergoing the large conformational change required. Dynactin and BICD2N can activate dynein by driving the dynein motors into a parallel form. Dynactin binding intrinsically pre-aligns dynein into a microtubule ready confirmation**.** Dynactin also constrains the range of movement of the individual motor domains. The comparison of dynein-dynactin-BICD2 complex with phi-particle shows that dynactin binding induces a rigid body twist of the heavy chains. The change in motor orientation is thus driven by conformational changes in the dynein tail (Mabuchi, Shimizu et al. 1976, Witman, Plummer et al. 1978, Nakamura and Masuyama 1979, Hoogenraad, Wulf et al. 2003, Zhang, Foster et al. 2017).

A cartoon structure (Figure 9) illustrates a simplistic way to observe dynein/dynactin/BicD2 complex. Examples of some studies of motor dependent roles are provided in the section specific for study of dynein/dynactin in *C. elegans*.

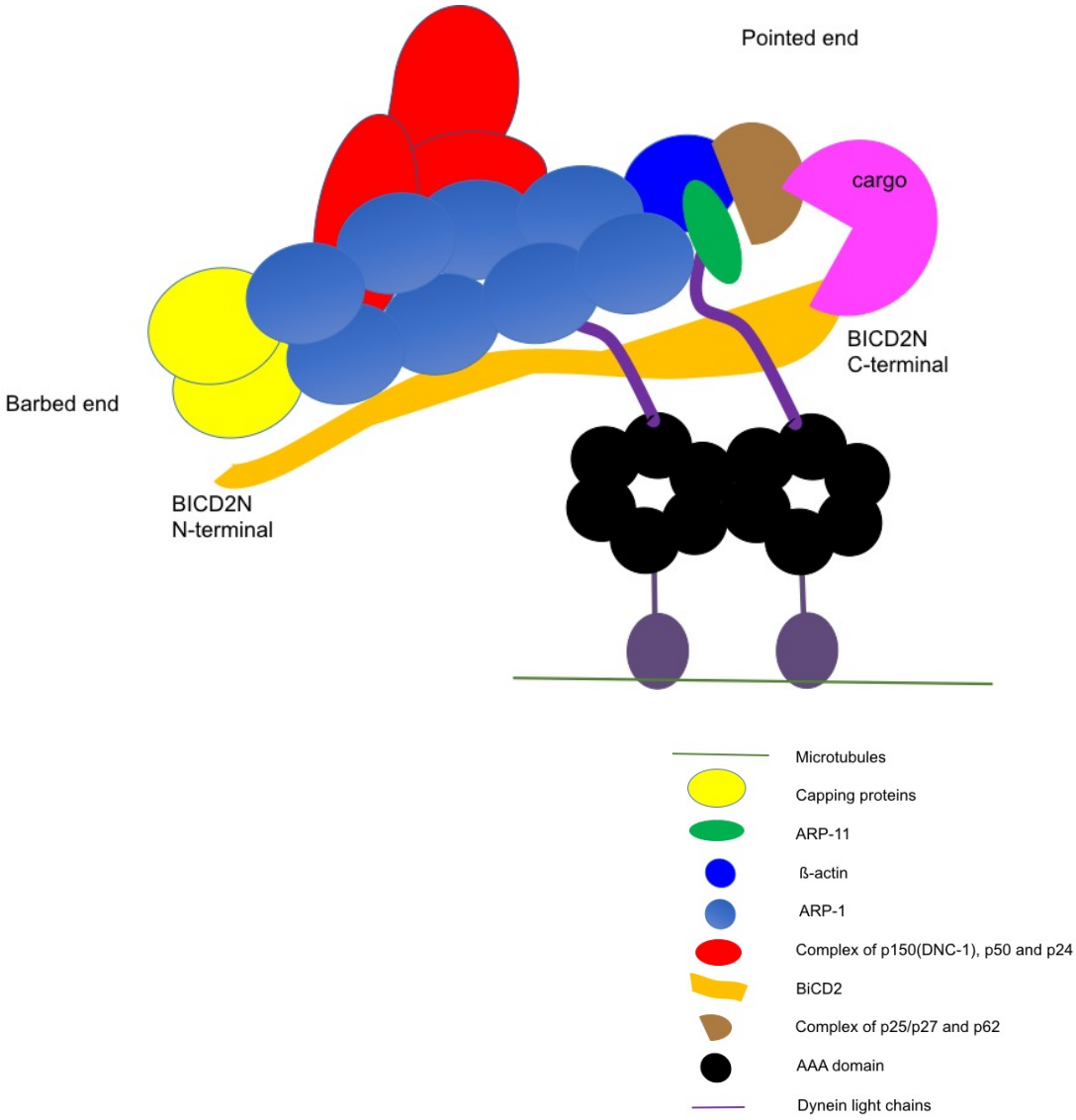

Figure 9. Cartoon structure of Dynein/dynactin-bicaudal D2 complex (Carter, Cho et al. 2011 ; McKenney, Huynh et al. 2014; Urnavicius, Zhang et al. 2015; Zhang, Foster et al. 2017).

vi. Motor independent roles of dynein/dynactin components

Dynein dynactin has been described to participate in a multitude of functions in a cell. Most of them, such as transport of mRNA, proteins and vesicles include their attachment with microtubules, using them as tracks and the motor function of dynein helps it slide along the tracks. Dynein motor does not change position while functioning for organelle positioning or spindle positioning, as it is attached to the cortex, but the motor role and their attachment to microtubules are still important. The dynein motor pulls microtubules, acting as cables either to orient or to position a certain organelle/structure. 'BUT' are there functions which are dynein motor independent? Here we explore couple of such cases.

In *C. elegans*, the PUF proteins FBF-1 and FBF-2 support germline progenitor maintenance by repressing production of meiotic proteins and use distinct mechanisms to repress their target mRNAs. Dynein light chain DLC-1 is an important regulator of FBF-2 function. DLC-1 directly binds to FBF-2 outside of the RNA-binding domain and promotes FBF-2 localization and function. By contrast, DLC-1 does not interact with FBF-1 and does not contribute to FBF-1 activity. the contribution of DLC-1 to FBF-2 activity is independent of the dynein motor. The contribution of motor activity was checked by performing *dhc-1(RNAi).* A *dlc-1(RNAi)* in *fbf-1* loss-of-function background gave sterility, whereas depleting *dhc-1* by using temperature sensitive allele *or195* under same conditions did not (Wang, Olson et al. 2016).

Genotype and temperature	Sterile (%)*	*n*
dlc-1(tm3153) 20°C	2±2	156
fbf-1(ok91); dlc-1(tm3153) 20°C	78±12	231
fbf-2(q738); dlc-1(tm3153) 20°C	1±2	180
dhc-1(or195); fbf-1(ok91) 15°C	4±1‡	181
dhc-1(or195) 15°C	5±1‡	158
dhc-1(or195); fbf-1(ok91) 20°C	3±2	245
dhc-1(or195) 20°C	2±0.4	185
dhc-1(or195); fbf-1(ok91) 24°C	10±1	210
dhc-1(or195) 24°C	8±2	153

*Sterile animals were identified by the absence of embryos in the uterus >24 h past the L4 larval stage, unless otherwise noted. Mean±s.d. shown. *n*, number of animals scored.
‡Animals grown at 15°C were analyzed 2 days post L4.

Table 1: Synthetic sterility of *fbf-1; dlc-1* mutants

A recent study focussed on Clathrin-mediated endocytosis (CME), which is an essential process among all eukaryotes. CME has roles in the maintenance of membrane composition, signalling, protein trafficking, polarity, virus uptake, and nutrient and drug internalization. The regulation of this endocytosis is not fully understood. *In yeast*, Tda2, an uncharacterised protein which localises at endocytic sites was suggested to be a component of actin module of endocytosis, as reflected by its colocalisation with well-established CME intermediate coat protein Sla1-RFP. The extent of the endocytic defect in *tda2Δ* cells is comparable to the one for other endocytic machinery mutants including Las17–MP8-12, a mutant displaying misregulation of actin polymerization during CME. Localization, timing, dynamics, and independence from the clathrin coat suggest that Tda2 is part of the late-stage endocytic machinery, likely the actin cytoskeleton. Tda2 fold is highly homologous to the dynein light chain of the *Drosophila melanogaster* TcTex1 type. Tda2 also shared structural homology with the *Saccharomyces cerevisiae* LC8-type dynein light chain, thereby implying Tda2 is a dynein light chain (Farrell, McDonald et al. 2017).

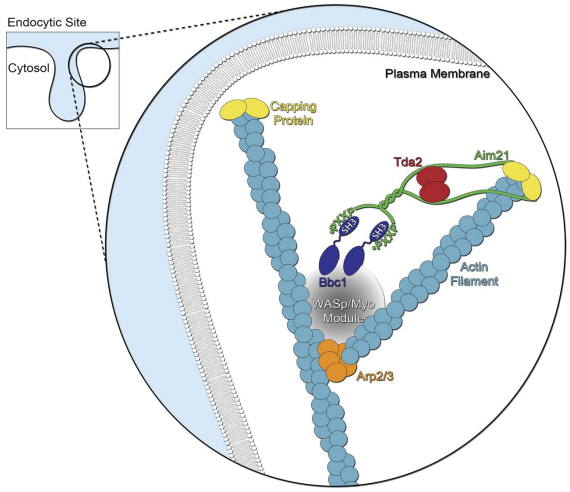

Figure 10. Tda-2 (a dynein light chain homologue) forms a complex with SH3 domain containing Aim-21, which is recruited to endocytic sites, where it interacts with actin-capping proteins and mediates its recruitment to barbed end of actin filament (Farrell, McDonald et al. 2017).

Microtubule-depolymerizing agent nocodazole was used to verify if Tda2 functions with or without dynein motor complex. Like previously known endocytic proteins, Sla1, Myo5, and Rvs167; Tda2 recruitment and lifetime was unaffected by microtubule depolymerisation. Live imaging analysis did not show any colocalization between Tda2-mCherry and Dyn2-GFP, the yeast LC8 dynein light chain component of the dynein motor complex. Immunoblotting analysis showed that Tda2 was present in total cell extracts but did not copurify with the dynein heavy chain, when TAP-tagged strain of the dynein heavy chain (*DYN1-TAP*) was used to purify the dynein motor complex under conditions that preserve

motor integrity and activity. The data indicate that Tda2 does not localize, function, associate, or interact genetically with the dynein motor complex and microtubules complex (Farrell, McDonald et al. 2017).

Tda2 forms a stable complex with Aim21 (protein of unknown function), as shown by size exclusion chromatography. GST-Aim21 specifically pull down His-Tda2, indicating a direct interaction between Tda2 and Aim21. Live-cell imaging showed Tda2-GFP and the well-established marker of filamentous actin Abp1-RFP had very similar dynamics at endocytic sites. Furthermore, actin-depolymerizing agent latrunculin A inhibited the recruitment of Tda2-GFP to endocytic patches. The Tda2–Aim21 complex binds actin-capping protein and regulates its recruitment to endocytic sites. A reconstituted Tda2–Aim21 complex, but not each protein separately, strongly and directly binds to actin-capping protein (Farrell, McDonald et al. 2017).

It has to be noticed that a new regulatory mechanism of the actin cytoskeleton during CME by a member of a protein family that has not been previously associated with function in endocytosis or actin polymerization has been discovered by these authors.

vii. Study of dynein/dynactin in *C. elegans*

Dynein/dynactin complex in *C. elegans* has not been explored extensively during embryonic elongation. Most of the studies of this complex in *C. elegans* have either been performed on adult animals or early embryos. I have tried to list a few studies out of several in this section of introduction, that illustrates the diversity of functions involving dynein/dynactin in *C. elegans.*

The study of interflagellar transport (IFT) in chemosensory cilia of adult *C. elegans*, using both single molecule and ensemble studies revealed the dynamics of dynein. IFT-dynein is the only motor available for retrograde transport in cilia as opposed to kinesin and OSM-3 for anterograde transport. Single-motor trajectories reveal unexpected, distinct features of IFT-dynein motility: diffusive behaviour at the ciliary base, pauses, turns, directed motion and switches between these behaviours. Stochastic simulations allow linking this single-molecule behaviour to the ensemble IFT-dynein distribution along the cilium, revealing that this distribution crucially depends upon the probability of single-motor directional switches (Mijalkovic, Prevo et al. 2017).

Studies such as the mechanisms governing spindle positioning were performed in the *C. elegans* one-cell stage embryo.

Every action in a cell is preceded by a biochemical activation, which in turn kicks in another reaction leading to a final action/response or change in the cell. An efficient network of signal transduction is thus essential for an efficient functioning of a living cell. Many types of coupling G-proteins define and tune the response by having varying specificity for different receptors (molecules that can pick up a stimuli). For example – if a receptor interacts with only one subtype of G protein, only one effector will be activated and thus the response would be very concentrated. G proteins consists of GTP hydrolysing α-subunit and a functional monomer of remaining two subunits ßγ. G proteins are inactive in heterotrimeric form, in which Gα is bound to GDP and ßγ subunit. Once activated Gα exchanges GDP with GTP and releases Gßγ. Both Gα and Gßγ subunits can activate downstream effector. Gα hydrolyses GTP to GDP, which promotes binding and subsequent inactivation of Gα and Gßγ subunits (Neer 1995). One of the very crucial action, regulated by G proteins is the spindle assembly and orientation.
Asymmetric cell divisions are a result of polarized distribution of cytoplasmic components and the proper alignment of the mitotic spindle. Both actin and microtubules have roles in proper spindle orientation (Hyman and White 1987, Hyman 1989, Hill and Strome 1990). Spindle position is set up on the axis of two centrosomes. Centrosome positions are abnormal in *gbp-1* mutants (Gß) just before nuclear envelope breakdown (NEBD). Centrosomes migrate onto abnormal axes and rotation of the nucleo-centrosomal complex in P1 cells is absent or late (Zwaal, Ahringer et al. 1996). Out of the two Gγ subunits in *C. elegans* i.e. *gpc-1* and *gpc-2*, only *gpc-2* (Gγ) *RNAi* showed embryonic lethality and spindle defects identical to Gß mutants, whereas embryos with *gpc-1 RNAi* were viable (Jansen, Thijssen et al. 1999, Gotta and Ahringer 2001). Simultaneous depletion of redundant Gα subunits *goa-1* and *gpa-16* led to 100% embryonic lethality with defects in proper segregation of centrosomes before NEBD, incorrect spindle orientations and incorrect paths of centrosome migration. Simultaneous *goa-1* and *gpa-16* RNAi (Gα RNAi) means a loss of Gα signalling and constitutive activation of Gßγ as Gα inhibits Gßγ. Indeed, Gß RNAi rescues centrosome defects in Gα RNAi embryo, which suggests that the over activity of Gßγ is responsible for failure to separate chromosomes. Tubulin is disorganised in Gα RNAi embryos and microtubule disrupting drugs produce the same kind of spindle defects as that of Gα RNAi, suggesting that tubulin might be the effector for Gα (Gotta and Ahringer 2001). G-protein regulators GPR-1 and GPR-2 associate with LIN-5 to form a complex and depend on LIN-5 for localization to the spindle and cell cortex. GPR-1/2 bind to Gα genes *goa-1* and *gpa-16.* Depletion of *lin-5, gpr-1* and *gpr-2* result in similar spindle positioning defects as that of Gα depletion. GPR domain of GPR-1/2 act as GDP dissociation inhibitor for Gα subunit GOA-1. The location of polarity proteins (PAR) is not affected in *lin-5* or *gpr-1/2* depleted embryos. LIN-5 and GPR-1/2 possibly act downstream of PAR proteins (Gotta, Dong et al. 2003, Srinivasan, Fisk et al. 2003). The protein LIN-5 is a homologue of mammalian NuMA (Nuclear mitotic

apparatus), which binds to dynein. The involvement of the dynein was confirmed when *dyrb-1* (dynein light chain roadblock type-1) came out as a candidate in an enhancer RNAi screen in *lin-5 (ev571ts)* and *gpr-1 (or574ts)* backgrounds. *dyrb-1* genetically interacts with *gpr-1* and *lin-5*. Co-disruption of dyrb-1 and gpr-1 results in a complete loss of viability and the embryos show spindle misalignment. LIN-5 and GPR-1/2 symmetrically activate cortically anchored dynein which pulls mitotic spindle towards posterior pole of the embryo. Spindle severing experiments following temporally restricted gene inactivation using *tbb-2(qt1ts)* and *dhc-1(or195ts)* microtubule stabilising drug exposure such as Taxol established that both microtubule dynamics and dynein generate pulling forces (Colombo, Grill et al. 2003, Couwenbergs, Labbe et al. 2007, Nguyen-Ngoc, Afshar et al. 2007). Antibodies against GOA-1/GPA-16 co-immunoprecipitates LIN-5 and antibodies against LIS-1 (a part of dynein complex) co-immunoprecipitates DHC-1, LIN-5, GPR-1/2. The dynein complex interacts with LIN-5 and GPR-1/2 and is recruited to cortex via myristoylated Gα protein which allow membrane attachment. Dynein attempts to move towards minus end of microtubules, but since it is anchored, microtubule experience a pulling force, which leads to depolymerisation of microtubule at plus ends. In meiotic cells LIN-5 forms a separate complex with calponin homology protein ASPM-1 and calmodulin CMD-1 at spindle poles, and contributes to the meiotic spindle positioning in conjunction with dynein motor (Nguyen-Ngoc, Afshar et al. 2007, van der Voet, Berends et al. 2009).

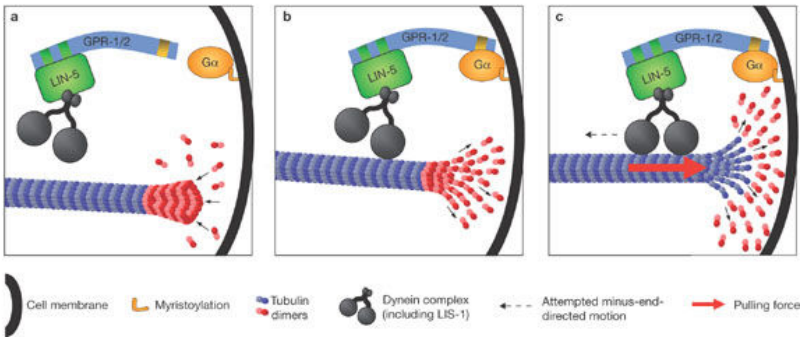

Figure 11. The dynein complex interacts in the cytoplasm with LIN-5, which binds to the N-terminus of GPR-1/2, which harbours TPR repeats (green boxes). (**b**) GPR-1/2 binds to the Gα proteins GOA-1 and GPA-16. Since the Gα proteins are myristoylated, the entire dynein–LIN-5–GPR-1/2 complex is recruited to the cell cortex, where dynein can bind to an astral microtubule growing toward the cortex. (**c**) Cortically anchored dynein generates a pulling force on the astral microtubule. The astral microtubule undergoes depolymerization, which is necessary for pulling to be productive (Nguyen-Ngoc, Afshar et al. 2007).

Both nuclear and cortical dynein cooperate to ensure timely centrosome separation, where the cortical dynein acts as a coupling device that transmits forces produced by polarized cortical actomyosin flows. Depletion of cortical dynein by *goa-1/gpa-16(RNAi)* slows down centrosome separation, while the

depletion of nuclear dynein by *zyg-12(ct350)* leads to excess separation of centrosomes along the cortex. Centrosome movement was totally impaired in *goa-1/gpa-16(RNAi) zyg-12(ct350)* embryos (Gonczy, Pichler et al. 1999, De Simone, Nedelec et al. 2016). Recently two populations of dynein – cortical LIN-5 bound and microtubule plus end bound were revealed to be responsible to ensure robust cortical pulling force generation by using CRISPR cas-9 tagged N-terminal DHC-1 (Schmidt, Fielmich et al. 2017).

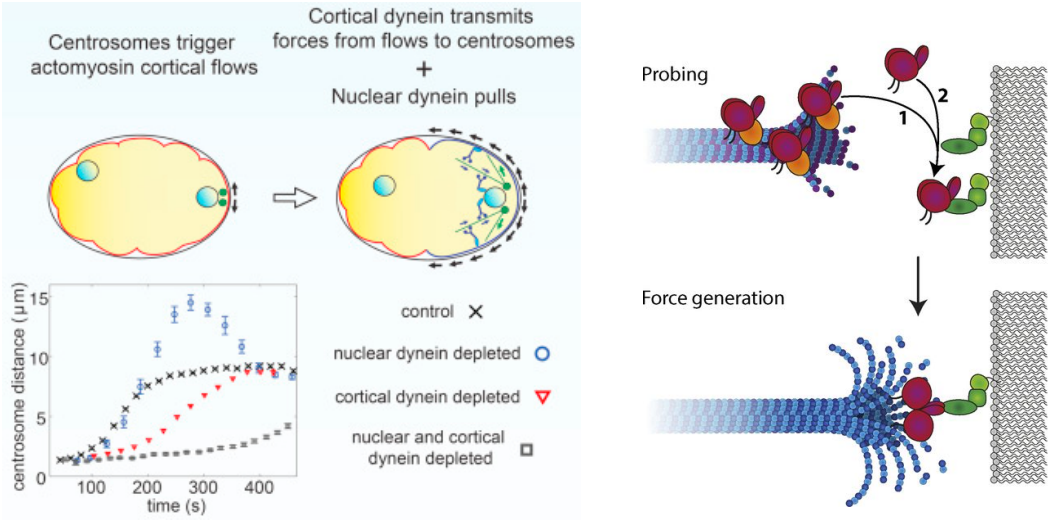

Figure 12. Centrosome separation in *C. elegans*. The centrosome is hold with the help of both cortical and nuclear dynein. Both cortical and nuclear dynein pull the centrosome (De Simone, Nedelec et al. 2016)

The two populations of DHC-1 – cortically bound and the microtubule bound as shown by Schmidt, Fielmich et al. 2017.

viii. Some tools to study dynein/dynactin complex

The null mutants of most of the dynein/dynactin components are early embryonic lethal. Therefore, it is quite a task to study the complex in late elongation stages. Temperature sensitive genes made it possible for us to study the effects of dynein/dynactin components in late elongation stages. *cap-1 (RNAi)* and RNAi of other genes such as *dlc-1* and *farl-11* also served us as a valuable tool in this study.

Gene	**Allele**	**Homozygote embryonic viability (15°C)**	**Homozygote embryonic viability (26°C)**	**Nucleotide change**	**Amino acid change**
dnc-1	*or404*	98.6%	0.0%	C1237T	R to C
sur-6	*or550*	72.8%	16%	T140C	W to R
egl-50	*n1086*	99%	65%	G145A	G to A
dhc-1	*or195*	95%	0%	-	G to D

Table 2 : Temperature sensitive (*ts*) alleles of/related to dynein/dynactin components used in this study (O'Rourke, Dorfman et al. 2007, O'Rourke, Carter et al. 2011).

7. C. elegans

i. Introduction

Classification
Kingdom – Animalia
Phylum – Nematoda
Class – Chromadorea
Order – Rhabditida
Family – Rhabditidae
Genus – Caenorhabditis
Species – *C. elegans*

The nematode *C. elegans* which was discovered by Dr. Sydney Brenner, is today an important model organism to study basic functions and interactions of eukaryotic cells, host-parasitic interactions and evolution. In the lab of Dr. Michel Labouesse and a lot of other laboratories around the world, this organism is used to study development and mechanotranduction.

ii. Why is this nematode so popular?

C. elegans is a free-living nematode. These organisms can be easily grown in NGM (nematode growth media) plates. It is used as a model organism in developmental biology, genetics and molecular biology because of its large brood size, rapid development, transparent body (ease to do microscopy), completely sequenced genome (ease of performing genetic manipulations) and an available wide array of mutants. Further the organism growth can be controlled, either by incubating it at 12 or 15°C which slows the development or accelerating the growth at 25°C. The L1 larvae of the organism can be frozen, just like bacteria at -80°C and stocked for future use. Newly hatched larvae are 0.25 mm long and adults are 1 mm long.

C. elegans display sexual dimorphism and X0 sex determination: self-fertilizing hermaphrodites which are XX and males which are X0. Males are rare and only 0.1-0.2 % of the progeny, which is a result of a rare meiotic non-disjunction of the X chromosome. The percentage of males can be increased by starving the plates or temperature shock.

iii. Life cycle and body plan

The life cycle of *C. elegans* is comprised of the embryonic stage, four larval stages (L1-L4) and adulthood. Each larval stage is separated by a molting event, where the larvae forms a new cuticle (apolysis) and sheds the old cuticle (ecdysis). *C. elegans* embryogenesis takes 16 hours at 20°C. It is divided into a. proliferative phase (350 minutes), which covers formation of embryonic founder cells and gastrulation and b. organogenesis/morphogenesis (490 minutes). The L1 larva hatches with 558 number of cells. *C. elegans* has an unsegmented, cylindrical body shape with an outer tube and an inner tube separated from each other by the pseudocoelomic space. The outer tube (body wall) consists of cuticle, hypodermis, excretory system, neurons and muscles, and the inner tube, the pharynx, intestine and, in the adult, gonad (Wormbook and Wormatlas).

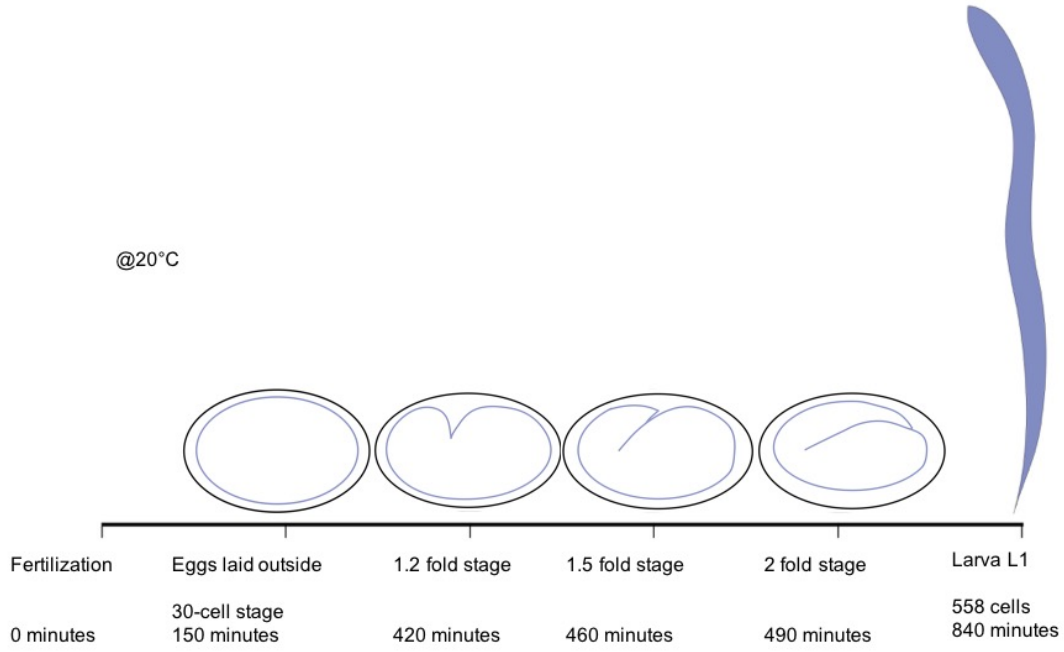

Figure 13. Time line of embryo growth. The embryo stages important for this study are shown here.

iv. Embryonic elongation – early and late

After the embryogenesis terminal differentiation of cells occurs without additional cell divisions, the embryo elongates threefold and takes form as an animal with fully differentiated tissues and organs. Morphogenesis starts with the "lima bean" stage. Epidermal cells are born at the end of gastrulation as a group of cells on the posterior and dorsal surface of the embryo. They form six rows of cells: two dorsal, two lateral, and two ventral rows (Sulston, Schierenberg et al. 1983, Heid, Raich et al. 2001). The first muscle twitches are observed at 475 min after fertilisation. The elongation can thus be divided into two phases

Early elongation – before muscles become active

Late elongation – after muscles become active

Actomyosin contraction drives the early phase of elongation and is regulated by the Rho kinase (*LET-502*) and the serine/threonine p21 activated kinase PAK-1. An evolutionary conserved, actin microfilament associated Rho-GAP(RGA-2) behaves as a negative regulator of LET-502/ROCK. The small GTPase RHO-1 is the preferred target of RGA-2 in vitro, and acts between RGA-2 and LET-502 in vivo. Time-lapse microscopy shows that loss of RGA-2 induces localised circumferentially oriented pulling on junctional complexes in dorsal and ventral epidermal cells. Specific expression of RGA-2 in dorsal/ventral, but not lateral, cells rescues the embryonic lethality of *rga-2* mutants. Hypercontractility mutants like *mel-11* or *rga-2* cause embryos to burst during elongation due to increased tension exerted on adherens junctions. Mutations in non-muscle myosin *nmy-1* suppress the rupturing phenotype of *rga-2(RNAi)* embryos, suggesting that rupturing requires actomyosin contraction. (Diogon, Wissler et al. 2007).

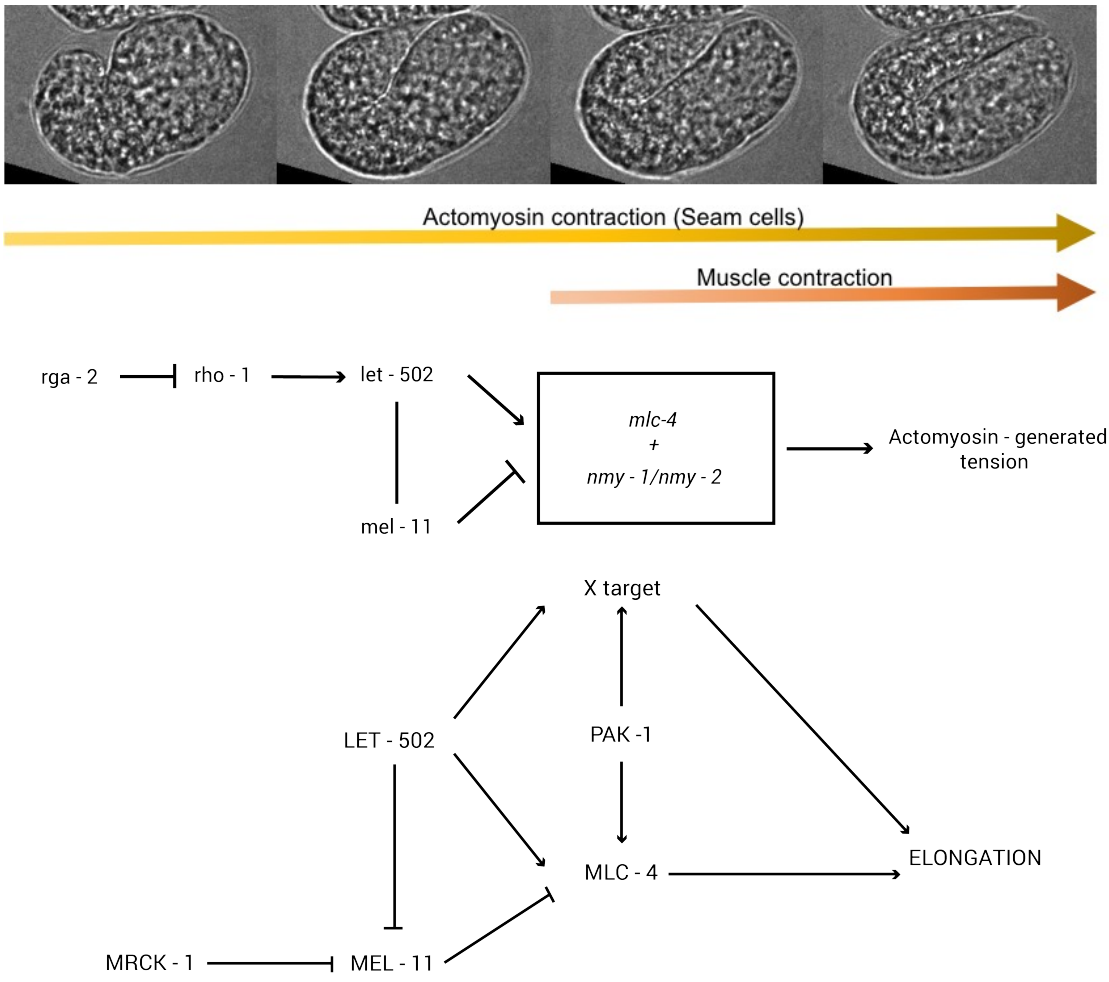

Figure 14. This figure shows the necessity of two kind of forces – actomyosin contraction and muscle contraction for *C. elegans* embryonic elongation. Myosin light chain (*mlc-4*) is regulated by Rho kinase LET-502 and phosphatase MEL-11 via phosphorylation and dephosphorylation, thereby regulating the actomyosin contraction. Both PAK-1 and LET-502 contribute to the phosphorylation of MLC-4 (Gally, Wissler et al. 2009).

The assembly of myosin II filaments, but not actin microfilaments, depends on the myosin regulatory light chain (MLC-4) and newly identified essential light chain MLC-5. Rescue experiments on *mlc-4* mutants with various constructs found out that MLC-4 is essential in seam cells. Phosphorylation of two evolutionary conserved MLC-4 serine and threonine residues is important for myosin II activity and organization. An RNAi screen for potential myosin regulatory light chain kinases found that the ROCK, PAK and MRCK homologs act redundantly. The combined loss of ROCK and PAK, or ROCK and MRCK, completely prevented embryonic elongation, but a constitutively active form of MLC-4 could only rescue a lack of MRCK. This suggests that ROCK and MRCK regulate MLC-4 and the myosin phosphatase. ROCK and PAK regulate at least one other target essential for elongation, in addition to MLC-4 (Gally, Wissler et al. 2009)

Late Elongation

The *C. elegans* epidermis is a single layered epithelium separated from musculature by a thin basement membrane on its basal surface. Four rows of muscles are attached to the ventral and dorsal epidermis by structures known as hemidesmosomes, making the epidermis, susceptible to the mechanical stress originating from contraction and relaxation of the underlying muscles. Thereby *C. elegans* embryonic elongation is a model in vivo system to study mechanical stress dependent changes in cell shape and junctional remodeling or regulation/activation of gene expression. *C. elegans* hemidesmosomes (CeHDs) signal to the epidermis through a mechanical input. Muscle contractions laterally stretch and squeeze the epidermis, a process comparable to the stretching of cultured cells grown on elastic membranes. Disruption of the CeHD core component, VAB-10A (a plectin and BPAG1e homologue), also strongly compromised this process, outlining the crucial role of CeHDs in transmitting muscle tension.

Tension provided by muscle contraction (external force for epidermis) recruits GIT-1 to hemidesmosomes (HD), which in turn facilitates further elongation by activating proteins such as *pak-1.* The pathway involves the scaffolding protein GIT-1 and its partner PIX-1, Rac GTPase, three signalling proteins found at the hemidesmosome (HD), and PAK-1. The phosphorylation of intermediate filaments is one of the outcomes of this pathway. Muscle defective mutants with no effective tension on epidermis arrest midway through elongation at the two-fold stage known as paralyzed at two-fold stage or Pat phenotype. Though *git-1, pix-1* and *pak-1* mutants are viable, suggesting that another pathway/s act/s in parallel to GIT-1/PAK-1 (Zhang, Landmann et al. 2011).

v. Hemidesmosomes and its components

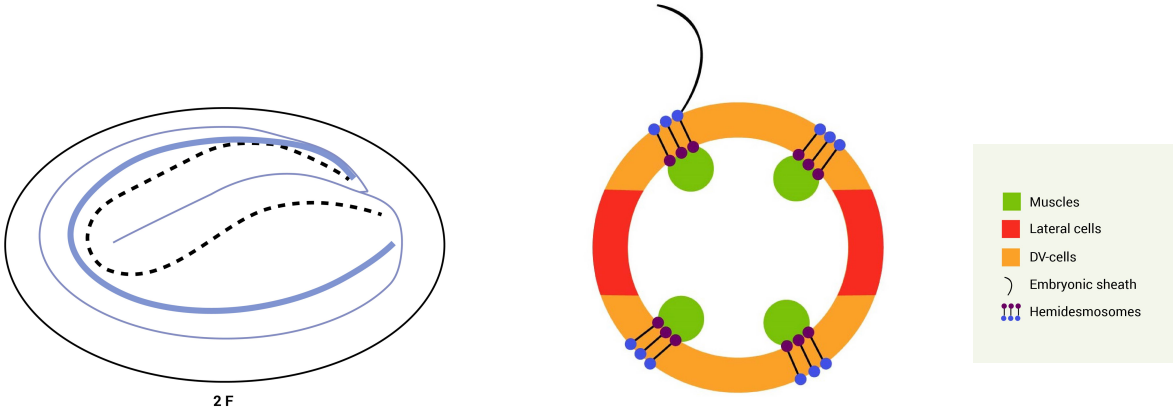

Figure 15. The four rows of CeHDs as seen in a 2-fold stage *C. elegans* embryo.
Cross section of a *C. elegans* embryo. The four rows of muscles connect to the epidermis via CeHD.

C. elegans hemidesmosomes (CeHDs) are structures that connect the underlying muscles to the epidermis. Its components correspond to IFB-1/IFA-3 and IFB-1/IFA-2 intermediate filaments and VAB-10A, a plakin homologous to BPAG1e, connects the intermediate filaments to the either sides. VAB-10 also has actin and microtubule binding sites, thereby supposedly connecting the hemidesmosomes to the cytoskeletal network. The transmembrane proteins to attach the VAB-10 on apical sides are muscle positioning and muscle attachment proteins MUP-4/MUA-3, whereas on the basal side, the attachment is provided by the myotactin LET-805. Other *C. elegans* hemidesmosome proteins are 'Ankyrin' repeat proteins such as VAB-19 and GIT-1. There are four hemidesmosomes in *C. elegans* along the four muscles – two dorsal and two ventral, which run along the four set of muscles in *C. elegans.*

The study following this introduction would be easier to understand if we know a bit more about the certain components of hemidesmosomes.

As mentioned previously, intermediate filaments impart mechanical stability to CeHDs. Intermediate filaments are anchored to hemidesmosomes through proteins belonging to Spectraplakin family. Spectraplakins are large multidomain proteins that connect actin, IFs, and microtubules. the nematode *Caenorhabditis elegans* encodes a single spectraplakin locus named *vab-10*. The *vab-10* locus, which has been identified by positional cloning, contains 32 exons, and undergoes multiple alternative splicing events. It produces two broad categories of alternative isoforms sharing a common 5′ region encoded by exons 1–15, with two distinct 3′ regions: VAB-10A and VAB-10B. Different domains and repeats are annotated in the figure16ii. Coimmunostaining of VAB-10A and IF perfectly colocalize, whereas VAB-10A and VAB-10B intercalate. *mc44* is a 1-kb deletion at the end of the 24th exon specific null allele for VAB-10B, whereas *ju281* is

point mutation in the last exon of VAB-10A and serves a null (Gally, Zhang et al. 2016). VAB-10(ΔSH3) is a new allele which lacks the SH3 domain in Spectrin repeat 3, created by CRISPR Cas-9 genome editing (Suman et al, unpublished data).

VAB-19 is a member of conserved family of Ankyrin repeat containing proteins that includes the human tumor suppressor Kank. *vab-19* mutants show muscle detachment and display aberrant actin organization. The loss in function of ß-spectrin SMA-1 partly rescues the VAB-19 mutations (Ding, Goncharov et al. 2003)

MUP-4 is an essential for embryonic epithelial morphogenesis and maintenance of muscle position. *mup-4* locus encodes a transmembrane protein, required for attachments between the apical epithelial surface and the cuticular matrix, and IF tethering. The extracellular domain includes epidermal growth factor-like repeats and two enterokinase modules and its intracellular domain is homologous to IF-associated protein filaggrin. MUP-4 colocalizes with epithelial CeHDs overlying body wall muscles, beginning at the time of embryonic cuticle maturation, as well as other sites of mechanical coupling (Hong, Elbl et al. 2001).

LET-805 encodes myotactin, which is a single transmembrane protein at the basal side of CeHDs. It connects the CeHDs to muscles and helps relay the contractile information of muscles to epidermis. The extracellular domain contains at least 32 fibronectin type III repeat. Muscular detachment is observed in myotactin mutants, once muscles become active. (Hresko, Schriefer et al. 1999).

GIT-1 is a scaffolding and GTPase associated protein (GAP), which recruits other proteins such as PAK-1 and Rac. It contains ankyrin repeats like VAB-19. It is maintained at the level of hemidesmosomes once muscles become active (Zhang, Landmann et al. 2011).

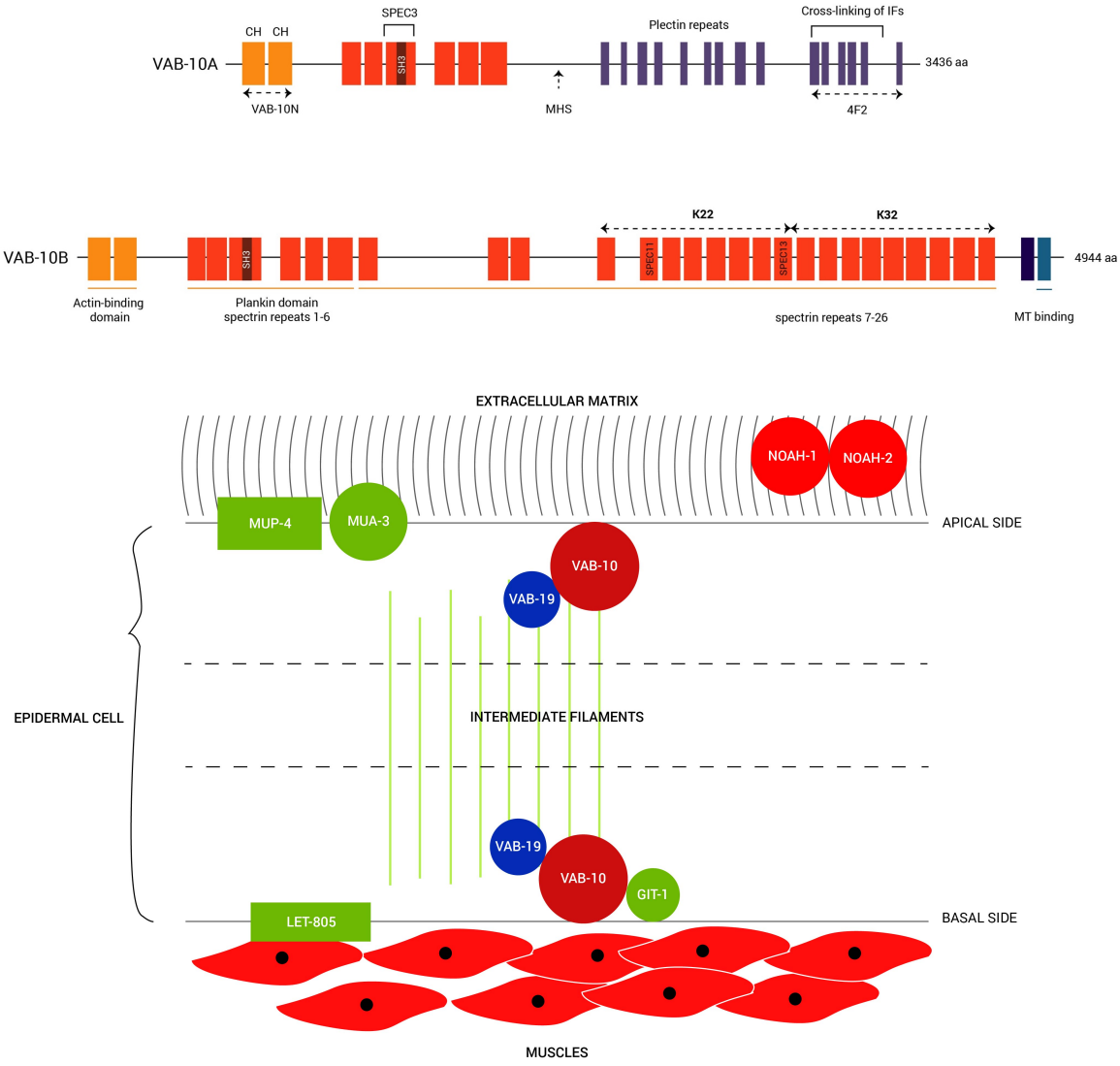

Figure 16. The top figure depicts the domain structure of VAB-10. The SH3 domain is hidden in the Spectrin repeat 3. The actin binding and the plakin domain are common in between VAB-10a and VAB-10b.

Bottom figure shows a cartoon structure of CeHD. CeHDs are structures connecting muscles to epidermis. Proteins like MUA-3 and MUP-4 are at the apical side of the CeHD. VAB-10 and VAB-19 are present at both apical and basal sides, whereas intermediate filaments hold the structure. LET-805 is present at the basal side.

Materials & Methods

II. Methods and Materials/Experimental Procedures

1. Nematode Strains

Wild-type (N2), *git-1(tm1962), pak-1(ok448)* and *vab-10(ΔSH3)* strains of *C. elegans* were maintained at 20°C. Worms were grown on NGM media (Brenner 1974). Strains carrying temperature sensitive alleles (ts) such as *egl-50(n1086), dnc-1(or404)* and *sur-6(or550)* were maintained at 15°C. For conditional inactivation of ts alleles, early L4 worms from all strains were selected and shifted to 25.5°C, 24 hours before the experiment, unless stated otherwise. Experiments were performed on the progeny of these worms. The strains used and prepared for this study are listed in Table 7 along with their genotypes.

2. Time Lapse – Growth Curves

Strains were kept at 20°C, 24 hours before the experiment for time lapse Differential Interference Contrast (DIC) microscopy. Time lapse at 20°C were performed using DM6000 Leica acquisition system using a step size of 0.3µm and time interval of 5-10 minutes for 10 hours. Time lapse done at 25.5°C were always performed at Zeiss Spinning Disk Microscope. Gravid adults were dissected; embryos were washed with M9 to remove the bacteria and mounted on 5% agarose pad for time-lapse microscopy. The lengths of the elongating embryos were measured using Image J and were normalized with respect to initial lengths of individual embryos. Growth curves were then plotted as a measure of time.

3. RNA Interference experiments and RNAi Screen

RNAi induced by bacterial feeding using specific clones from Ahringer library. L3/L4 larvae were placed on feeding plates 24 hours before the experiment. Progeny of these worms were used for experiments. RNAi by injection was used for genes, which cannot be efficiently knocked down by feeding. Specific dsRNA was prepared using the Ambion mMessage mMachine® kit and it was then purified by Qiagen RNeasy® MinElute® Cleanup kit. The ds RNA was injected in L4 worms. An illustration of the RNAi assay is provided in Figure 3.

For RNAi screen, wild type gravid adults were bleached and leaving the embryos overnight in M9 medium synchronized the embryos. In the absence of food, all embryos hatch and stay at L1 larval stage. These synchronized L1 can now be transferred directly to RNAi plates or to 20°C on NGM plates for them to

grow to L4 larval stage. L4 animals are then transferred to RNAi plates. Animals were left there for 5 days at 20°C temperature and then the embryos were checked under DM6000 microscope for defects. To prepare the RNAi plates, the bacteria from the RNAi library were inoculated at 37°C overnight and induced with 1mM IPTG for three hours. The bacterial strain used is HT115(DE3), an RNase III-deficient strain of E. coli in which expression of T7 RNA polymerase is induced by addition of isopropyl-β-d-thiogalactopyranoside (IPTG) bacteria, and is therefore ideal for RNAi by feeding experiments.

4. Rescue constructs and experiments

arp-1 was amplified in three fragments from genomic DNA using Thermo Scientific Phusion high-fidelity DNA polymerase. Three fragments had exon 1 & 2; exon 3 & 4, and exon 5 & 3'UTR of *arp-1* respectively. We introduced the first fragment consisting of exon 1 and 2 into pJET blunt end cloning vector by using Thermo Scientific Clonejet PCR cloning kit. The other two fragments were inserted by using megawhop cloning. Tissue specific constructs were generated by introducing epidermal specific 432 bp long or 1.1 kb *dpy-7* promoter (Gilleard, Barry et al. 1997)or muscle specific 2.4 kb *myo-3* promoter (Merris, Kraeft et al. 2004). The promoters were inserted into the *arp-1* construct by using NEBuilder® HiFi DNA Assembly Gibson Cloning kit. The mix was incubated at 50°C for 15 minutes to 1 hour depending on the size of the insert. We confirmed the sequence and the frame of the sequence by GATC sequencing it. The constructs were microinjected into gravid *N2 (wild type)* adults with injection markers pRF4 (roller) and pCFJ90 (red pharynx). The progeny with transgene was selected with the help of selection marker (red pharynx). The animals with red pharynx were then crossed to the double mutant *egl-50; git-1* to obtain the mutants with rescue constructs. The single and the double mutants with the rescue construct were chosen with the help of the selection marker. To check whether our constructs rescue the mutants, we chose red pharynx L4 animals from N2, single mutants *git-1* & *egl-50* and the double mutant *egl-50; git-1* and transferred them to the restrictive temperature 25.5°C. The animals were dissected and the embryos were washed, counted and transferred back to 25.5°C incubation. The embryos were recounted after 12 hours. The percentage of surviving embryos was calculated by taking ratio of post 12 hours and initial number of embryos.

An outline of the rescue construct plasmids is provided in Figure 2.

5. CRISPR/Cas9 fluorescent knock-in transgenic worm generation

We followed established protocols for genome editing by use of CRISPR/Cas9. For the method described in (Dickinson, Ward et al. 2013), we amplified a 2 kb segment on the Carboxy terminus of the target gene from genomic DNA and cloned into pJET vector to prepare the homology repair template. We inserted GFP sequence in a way that 1500 bp are before GFP and 500 bp are after GFP. These 1500 bp and 500 bp segments function as homology arms. We used www.crispr.mit.edu to select a PAM site. PAM site in the template was modified to avoid Cas9 enzyme from acting on it. Single guide RNA sequence was cloned in pDD162 plasmid by megawhop cloning. All constructs were purified using Invitrogen Purelink™ Quick Plasmid miniprep kit. The injection mixture consisted of 50-100ng/µl of the template, 50-70ng/µl of pDD162, the injection markers 100ng/µl of pRF4 and 2.5ng/µl of pCFJ90. Young adults were then injected with this mixture and kept at 20°C. The F1 progeny was selected with the help of injection markers. F1 generation progeny expressing roller marker or red pharynx were separated and genotyping was performed to look for positive insertions. GATC sequencing was performed to confirm the CRISPR event. The CRISPR generated strain was further tested for fluorescence by Fluorescence dissecting microscope. The method is illustrated in Figure 4.

To follow the method based on Self-excising drug selection cassette (Dickinson, Pani et al. 2015), we amplified 700 bp arms flanking the site of insertion from genomic DNA by using Thermo Scientific Phusion High-Fidelity DNA polymerase. The plasmids pJJR82 and pJJR83 were predigested by AvrII and SpeI for Carboxy terminal insertion and by ClaI and SpeI for Amino terminal insertion. The left and right arm were assembled with the digested plasmid by using NEBuilder® HiFi DNA Assembly Gibson Cloning kit. The resulting plasmid was then injected into young adult worms. The F1 progeny was screened for rollers with no red pharynx. Roller homozygotes were separated by screening F2 generation. The homozygous rollers were given a temperature shock to excise the cassette. The insertion of the fluorescent tag was confirmed by GATC sequencing. The method is illustrated in Figure 5.

6. Genetic Interaction/Lethality count

Genetic interaction between genes was elucidated by crossing the strains carrying the variations. Males were created either by temperature shocking L4 animals at 32°C for two hours or by crossing with *N2* males. These males from one strain were crossed to L4 hermaphrodite of the other strain. The screening of the homozygotes was done in F2 generation either by PCR or by visible phenotypes. A library of mutants was created, enlisted in Table 7. The mutant and the N2 were incubated at 25.5°C for 24 hours. Adults were dissected, embryos were washed, counted and incubated at 25.5°C. Embryos were recounted after 12 hours. The percentage of surviving embryos was calculated by taking ratio of post 12 hours and initial number of embryos.

RNAi knock down was performed if the mutations of certain genes were early embryonic lethal. The RNAi was performed as described previously. The counting was done in the same manner.

7. Spinning Disk Microscopy: -

Gravid adult worms were dissected, washed with M9 and mounted on a 2 % agarose pad. Embryos were then staged with the help of growth curves and imaged. Different wavelengths of laser were used for illuminating different fluorescent tags. The microscopy settings used intensity measurement for each marker is tabulated in Tables 1-2. The temperature incubation was maintained at 25.5°C during the course of microscopy. The program Metamorph was used to set the parameters for imaging.

To perform the actin texture analysis, the embryos were put on the slide with excess bacteria, without washing the embryos. The bacteria on the slide deplete the oxygen, which slows the rotation movement of the embryos (sleeping embryos). This made it easier to image the actin texture in embryos.

Table 1.

Marker	CAP-1::GFP	DHC-1::eGFP	FARL-11::GFP	mCherry::NOAH-1
Laser	CSU 491	CSU 491	CSU 491	CSU 561
Laser power	25%	25%	50 %	60 %
Gain	3(4X)	3(4X)	3(4X)	3(4X)
Digitizer	10 MHz	10 MHz	10 MHz	10 MHz
EM gain	300	300	300	300
Exposure time	100 ms	100 ms	100 ms	100 ms
Step Size	0.3 µm	0.3 µm	0.5 µm	0.5 µm
Temperature	25.5°C	25.5°C	25.5°C	25.5°C

Table 2.

Marker	LET-805::GFP	MUP-4::GFP	PAR-3::GFP	VAB-10a::mCherry
Laser	CSU 491	CSU 491	CSU 491	CSU 561
Laser power	10%	20%	20 %	30%
Gain	3(4X)	3(4X)	3(4X)	3(4X)
Digitizer	10 MHz	10 MHz	10 MHz	10 MHz
EM gain	300	300	300	300
Exposure time	100 ms	100 ms	100 ms	100 ms
Step Size	0.5 µm	0.3 µm	0.3 µm	0.5 µm
Temperature	25.5°C	25.5°C	25.5°C	25.5°C

Fluorescence Recovery After Photobleaching (FRAP)

Gravid adult worms were dissected, washed with M9 and mounted on a 2 % agarose pad. Embryos were then staged with the help of growth curves. We performed FRAP on staged 1.5-fold embryos. To perform FRAP on HDs,

we chose LET-805::GFP as a marker for HD. The settings are as described in Table 4a and 4b. To calibrate the microscope, a calibration slide was prepared. 'Lyreco penstyle highlighter Liquid Ink Assorted Neon green' marker was used to prepare a square mark on the slide and a cover slip was placed on it and sealed with nail paint. The calibration settings are as mentioned in Table 3. The microscope was set on FRAP mode before starting the experiment. The temperature of the microscope was maintained at 25.5°C. FRAP was performed using Metamorph software.

Table 3.

LET-805::GFP – Calibration FRAP		
a.	Laser type	CSU FR 491
b.	Acquisition laser power (ilas)	15 %
c.	Calibration laser power (FRAP)	15 %
d.	Gain	1X
e.	Digitizer	1.25 MHz
f.	EM gain	-
g.	Exposure time	10 ms
h.	Step Size	0.5 µm
i.	Temperature	25.5°C
j.	Objective	63X

Table 4a.

LET-805::GFP – FRAP settings		
a.	Laser type	CSU FR 491
b.	Acquisition laser power (ilas)	15 %
c.	Calibration laser power (FRAP)	15 %
d.	Gain	3(4X)
e.	Digitizer	10 MHz
f.	EM gain	300
g.	Exposure time	100 ms
h.	Step Size	0.5 µm
i.	Temperature	25.5°C
j.	Objective	63X

Table 4b.

Parameters for FRAP on LET-805::GFP			
	Area to bleach – 25 *25 au diameter circle		
	Repetition	45	
	Depth	1	
		Time (sec)	**Interval (sec)**
	Pre-bleach acquisition –	6.00	3.00
	Bleach	0.27	
	Post Bleach 1	12.00	3.00
	Post Bleach 2	300	10

For FRAP on Junctions, we chose the Crispr-Cas9 construct marker of e-cadherin e-CAD::GFP (Dickinson and Goldstein 2016). The settings and parameters are summarized in Table 6a/b. Calibration slide was prepared described as described above. The calibration settings are mentioned in Table 5.

Table 5.

E-CAD::GFP – Calibration FRAP		
a.	Laser type	CSU FR 491
b.	Acquisition laser power (ilas)	10 %
c.	Calibration laser power (FRAP)	15 %
d.	Gain	1X
e.	Digitizer	1.25 MHz
f.	EM gain	-
g.	Exposure time	10 ms
h.	Step Size	0.5 µm
i.	Temperature	25.5°C
j.	Objective	100X

Table 6a.

Junction - E-CAD::GFP – FRAP settings		
a.	Laser type	CSU FR 491
b.	Acquisition laser power (ilas)	15 %
c.	Calibration laser power (FRAP)	15 %
d.	Gain	3(4X)
e.	Digitizer	10 MHz
f.	EM gain	300
g.	Exposure time	100 ms
h.	Step Size	0.5 µm
i.	Temperature	25.5°C
j.	Objective	100X

Table 6b.

Parameters for FRAP on E-CAD::GFP			
	Area to bleach – 15 *15 au diameter circle		
	Repetition	45	
	Depth	1	
		Time (sec)	**Interval (sec)**
	Pre-bleach acquisition –	6.00	3.00
	Bleach	0.135	
	Post Bleach 1	12.00	3.00
	Post Bleach 2	180	10

Immunostaining

The slides were coated with Sigma Poly-L-lysine (0.1 % w/v solution in water) and kept at 65°C overnight. The embryos were staged using synchronized hermaphrodites and mounted on the slides. Excess M9 was removed and embryos were allowed to settle down and attach to the poly-L-lysine. A cover slip was placed carefully on it and the slide was transferred to -80°C. It could be stored at this point. After 15 minutes, slide was transferred from -80°C to liquid Nitrogen. The cover slip is removed instantly to allow the eggshell to undergo freeze fracture. The slide is immediately dipped in methanol kept at -20°C. This step is followed by a quick wash by PBS and block (PBS 1X, Tween 0.1%, BSA 0.5 %, milk 0.5 %) solution is then put on the wells containing the embryos on the slide for an hour.
The block solution is then removed and the wells containing embryos are incubated overnight in the primary antibody diluted in block solution at 4 °C. The primary antibody was diluted 200-400 times. The wells are rinsed 3-5 times with block solution to get rid of excess primary antibody. The wells with embryos are covered with secondary antibody (diluted 200-400 times) and kept in dark at room temperature for three hours. The secondary antibody is then washed and 'Vectashield mounting medium for fluorescence' is mounted on the slide. A cover slip is placed gently and is sealed by using nail paint. The slide can nicely be stored for imaging at this point.

8. Image Analysis and Quantification

Image J was primarily used to perform all image analysis. The mean intensity was measured by selecting an area on the junction, HD or the extracellular matrix (ECM). Mean intensity was normalized with the background intensity. A mean of 10-15 embryos was taken and intensities of different mutants were plotted.

Analysis of FRAP movies was done manually with help of ImageJ. The area selected to perform FRAP in Metamorph software had to be transferred to ImageJ for analysis purpose. Metamorph ROI manager plugin was downloaded and installed in ImageJ for this.
The scheme of ImageJ commands is as follows –

1. Open the movie in Image J
2. Create Z projection. Image - Stacks - Z projection
3. File – Import – Metamorph ROI
4. Image – Overlay – Add Selection
5. Crop the movie to appropriate size
6. Image – Overlay – To ROI manager
7. Registration – Stackreg
8. Click the area to make it active
9. Plot Z-axis profile
10. Analyze – Summarize – Paste the values in excel file for analysis.

The values are then normalized against the background intensity and plotted against time. The recovery curves thus obtained are compared among different mutants.

9. Quantitative Polymerase Chain Reaction (qPCR)

RNA extraction and purification

The bench and the pipettes were washed with 100 % ethanol and RNase away before the experiment. The worms were collected from the NGM plates and bleached in 2 ml of bleach solution (5 ml H_2O, 1.5 ml NaOCl and 0.5 ml of 10N NaOH). An excess of M9 was added to stop the bleach reaction. It was then centrifuged at 2000 rpm for a minute to pellet the embryos. The bleach was removed using a vacuum pump. The embryos were washed 4 times with M9 buffer to get rid of the bleach completely. The embryos were then put in Omega RNA solv reagent and flash freeze in liquid nitrogen. Pellet pestles cordless motor was used to crush the frozen embryos. This was used to extract RNA using the Chloroform-Isopropanol mixture. The RNA extract was then purified with RNeasy® Minielute™ Cleanup kit. The RNA was aliquoted and stored at -80°C till further use.

cDNA preparation

Primer $p(dT)_{15}$ for cDNA synthesis and Roche First strand cDNA Synthesis kit for RT-PCR (AMV) was used to prepare cDNA.

Sigma-Aldrich SYBR® Green JumpStart™ Taq was used to perform the qPCR. Relative quantification was performed on the Cp (Cycle) values obtained using *act-1, eif-3C* and *Y4510D.4 act-1, eif-3C* and *Y4510D.4* (Zhang, Chen et al. 2012) genes as housekeeping genes.

Stastical Analysis

For growth curves, standard error of mean have been measured. For L1 length measurement, intensity measurement and rescue experiments student t test was performed using excel and matlab. For contraction time, actin continuity and orientation we applied for all genotypes a paired t-test using Matlab.

Figures and Strain list

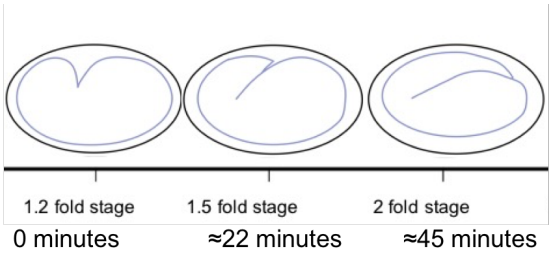

Figure 1. Staging the embryos. The embryos are staged with respect to the 1.2-fold stage. At the temperature of 25°C, embryos reach 1.5-fold after 20-25 minutes and at 2-fold after 45-50 minutes. All embryos are staged by using this time scale.

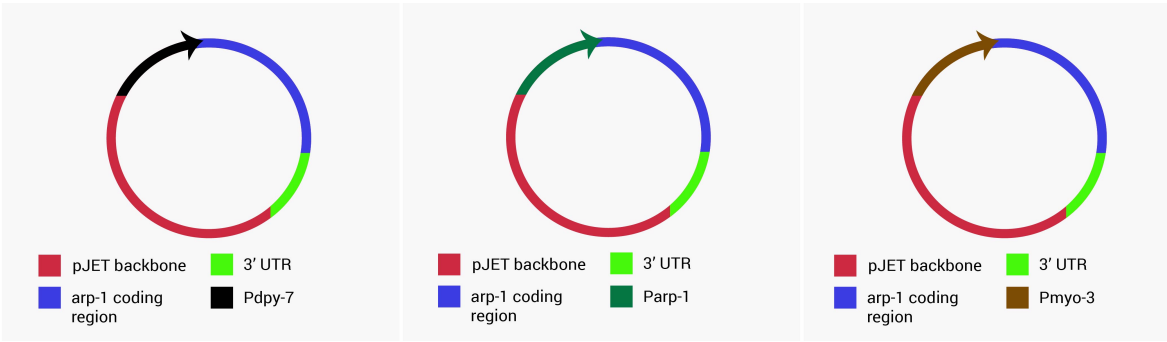

Figure 2. The schematic of the constructs designed for the rescue experiments. We used epidermal promotor *dpy-7*, muscle promotor *myo-3* as tissue specific rescue and wild type promotor as a control.

Step 1. Inoculate RNAi plasmid containing HT115 bacteria in 1 ml 'Ampicillin containing LB'

Step 2. Incubate overnight at 37°C

Step 3. Add 4 ml 'Ampicillin containing LB' and 15µl of 1M IPTG and incubate for 3 hours at 37°C

Step 4. Centrifuge – remove 4 ml supernatant

Step 5. Mix and plate – let the plates dry in dark

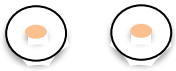

Step 6. Put L4 worms on the plate for 24 hours before experiment

Figure 3. RNAi feeding protocol

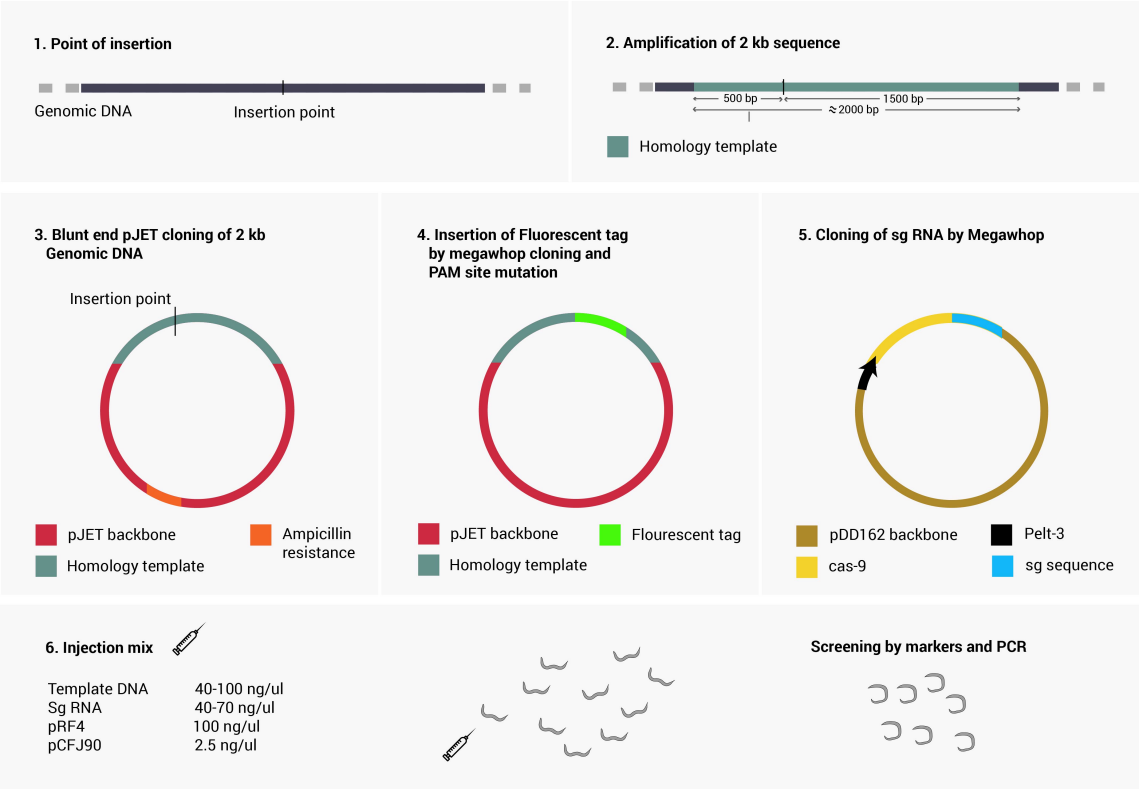

Figure 4. Strategy of CRISPR- Cas9 mediated gene editing by 500 base pair and 1500 base pair homology arms on either side of the insertion (Dickinson, Ward et al. 2013). The steps are illustrated here. We selected a point of insertion in a particular gene. The insertion can be on the ends of the protein i.e. N-terminal insertion, a C-terminal insertion or somewhere in the middle of the protein. The genomic DNA flanking this point of insertion was then amplified by polymerase chain reaction (PCR) and inserted into the blunt end cloning vector pJET. Next the fluorescent tag was inserted by using megawhop cloning or Gibson cloning (Gibson, Young et al. 2009, Miyazaki 2011). We used the same methods to clone the single guide fragment in the pDD162 vector, which expresses the protein Cas-9. The single guide (sg) sequence was selected using the software available online at crispr.mit.edu (Haeussler, Schonig et al. 2016). The injection mix was prepared with these plasmids and injection markers. Young adults were injected with this mix. The transgenic animals were selected by looking for roller and red pharynx markers. The screen for the insertion was then done by PCR and confirmed by fluorescence microscopy.

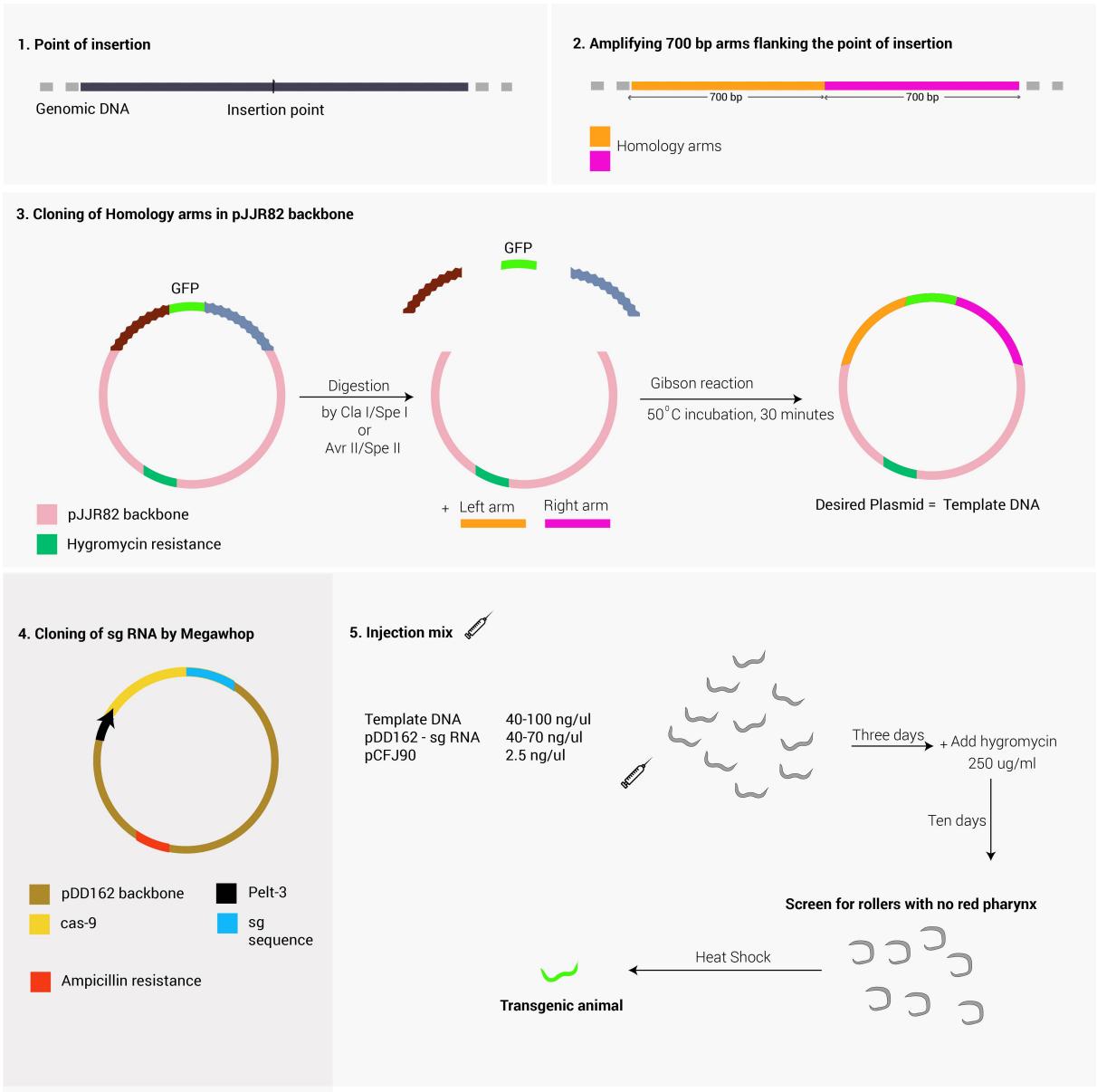

Figure 5. Strategy of CRISPR- Cas9 mediated gene editing by streamlined genome engineering with a self-excising drug selection cassette (Dickinson, Pani et al. 2015). The steps are illustrated here. We selected a point of insertion in a particular gene. The insertion can be on the ends of the protein i.e. N-terminal insertion, a C-terminal insertion or somewhere in the middle of the protein. We amplified 700 base pair arms on the either side of the insertion site from the genomic DNA. The plasmid containing the fluorescent marker (pJJR82, if the marker is GFP) along with the hygromycin resistance cassette is then digested and Gibson reaction is performed with the two amplified 700 bp arms. The desired plasmid containing both the 700 base pairs arms is screened by using colony PCR method. We used megawhop to clone the single guide fragment in the pDD162 vector, which expresses the protein Cas-9. The single guide (sg) sequence was selected using the software available online at crispr.mit.edu (Haeussler, Schonig et al. 2016). The injection mix was prepared with these plasmids and injection markers. Young adults were injected with this mix. The transgenic animals were selected by looking for roller without red pharynx. The screen for the insertion was then done by PCR and confirmed by fluorescence microscopy.

Table 7. Library of strains created for this study

S.no.	Lab identification number	*Genotype*
1	ML2661	*mcIs43[Plin-26::ABDvab-10-mcherry, Pmyo-2::GFP] IV; mcIs35[Plin-26court::YFP-tba-2, pat-4-CFP, pRF4] V*
2	ML2662	*mcIs43[Plin-26::ABDvab-10-mcherry, Pmyo-2::GFP] IV; mcIs35[Plin-26court::YFP-tba-2, pat-4-CFP, pRF4] V; git-1(tm1962) X*
3	ML2691	*par-3::gfp III; git-1(tm1962) X*
4	ML2692	*egl-50(n1086) II; par-3::gfp III*
5	ML2693	*egl-50(n1086) II; par-3::gfp III; git-1(tm1962) X*
6	ML2657	*unc-119(ed3) III; hmp-1(mc60[hmp-1::mTFP-1;loxP::unc-119(+)::loxP]) V; git-1(tm1962) X*
7	ML2694	*egl-50(n1086) II; unc-119(ed3) III; hmp-1(mc60[hmp-1::mTFP-1;loxP::unc-119(+)::loxP]) V*
8	ML2695	*egl-50(n1086) II; unc-119(ed3) III; hmp-1(mc60[hmp-1::mTFP-1;loxP::unc-119(+)::loxP]) V; git-1(tm1962) X*
9	ML2696	*git-1(tm1962) X; mcIs88[Pspc-1::spc-1::gfp; Pmyo-2::mCherry]*
10	ML2697	*egl-50(n1086) II; mcIs88[Pspc-1::spc-1::gfp; Pmyo-2::mCherry]*
11	ML2698	*egl-50(n1086) II; git-1(tm1962) X; mcIs88[Pspc-1::spc-1::gfp; Pmyo-2::mCherry]*
12	ML2654	*git-1(tm1962) X; XnIs94 [HMR-1::GFP]*
13	ML2655	*egl-50(n1086) II; XnIs94 [HMR-1::GFP]*
14	ML2656	*egl-50(n1086) II; XnIs94 [HMR-1::GFP]; git-1(tm1962) X*
15	ML2605	*git-1(tm1962) X; unc-119(ed3)III; let-805(mc73) III*
16	ML2606	*egl-50(n1086) II; unc-119(ed3) III; let-805(mc73) III*
17	ML2607	*egl-50(n1086) II; unc-119(ed3) III; let-805(mc73) III; git-1(tm1962) X*
18	ML2701	*mcIs67 [dpy7p::LifeAct::GFP; unc-119(+)] V; stIs10088[hlh-1::his-24::mCherry, unc-119(+)]; git-1(tm1962) X*
19	ML2702	*egl-50(n1086) II; mcIs67 [dpy7p::LifeAct::GFP; unc-119(+)] V; stIs10088[hlh-1::his-24::mCherry, unc-119(+)]*
20	ML2700	*egl-50(n1086) II;mcIs67 [dpy7p::LifeAct::GFP; unc-119(+)] V; stIs10088[hlh-1::his-24::mCherry, unc-119(+)]; git-1(tm1962) X*
21	ML2649	*noah-1(mc61[noah-1::mCherry; loxP::unc- 119(+)::loxP]) I; unc-119(ed3) III; git-1(tm1962)X*
22	ML2650	*egl-50(n1086) II; noah-1(mc61[noah-1::mCherry; loxP::unc- 119(+)::loxP]) I; unc-119(ed3) III*
23	ML2651	*egl-50(n1086) II; noah-1(mc61[noah-1::mCherry; loxP::unc- 119(+)::loxP]) I; unc-119(ed3) III; git-1(tm1962) X*
24	ML2690	*git-1(tm1962) pak-1(ok448) X*
25	ML2663	*dhc-1(he264[egfp::dhc-1]) vab-10(mc100[vab-10A::mCherry + LoxP]) I*

26	ML2646	*git-1(tm1962) dlg-1::gfp X*
27	ML2647	*egl-50(n1086) II; dlg-1::gfp X*
28	ML2648	*egl-50(n1086) II; git-1(tm1962) dlg-1::gfp X*
29	ML2638	*cap-1[mc76{cap-1::GFP;unc-119(+)}]IV; git-1(tm1962)X*
30	ML2709	*vab-10[mc109{vab-10A(∆SH3)::mCherry + LoxP}] I; egl-50(n1086) II*
31	ML2710	*dhc-1(he264[egfp::dhc-1]) I; mcIs43[Plin-26::ABDvab-10::mCherry, Pmyo-2::GFP] IV*
32	ML2721	*hmr-1(cp21[hmr-1::GFP + LoxP]) I; cap-1[mc76{cap-1::GFP; unc-119(+)}] IV*
33	ML2722	*cap-1[mc76{cap-1::GFP;unc-119(+)}] IV; hmp-1(mc60[hmp-1::mTFP-1; loxP::unc-119(+)::loxP]) V*
34	ML2723	*git-1(tm1962)X; goeIs3 [myo-3p::SL1::GCamP3.35::SL2::unc54 3'UTR + unc-119(+)]*
35	ML2724	*egl-50(n1086) II; goeIs3 [myo-3p::SL1::GCamP3.35::SL2::unc54 3'UTR + unc-119(+)]*
36	ML2725	*egl-50(n1086) II; goeIs3 [myo-3p::SL1::GCamP3.35::SL2::unc54 3'UTR + unc-119(+)]; git-1(tm1962) X*
37	ML2727	*hmr-1(cp21[hmr-1::GFP + LoxP]) vab-10[mc109{vab-10A(∆SH3)::mCherry + LoxP}] I*
38	ML2739	*hmr-1(cp21[hmr-1::GFP + LoxP]) I; git-1(tm1962) X*
39	ML2740	*hmr-1(cp21[hmr-1::GFP + LoxP]) I; egl-50(n1086) II; git-1(tm1962) X*
40	ML2741	*hmr-1(cp21[hmr-1::GFP + LoxP]) I; egl-50(n1086) II*
41	ML2763	*mup-4(mc121[mup-4::mCherry + LoxP]) III*
42	ML2767	*dhc-1(he264[egfp::dhc-1]) I; cap-1[mc76{cap-1::GFP; unc-119(+)}] IV*
43	ML2768	*vab-10(mc100[vab-10A::mCherry + LoxP]) dhc-1(he264[egfp::dhc-1]) I*
44	ML2769	*let-805(mc119[let-805::mMaple3; unc-119(+)]) III*
45	ML2636	*ifb-1(mc108[ifb-1::GFP]) II*
46	ML2302	*(farl-11::gfp)*
47		*egl-50(n1086) II; pak-1(ok448) X*
48		*mcIs86[lin-26p::ABD::mkate; myo-2p::mCherry]; cap-1[mc76{cap-1::GFP; unc-119(+)}] IV*
49		*cap-1[mc76{cap-1::GFP;unc-119(+)}] IV; hmp-1(mc60[hmp-1::mTFP-1;loxP::unc-119(+)::loxP]) V*
50	ML2775	*mup-4(mc121[mup-4::mCherry + LoxP]) III; git-1(tm1962) X*
51	ML2776	*egl-50(n1086) II; mup-4(mc121[mup-4::mCherry + LoxP]) III*
52	ML2777	*egl-50(n1086) II; mup-4(mc121[mup-4::mCherry + LoxP]) III; git-1(tm1962) X*
53		*let-805(mc119[let-805::mMaple3; unc-119(+)]) III; git-1(tm1962) X*
54		*egl-50(n1086) II; let-805(mc119[let-805::mMaple3; unc-119(+)]) III*
55		*egl-50(n1086) II; let-805(mc119[let-805::mMaple3; unc-119(+)]) III; git-1(tm1962) X*
56		*vab-10(mc100[vab-10A::mCherry + LoxP]) I; git-1(tm1962) X*

57		*vab-10(mc100[vab-10A::mCherry + LoxP]) I; egl-50(n1086) II*
58		*vab-10(mc100[vab-10A::mCherry + LoxP]) I; egl-50(n1086) II; git-1(tm1962) X*
59		*vab-10(mc100[vab-10A::mCherry + LoxP]) I; let-805(mc73[let-805::GFP; unc-119(+)]) III; git-1(tm1962) X*
60		*vab-10(mc100[vab-10A::mCherry + LoxP]) I; egl-50(n1086) II; let-805(mc73[let-805::GFP; unc-119(+)]) III*
61		*vab-10(mc100[vab-10A::mCherry + LoxP]) I; egl-50(n1086) II; let-805(mc73[let-805::GFP; unc-119(+)]) III; git-1(tm1962) X*
62		*vab-10(mc100[vab-10A::mCherry + LoxP]) I; cap-1[mc76{cap-1::GFP; unc-119(+)}] IV*
63		*mcEx971(Pmyo-3::arp-1)*
64		*egl-50(n1086) II; git-1(tm1962); mcEx971(Pmyo-3::arp-1)*
65		*vab-10(mc100[vab-10A::mCherry + LoxP]) I; egl-50(n1086) vab-19(mc104[vab-19::mCherry) II*
66		*vab-10(mc100[vab-10A::mCherry + LoxP]) I; vab-19(mc104[vab-19::mCherry) II*
67		*vab-19(mc104[vab-19::mCherry) egl-50(n1086) II*
68		*mcEx970(Pdpy-7::arp-1)*
69		*mcIs54 [dpy-7p::spastin^mCherry ; unc-119+]*
70		*egl-50(n1086) II; git-1(tm1962) X; mcEx970(Pdpy-7::arp-1)*

Results

Results

A novel dynein independent role of dynactin in *C. elegans* embryonic elongation.

Saurabh Tak[1,2], Christelle Gally[2], Loan Bourdon[1], Shashi Kumar Suman[1,2], Sarah Hoff-yoessle[2], Agnes Aubry[2], Alicia Lardennois[1] and Teresa Ferraro[1], Michel Labouesse[1,2].

1. Institut de Biologie Paris, Seine, UPMC, Paris
2. Institut de Génétique et de Biologie Moléculaire et Cellulaire, Strasbourg

III. Results - Table of contents

1. Elongation continues in *git-1/pak-1* null mutants.

It has been previously shown (Williams and Waterston 1994, Zhang, Landmann et al. 2011) that muscle tension is important for embryonic elongation. In the absence of muscle tension, elongation is halted, and embryos are paralyzed at two-fold stage (pat). Muscle tension is responsible for compressing and squeezing the epidermis laterally. As a result, epidermis experiences a tension which is detected by a mechanosensory molecule (Red question mark, Figure 1. i) to in turn induce the recruitment and maintenance of the G protein coupled receptor kinase interactor GIT-1. GIT-1 interacts, binds and induce conformational changes in PIX-1, which allows it to activate Rac. Activated Rac/CED-10 activates the kinase PAK-1, which phosphorylates the intermediate filament IFA-3. The phosphorylation of intermediate filament is one outcome of this pathway. The phosphorylation of intermediate filaments strengthens CeHDs and allow further elongation. Therefore, hemidesmosome remodels via PAK-1 – PIX-1 – GIT-1 signaling (Figure 1.i) which promotes embryonic elongation via intermediate filament phosphorylation. We expected *git-1* and *pak-1* null mutants to be arrested at 2-fold stage, like in the case of paralyzed at two-fold (pat) phenotype. However, *git-1(tm1962)* and *pak-1(ok448)* null mutants are viable (Figure 3.iii), although they are shorter than the wild type embryos at hatching. Therefore, we propose the existence of parallel pathway/s to the one described before (Zhang, Landmann et al. 2011).

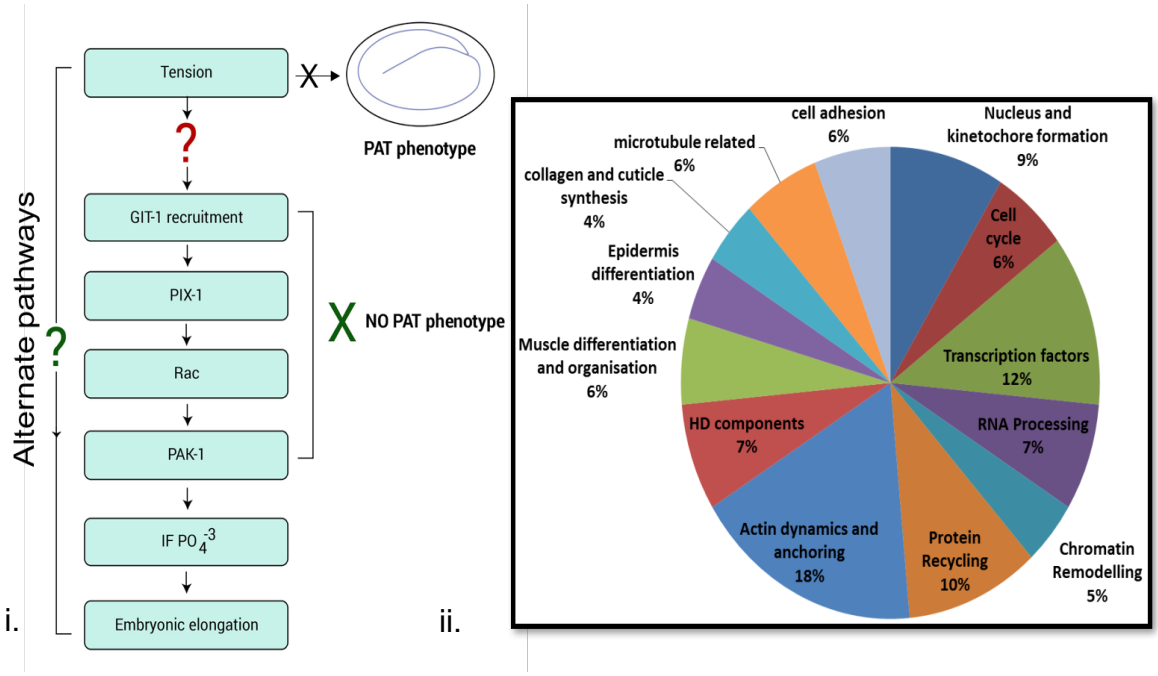

Figure 1. i. Mechanotransduction pathway in CeHDs. Epidermis gets compressed and squeezed by muscle contraction and relaxation cycles. In the absence of tension, embryos arrest and paralyze at the two-fold stage (pat). This tension on epidermis leads to recruitment and maintenance of GIT-1 at the level of CeHD, which in turn recruits PIX-1 by binding to it and activates it. Activated PIX-1 activates Rac/CED-10, which in turn activates PAK-1, resulting in IFA-3 intermediate filament phosphorylation (IF PO_4^{-3}). This allows strengthening of CeHDs, allows further elongation (Zhang, Landmann et al. 2011). Since git-1/pak-1 mutants are viable, it predicts the existence of alternative pathways acting downstream of the tension provided by muscles.

ii. To reveal the components acting in parallel pathway/s, we performed a genome wide enhancer RNA interference screen in *git-1(tm1962)* mutant background to look for two-fold arrest, body morphology defects (BMD) and pat phenotypes. A summary of the 78 candidates identified from this screen is provided here.

2. Components in alternate pathway/s are revealed by performing Genome wide RNAi screen in *git-1(tm1962)* background.

In the absence of muscle tension GIT-1 is not maintained at the level of CeHDs. Though the null mutants of *git-1 (tm1962)* or *pak-1(ok448)* are viable. It led us to predict the existence of alternative pathways acting downstream of the tension provided by muscles. To determine, which proteins/molecules act in the parallel pathway/s, an RNAi screen was designed. *git-1* is expressed in the epidermis and nerve rings but not in muscles; it is a known scaffolding protein and located at hemidesmosomes (the structures which hold muscle and epidermis together), whereas *pak-1* is ubiquitously expressed in most tissues. Therefore, *git-1* serve as a better candidate than *pak-1* to perform the screen. A genome wide enhancer RNAi screen in the *git-1(tm1962)* mutant background was performed (Figure 1.ii) to look for body morphology defects (bmd) and paralyzed at two-fold arrest (pat). Screen performed starting with L1 larvae allowed the identification of the new candidates with no obvious embryonic phenotypes, whereas screen performed starting with L4 larvae allowed the identification of candidates with early embryonic and maternal phenotypes. The figure 2 illustrates the screen strategy (details in methods and materials).

The phenotypes of *vab-10* validated the screen. *vab-10* has peculiar phenotype with a pinched nose, arresting at 2-2.5-fold stage. Almost 80 candidates were identified from the screen (Table 2), which are summarized in Figure 1.ii. We narrowed the candidates on the basis of their strength of interaction with *git-1*. Candidates with more than 70% BMD were selected (Table 1), whereas the individual depletion did not produce a significant defect or the 2-fold arrest increased significantly with *git-1*. Dynein/dynactin subunits and the proteins related to dynein/dynactin such as *dlc-1*, *cap-1* and *farl-11, zyg-12* were narrowed out. Henceforth, we shifted our focus to studying the Dynein/Dynactin complex.

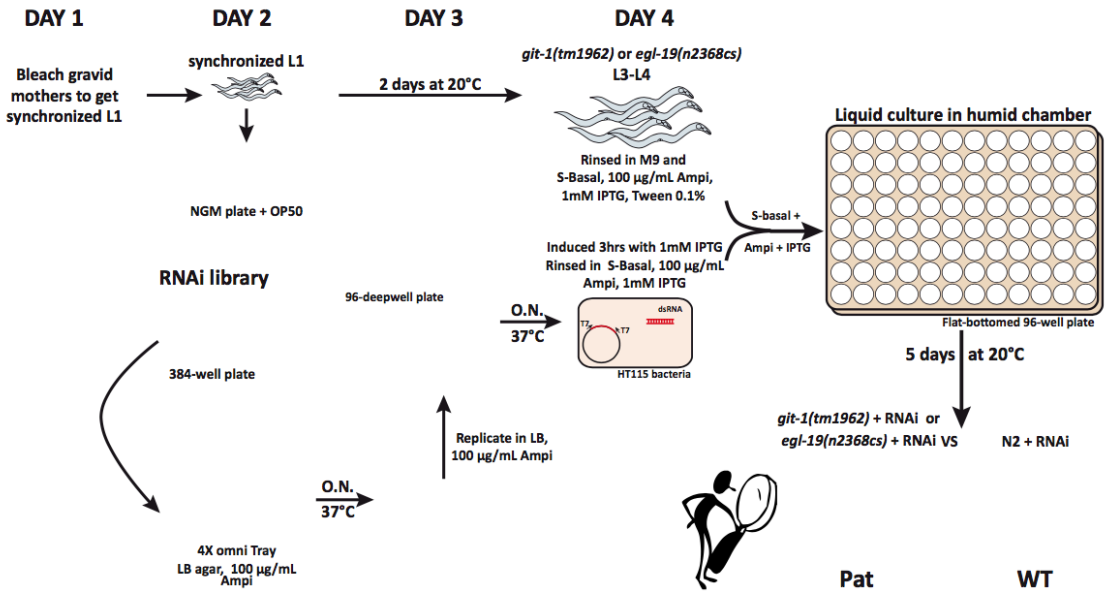

Figure 2. The strategy of genome-wide RNAi enhancer screen. To make the screen efficient and faster, RNAi feeding was done using liquid culture in 96 well-plates. Embryos were synchronized by bleaching the gravid adults and the resulting L1 larvae were kept at 20°C to let them grow to L4 larvae. L4 larvae were transferred to RNAi cultures and the embryos were checked under DM6000 DIC microscope after 5 days (Kamath and Ahringer 2003).

3. Depleting dynein/dynactin subunits in the *git-1(tm1962)* mutant background leads to two-fold stage arrest.

Characterization of the interaction of dynactin mutants was done by combining dynactin subunit mutants with *git-1(tm1962).* The null alleles of dynein/dynactin mutants are early embryonic lethal. To overcome this, we relied on the use of temperature sensitive alleles and RNA interference technique, which allowed us to study late elongation. The mutation *egl-50(n1086)* is a temperature sensitive allele of *arp-1* (Bill Schaffer, personal communication) that corresponds to a point mutation in the second exon of arp-1 (Figure 3.i) which encodes a homologue of human protein centractin (Clark and Meyer 1992). This conditional mutant is viable at 15°C, but lethal at the restrictive temperature 25.5°C. We constructed double mutant strains using *egl-50(n1086ts)* and *git-1(tm1962)* to get the *egl-50(n1086); git-1(tm1962)* (hereafter referred as *egl-50; git-1* for ease) and examined its embryonic lethality. The double mutant *egl-50; git-1* arrested at the 2-fold stage at 25.5°C (Figure 3.iii and 3.iv). We found that *egl-50(n1086); pak-1(ok448)* arrests at 2-fold stage too*,* thereby suggesting that *git-1* and *pak-1* interact with *egl-50* in a similar manner and thus probably act in the same pathway. A closer inspection revealed three phenotypes in the double mutant *egl-50; git-1* background i.e. 2-fold arrest, collapsing embryos and retracting embryos (Figure 4.i, ii). To test whether other dynactin subunits had the same effect on the elongation or the effect is confined to *arp-1*, I combined *dnc-1(or404ts)* and *git-1(tm1962)* to obtain *dnc-1(or404ts); git-1(tm1962)* (hereafter referred as *dnc-1; git-1* for ease) and examined its embryonic lethality. *dnc-1* codes for the *C. elegans* orthologue of the *p150* subunit of dynactin in mammals. The ts allele *or404* is a missense mutation of Arginine to Cysteine at position 1237 (Figure 5.i). At the restrictive temperature of 25.5°C, it has 20-30% viability and reduced brood size. The high early embryonic lethality in *dnc-1* mutants is a result of spindle alignment defects. Indeed all dynactin mutants produce early embryonic lethality, because of the requirement of dynactin in early embryonic stages (Skop and White 1998). The double mutant *dnc-1; git-1* embryos that surpass the early embryonic lethality arrest at the 2-fold stage at the restrictive temperature of 25.5°C (Figure 5.iii, iv).

Further, RNAi of *cap-1*, another subunit of dynactin, which codes for capping protein, in *git-1(tm1962)* or *pak-1(ok448)* mutant background results in 2-fold arrest of the embryo (Figure 23). Depleting *farl-11*, a known suppressor of conditional *dhc*-1 mutants in *git-1* mutant background resulted in a two-fold arrest phenotype too. These results prove that the complex dynein/dynactin genetically interacts with *git-1* and *pak-1*.

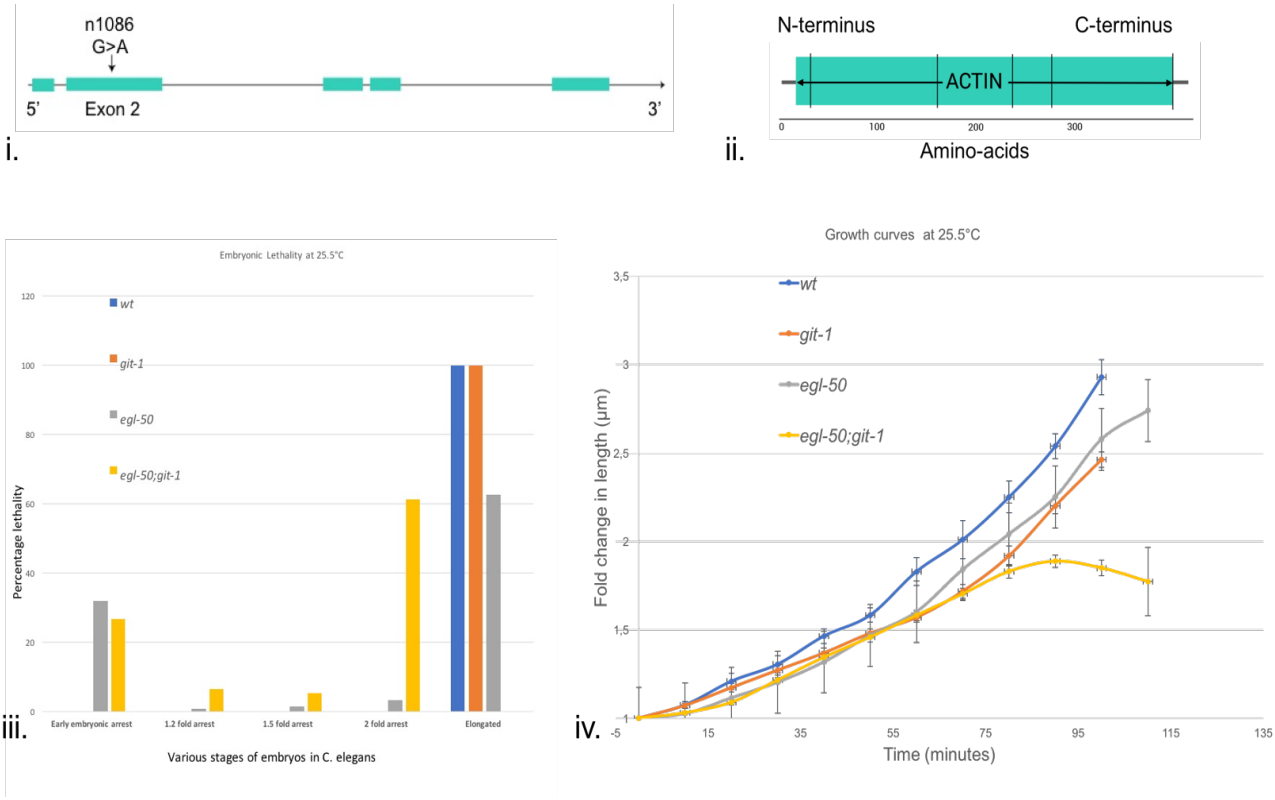

Figure 3 i. Location of single point missense mutation in the *egl-50(n1086ts)* allele.
ii. The protein coding region of ARP-1 codes for single Actin domain like in the G-actin subunits. The vertical lines show the position of introns.
iii. Lethality was checked at various embryonic stages. The percentage arrest of embryos at the 2-fold stage increases in *egl-50; git-1* background (n>240, for all genotypes).
iv. *egl-50(n1086ts)* genetically interacts with *git-1(tm1962)* and the embryos arrest at the 2-fold stage at the non-permissive temperature of 25.5°C, whereas the single mutants are viable (n>9 for all genotypes).

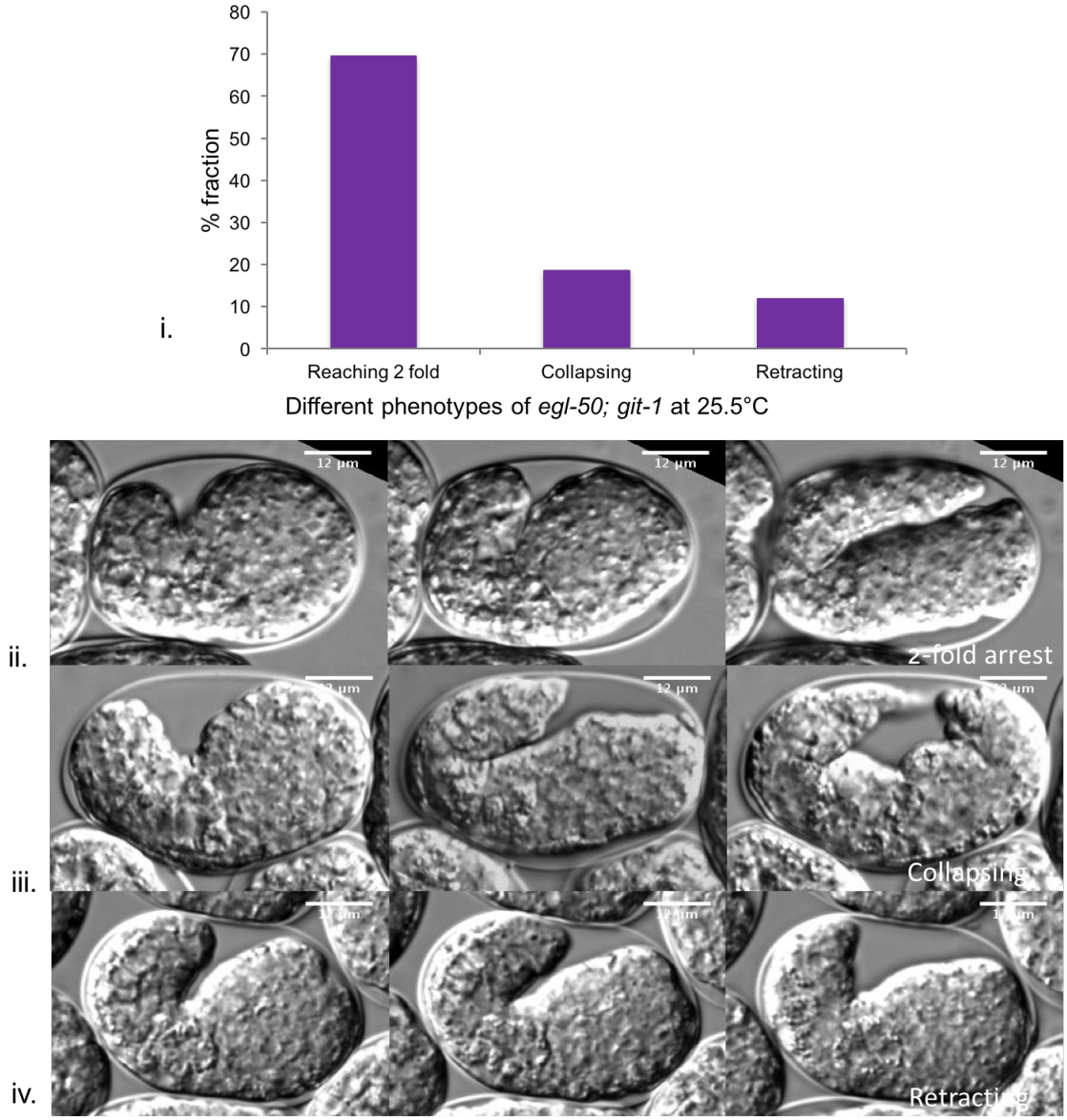

Figure 4. The double mutant *egl-50; git-1* shows phenotypic variability at the restrictive temperature of 25.5°C. The three phenotypes are 2-fold arrest, collapsing embryos and retracting embryos. **i.** The percentage of each of these embryos present in the total population is given in this graph (n>100).

ii, iii, iv – The panel shows the phenotypic variability of the *egl-50; git-1* embryos. All the embryos were staged with respect to 1.2-fold stage. In a 2-fold arrest, embryos grow normally up to 2-fold and arrest at this stage. Collapsing embryos can grow normally till 1.5 or 1.7-fold stage and then pinch, shrink or explode from their heads. Retracting embryos grow till 1.5-fold, and then retract back to 1.2-fold.

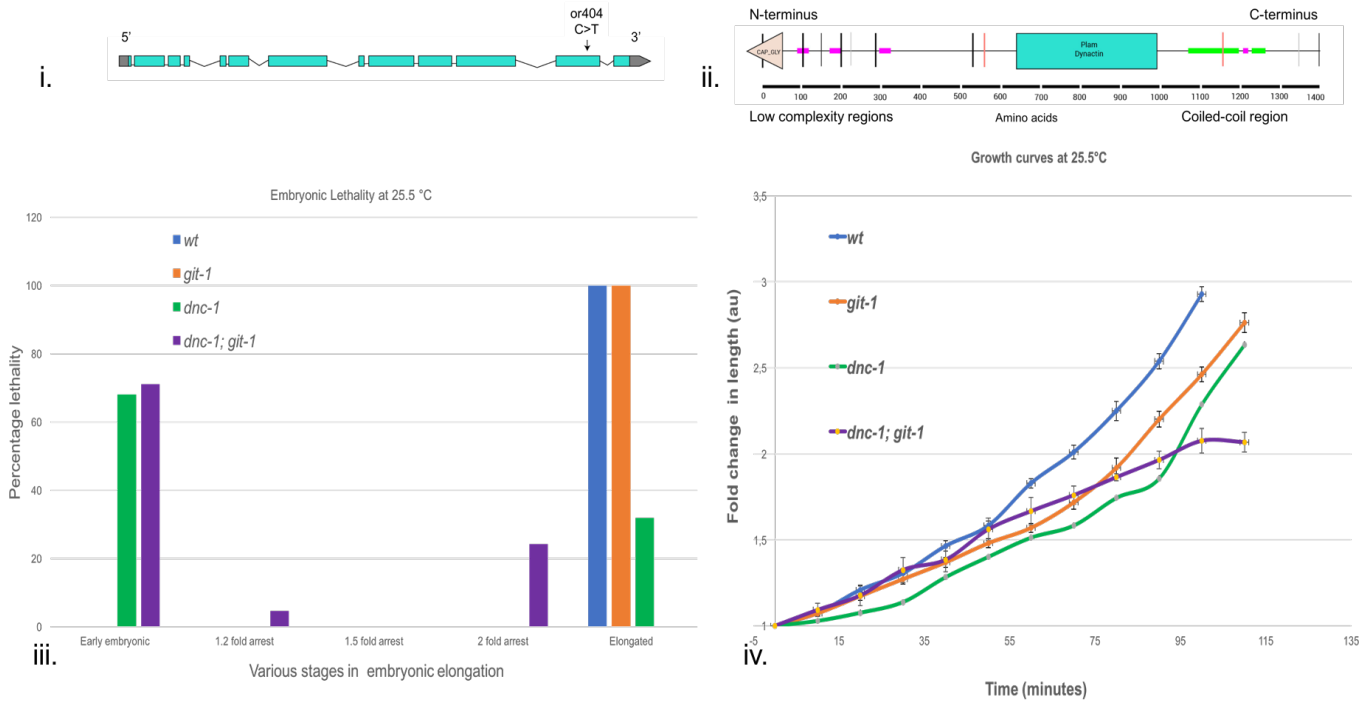

Figure 5 i. Location of single point missense mutation in *dnc-1(or404ts)* allele.

ii. The SMART domain structure from protein coding region of DNC-1 is shown.

iii. Lethality was checked at various embryonic stages. The percentage arrest of embryos at the 2-fold stage increases in the *dnc-1; git-1* background (n>100, for all genotypes).

iv. *dnc-1(or404ts)* genetically interacts with *git-1(tm1962)* and the embryos arrest at the 2-fold stage at the non-permissive temperature of 25.5°C, whereas the single mutants are viable (n>9 for all genotypes).

Table 1. Candidates, related to the dynein/dynactin complex, showing strong interaction (increase in the 2-fold arrest) with *git-1(tm1962)* are listed here.

Protein	Allele/RNAi	Interaction with *git-1 (tm1962)*
Centractin	*egl-50(n1086ts)*	2-fold arrest (major phenotype)
Capping protein - 1	*cap-1*	2-fold arrest
Dynactin	*dnc-1(or404)*	2-fold arrest
Dynein light chain	*dlc-1*	2-fold arrest*
FAR-11(Factor arresting DHC-1 lethality) like (FARL-11)	*farl-11*	2-fold arrest

* *dlc-1(RNAi)* causes very high lethality. *dlc-1* is known to act independently of dynein and has varied functions such as transcriptional regulator. Therefore, is hard to study.

The growth curves of both the double mutants (*dnc-1; git-1* and *egl-50; git-1*), display the growth rates of all the mutants similar to the wild type, till the arrest at the 2-fold stage. Therefore, the first part of the elongation, which depends on non-muscle myosin II contractility is most likely normal.

What are the morphological changes that accompany the 2-fold arrest? The morphological changes might provide a clue for what goes wrong in these double mutants. To investigate this, we measured the egg shell length, head width and body lengths of the embryos at the 2-fold stage. Variable sizes of the double mutants as compared to the wild type or the single mutants were observed (Figure 6). We compared the head width to that of total length of the embryo. A MATLAB code recognizes the line passing through center of the embryo body along the length, after a perimeter of the embryo is drawn by hand. The width of the head was measured at 20% of the total length of the embryo, starting from the tip of the mouth. The embryos with large heads were observed to have elongation defects. In *git-1* mutants, heads are slightly bigger and the L1 larvae of *git-1* mutants can be selected by looking at their large heads. The double mutant *egl-50; git-1* embryos have significantly larger than that of the single mutants (Figure 6). Similar results were found for the *cap-1(RNAi)* and the *farl-11(RNAi)* in *git*-1 mutant background. Embryos with these combinations (co-depletion of one of the subunits of dynactin along with *git-1* or *pak-1* null mutants) displayed elongation defects and arrested at the 2-fold stage. We also observed other elongation defective mutants in the lab also displayed larger heads. This suggests that squeezing of head is important in order for the elongation to continue normally.

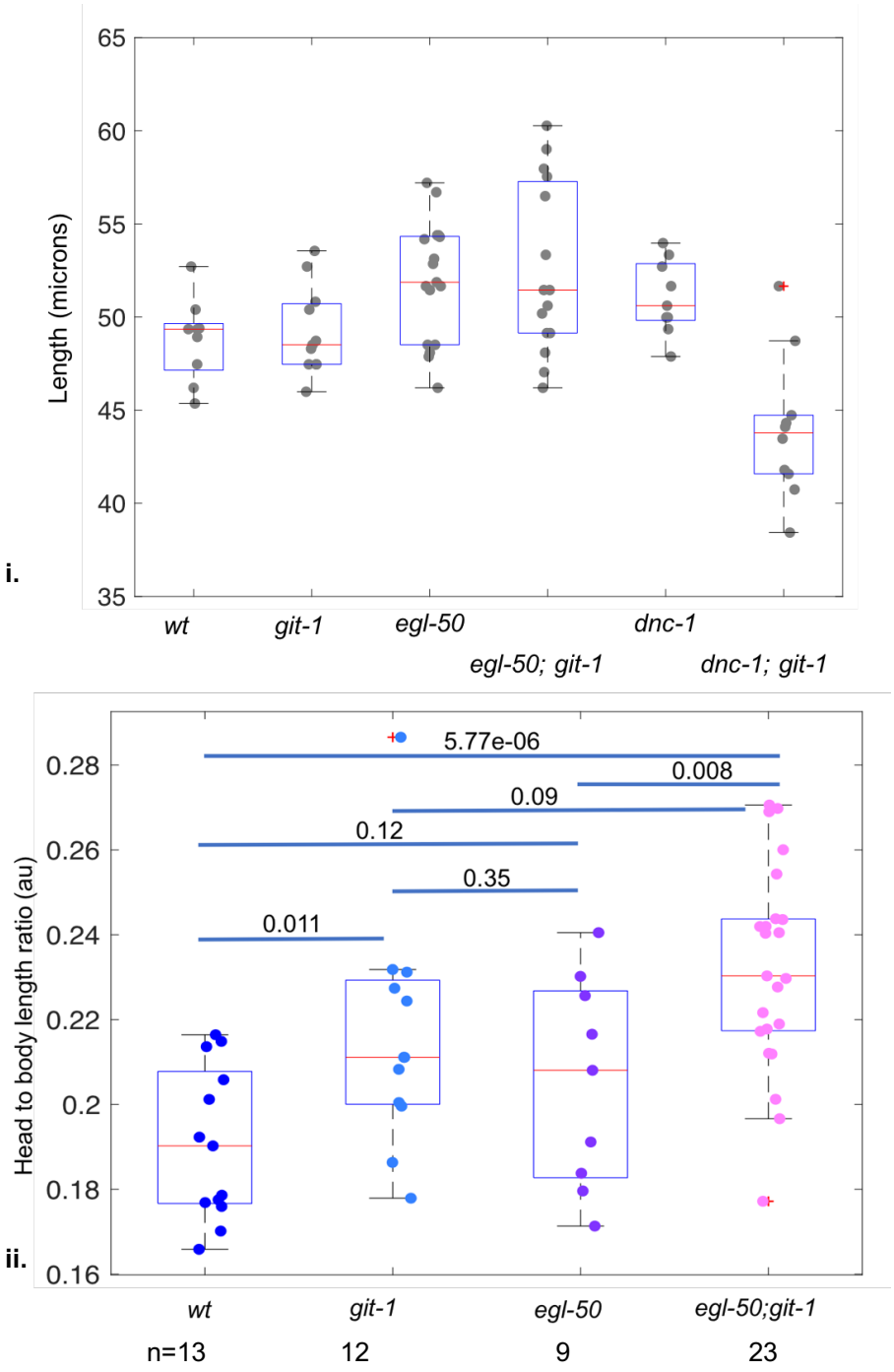

Figure 6. Morphological changes in double mutant embryos. **i.** The egg shell lengths variation of the egg shell measured in the double mutants *egl-50; git-1* and *dnc-1; git-1* with single mutant and wild type controls (n>9, for all genotypes). The double mutants vary more than the wild type and the single mutants.

ii. Head to body length ratio. The head of *egl-50; git-1* animals is significantly larger than the single mutants and the wild type animals. The width of the head was chosen by drawing a perpendicular at 20% of the total length of the embryo from the mouth (n>10, for all genotypes). The head width was then normalized with body length and the data is plotted here.

4. Which cellular structure/s can be causing these defects?

a. Creation of a library of markers and Intensity analysis

It is well established, at this point in this manuscript, that the double mutants mentioned above, all show an elongation defect and arrest at the two-fold stage. To probe which component of what structure is the reason behind the 2-fold stage arrest, we combined markers of various structures in the cell in *egl-50; git-1* background. Next we raised the question of what is the role of Dynein/Dynactin in late elongation of *C. elegans* embryo. As outlined in the introduction, cytoplasmic dynein is a microtubule-based motor that functions in vesicular and organelle transport. The lab recently showed that microtubule depleted embryos (spastin overexpressed) have a normal elongation, unless combined with *let-502(sb112ts)* (Quintin, Wang et al. 2016). Furthermore, that study found out that the levels of the basal hemidesmosome receptor, known as LET-805, decreased in *let-502(sb112ts)* embryos overexpressing spastin (Quintin, Wang et al. 2016). We thus explored what is *let-805::gfp* level in the double *egl-50; git-1* mutant background. (Figure 7). All embryos were staged as shown in methods and materials with respect to 1.2-fold stage. To image the 1.5-fold stage, imaging was done 20-25 minutes after the 1.2-fold stage and to image the 2-fold stage imaging was done 45-50 minutes after 1.2-fold stage.

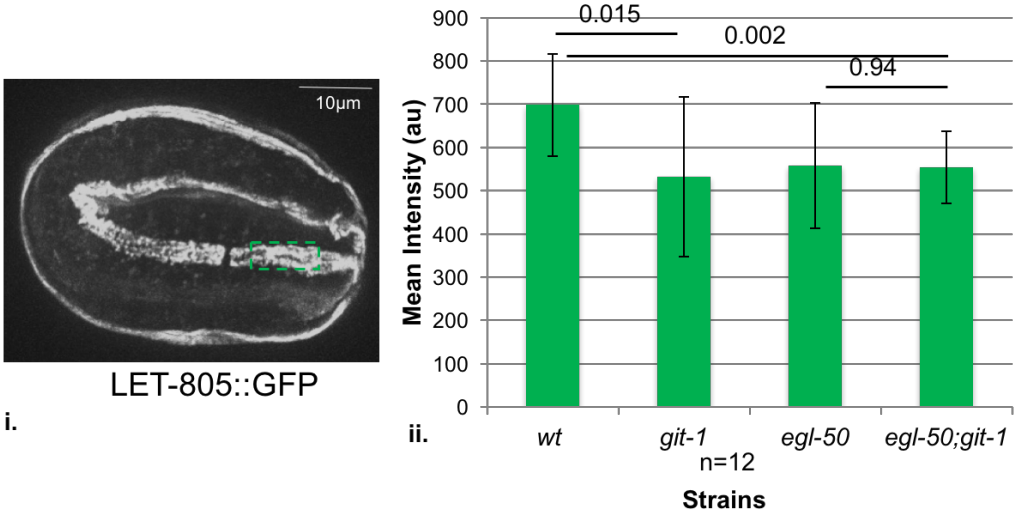

Figure 7. The *C. elegans* hemidesmosomes as observed by the basal hemidesmosome marker LET-805::GFP. The intensity of fluorescence at the hemidesmosome was compared. The green box shows the region in head, for which intensity was compared. Background was subtracted from the intensity. The intensity of wild type to double mutant is significantly different, but the intensity change between *egl-50* and the *egl-50; git-1* is not significant. The bars represent standard deviation.

There was no significant difference in the mean intensity of *let-805::gfp* (basal side marker of CeHD) among the single mutants and the double mutant (Figure 7). Despite this, I found defects (hemidesmosome breaking) in CeHDs, though the defects were either not striking or not present in all 2-fold arrested embryos. To probe further, I created a library of markers in the *egl-50; git-1* background to look for structural and dynamic defects (Table 7 from method and materials). We did not observe any major organization defects of the actin cytoskeleton (Figure 9.i). The extracellular matrix (ECM) protein NOAH-1, which is essential for *C. elegans* embryonic integrity and elongation (Vuong-Brender, Suman et al. 2017) was not affected in the *egl-50; git-1* background (Figure 8).

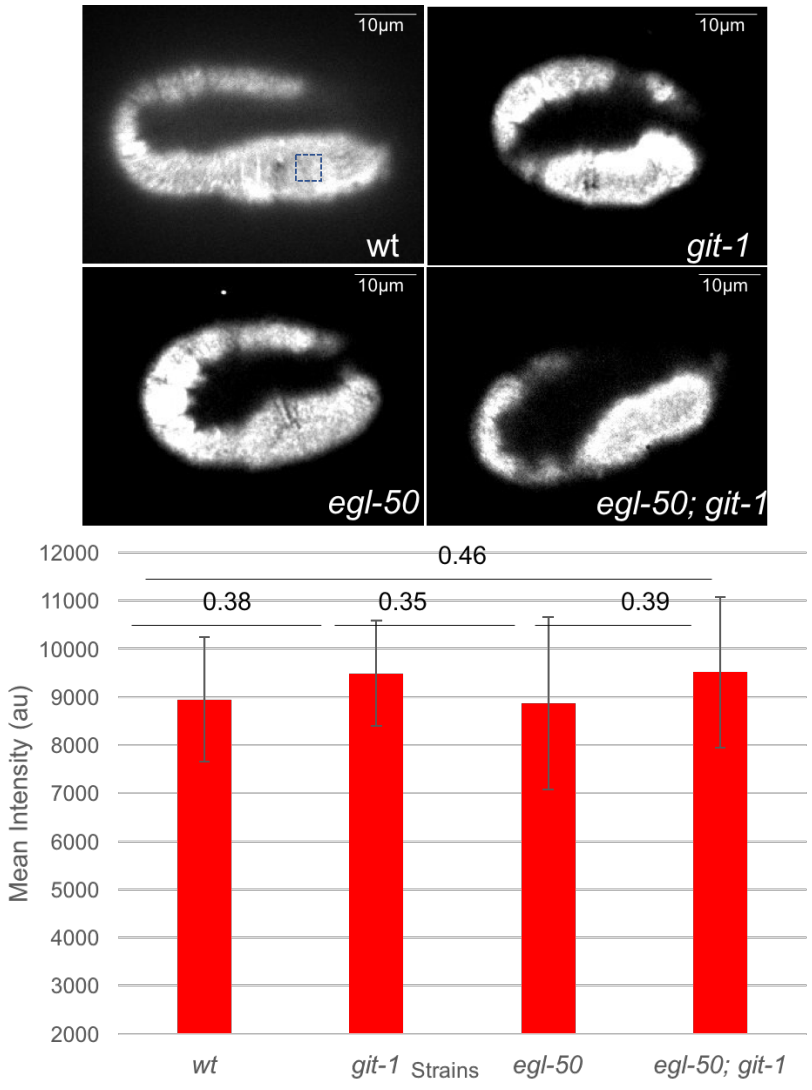

Figure 8. The *C. elegans* ECM as observed by the ECM marker mCherry::NOAH-1. The intensity of the ECM at DV cells was compared. The green box shows the region in head, for which intensity was compared. Background was subtracted from the intensity. The intensity of wild type to double mutant is significantly different, but the intensity change between *egl-50* and the *egl-50; git-1* is not significant (n>10). The bars represent standard deviation.

Next I examined HMR-1::GFP (Marston, Higgins et al. 2016). E-cadherin (*hmr-1*) is a component of the cadherin-catenin complex (CCC). Neither the localization nor the intensity of HMR-1::GFP at the 12 junctions I examined, were affected. Nevertheless, I observed a popping seam cell defect in a small population (20%) of the embryos (Figure 9.ii). In the popping seam cell defect, one of the seam cells pops out of the lateral epidermis towards the ventral or dorsal epidermis. Similarly, a fluorescent CRISPR construct marker of PAR-3 *(Marston, Higgins et al. 2016),* a component of Partitioning complex, did not show any significant changes in the pattern of expression (Figure 10). I prepared a GFP-fused CRISPR construct of *mup-4* (apical side marker of HD) and examined it. The intensity was changed significantly in between the wild type and the double mutant, though we need the single mutant controls to appropriately draw a conclusion here. The hemidesmosome also spreads irregularly. We are currently examining it in vivid detail (Figure 11).

i.

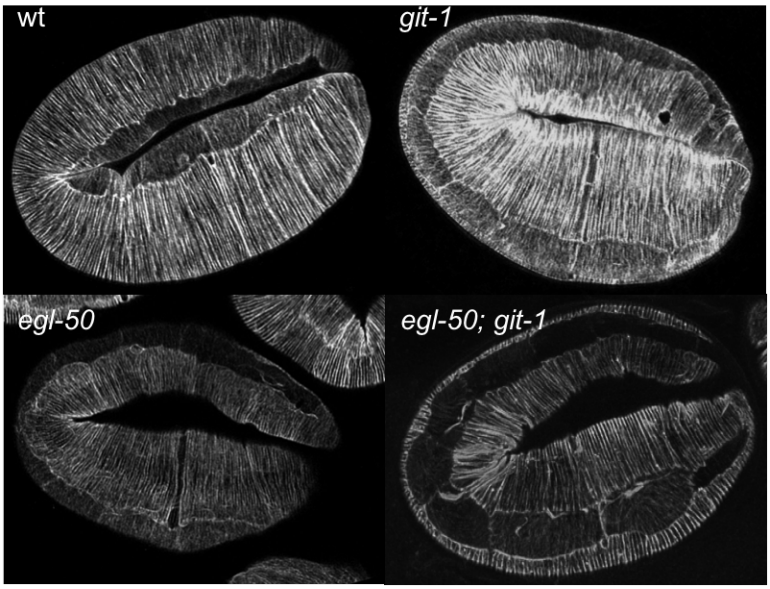

ii.

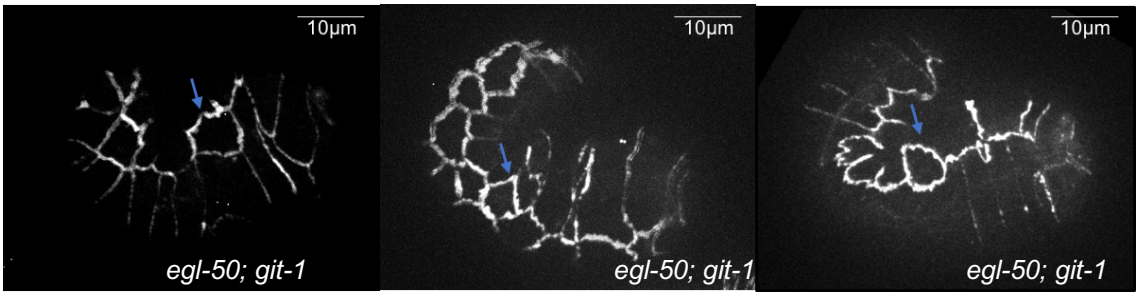

Figure 9. **i**. The *C. elegans* actin cytoskeleton as observed by the epidermal actin marker *Pdpy-7::LifeAct::GFP*. The actin pattern is not affected immediately. Imaging was performed on the sleeping embryos and the images were then deconvoluted (n>10).

ii. The HMR-1::GFP marker was used to image the junctions. We observed a seam cell alignment defect in 20-30% of the population in the double mutant *egl-50; git-1*. A seam cell pops out of the lateral epidermis towards dorsal or ventral epidermis (n>10). The blue arrow shows a cell from seam cells moving towards dorsal or ventral epidermis.

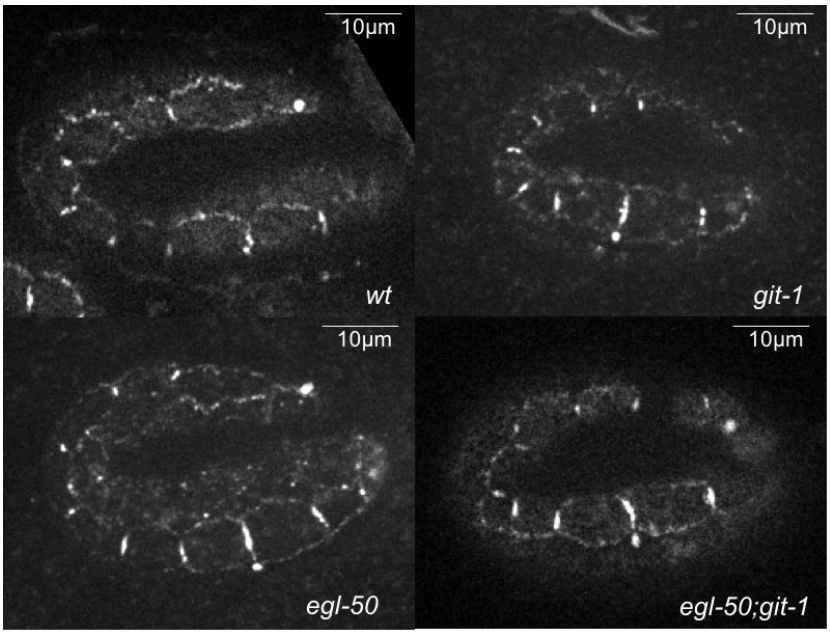

Figure 10. The marker PAR-3::GFP was used to image the PAR-3. We did not observe any defects in any of the mutants (n>10).

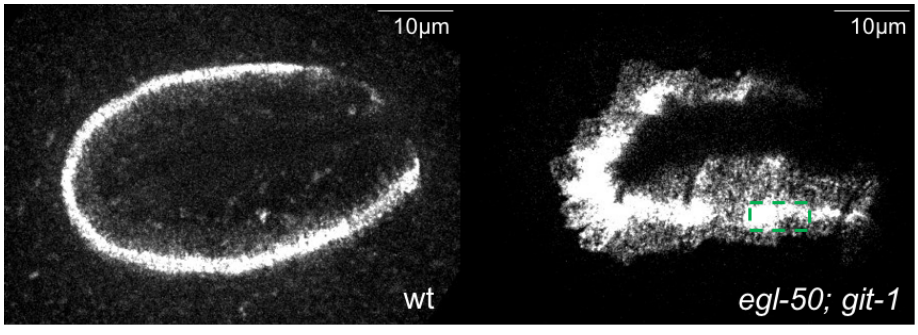

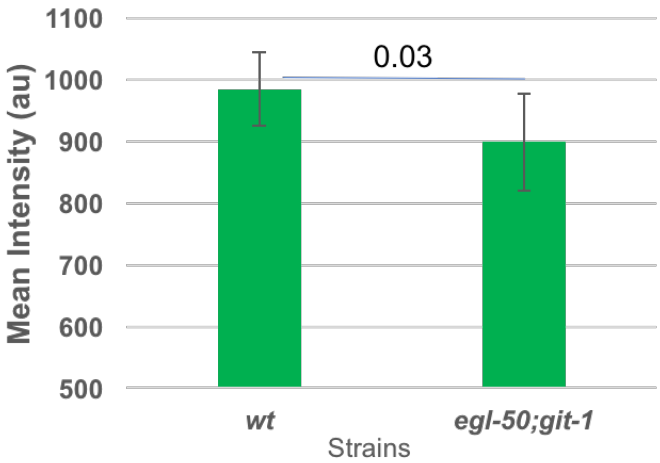

Figure 11. Examining the apical side marker of hemidesmosome, MUP-4::GFP showed an irregularity and spreading of hemidesmosome in dorso-ventral direction the *egl-50; git-1* embryos. The mean intensity difference between the wild type and the *egl-50; git-1* mutant is significant (n=10). The mean intensity was measured in the head region as shown by the green dashed box. The bars represent standard deviation.

The protein components from junctions and extracellular matrix did not show decrease in the intensity. The actin cytoskeleton is not immediately affected. The polarity of PAR-3 in junctions, where PAR-3 is more concentrated on the seam-seam junctions than the seam-dorsal or seam ventral junctions, is maintained and not disturbed in both single mutants and the double mutant. Therefore, dynein/dynactin is not responsible for maintaining or regulating the PAR-3 polarity. Since we did not see any actin aberrations, we conclude that there are no defects in actin turnover and alignment in the double mutant.

5. The FRAP profile of Myotactin (LET-805) on dorsal and ventral hemidesmosomes in the double mutant *egl-50; git-1* is asymmetric.

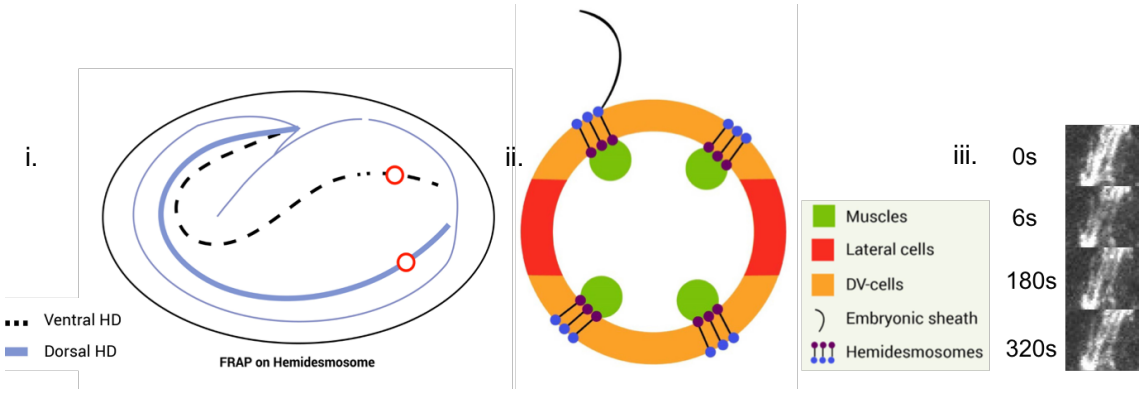

Figure 12. i. Ventral and dorsal hemidesmosome are shown in a 1.5-fold embryo. FRAP was performed on both ventral and dorsal CeHD, the red circles denote the position. **ii.** A cross section of *C. elegans* embryo. *C. elegans* hemidesmosomes are structures that connect the 4 sets of muscles to the epidermis. **iii.** A typical FRAP progression. The region was bleached at t=6s and the recovery was observed for 6 minutes.

Since minor defects were observed in *C. elegans* hemidesmosome (CeHDs) by using LET-805::GFP, and dynein/dynactin is a motor protein, I explored the possibility of dynamic defects by using 'Fluorescence recovery after Photobleaching' (FRAP) on CeHDs using LET-805::GFP as a marker. There are four rows of CeHDs as previously described – two ventral and two dorsal. FRAP was performed separately on ventral and dorsal CeHDs (Figure 12). 30% recovery (mean mobile fraction) in fluorescence was observed in the wild type for both dorsal and ventral hemidesmosome after six minutes, whereas in the double mutant *egl-50; git-1*, an asymmetric recovery on ventral and dorsal hemidesmosome was observed. The ventral hemidesmosome fluorescence recovery decreased to 20%, while the fluorescence recovery at the dorsal hemidesmosome increased to 40% (Figure 13) as compared to the wild type. The implications and probable causes of symmetric recovery at the level of hemidesmosome in wild type and the symmetry breaking in the double mutant *egl-50; git-1* background will be discussed in the discussion section.

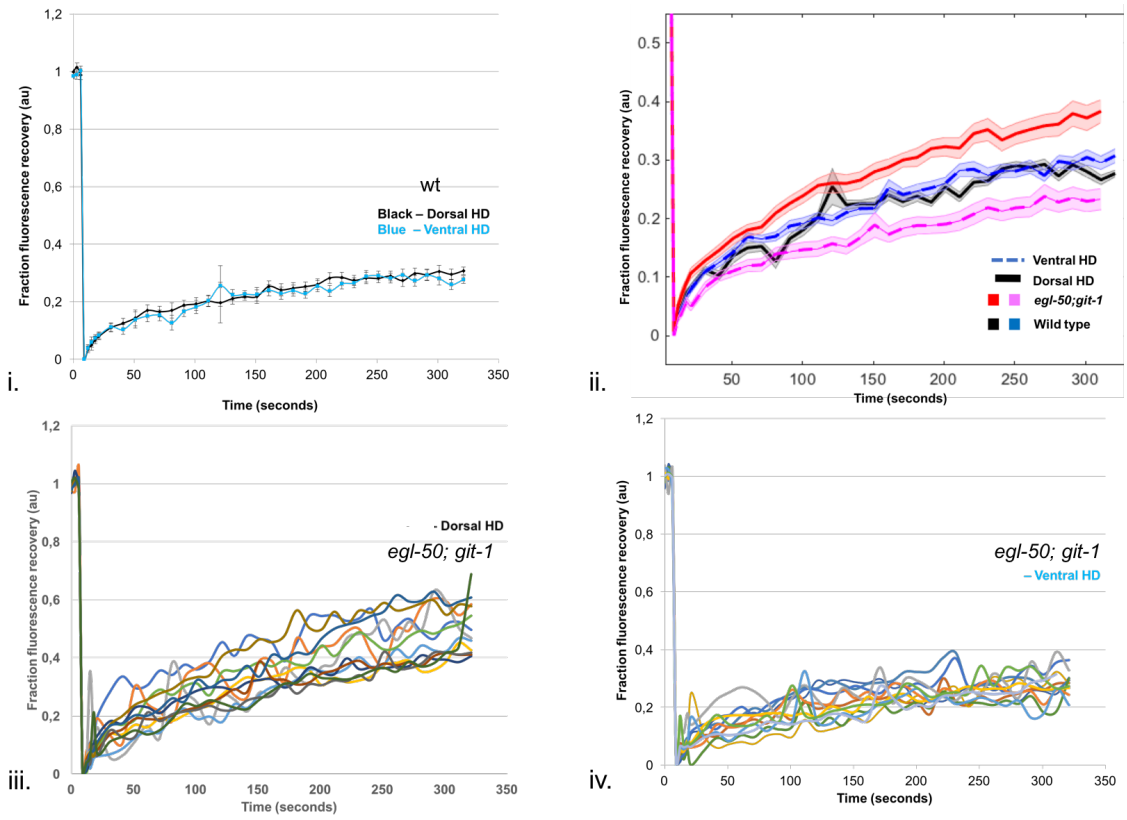

Figure 13. i. FRAP performed on the CeHDs using LET-805::GFP as a marker exhibited 30% fluorescence recovery rate in wild type background. The bars represent standard error.

ii. FRAP profiles of dorsal and ventral CeHDs in wild type compared to the *egl-50; git-1* mutant. The average recovery rate on ventral CeHDs in the *egl-50; git-1* decreases as compared to the *wt*, while the average recovery rate on dorsal CeHD in the *egl-50; git-1* increases as compared to the *wt*.

iii. Range of individual FRAP recovery curves from dorsal CeHD in *egl-50; git-1* background. The trend shows an increase in the recovery fraction of LET-805::GFP.

iv. Range of individual FRAP recovery curves from ventral CeHD marker in *egl-50; git-1* background. The trend shows the decrease of the fraction recovery.

6. Genetic interaction of the dynactin subunit *egl-50(n1086ts)* mutant and *cap-1(RNAi)* with *vab-10(Δsh3)* reveals apico-basal detachment of hemidesmosomes

At this point in this project, it had become very important to check the interactions of dynactin component *egl-50* with other known players involved in elongation. To determine this, I depleted dynactin subunits in combination with *vab-10* mutants. The *vab-10* gene encodes two sets of isoforms that are reminiscent of the spectraplakin proteins Plectin/BPAG1e (VAB-10A) and MACF1a/BPAG1a (VAB-10B) The VAB-10 proteins are essential to connect the epidermis to the cuticle apically and to the muscles basally in *C. elegans*. VAB-10A has actin and intermediate filament binding domains, whereas VAB-10B displays an actin and a microtubule binding domain (Figure 14) (Gally, Zhang et al. 2016). VAB-10A and B share a common N terminal part containing and Actin Binding Domain (ABD in short) and six spectrin repeats, one of which harbors a hidden SH3 domain; their distinct C terminal parts contain an intermediate filament-binding region for VAB-10A and a microtubule-binding domain for VAB-10B.

In a separate study from the lab. (Suman et al, unpublished data), the SH3 domain from spectrin repeat 3, present in both VAB-10A and VAB-10B was deleted (hereafter termed as *vab-10(Δsh3)*) using the CRISPR-cas9 genome editing method. Time lapse analyses of *vab-10(Δsh3)* revealed a wild type like growth curve with no obvious phenotypes but a strong genetic interaction with *git-1* and *pak-1* mutations characterized by elongation arrest slightly beyond the 2-fold stage. Combining *egl-50* with *vab-10(Δsh3)::mcherry; let-805::gfp* resulted in two-fold arrest of the embryos (Figure 7c). While there were no hemidesmosome defects either in *egl-50* or *vab-10(Δsh3)::mcherry*, 100% apico-basal detachment of both *vab-10* and *let-805* at the turn, at the level of hemidesmosomes, was observed for the double mutant (Figure 7b). A two-fold arrest was also seen by performing *cap-1 RNAi* in *vab-10(Δsh3)::mcherry* background (Figure 15).

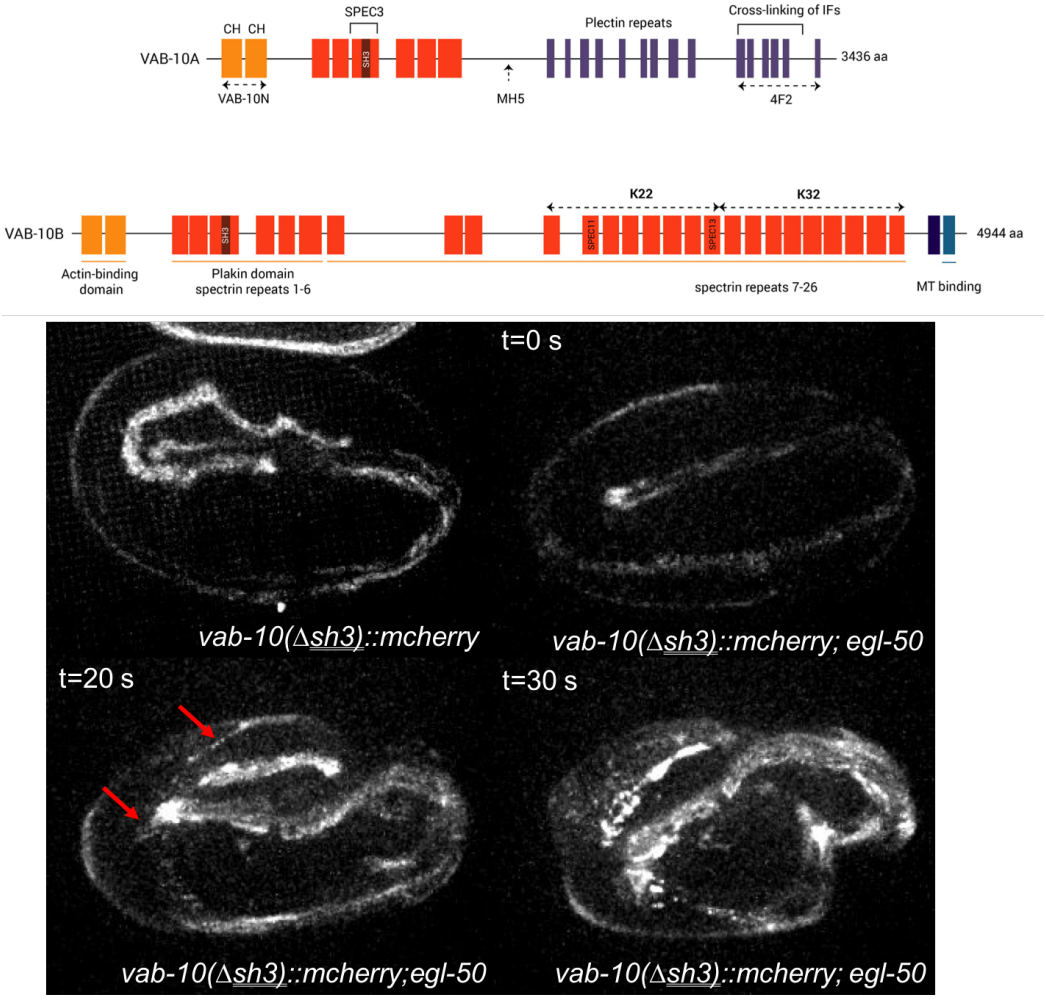

Figure 14. Schematic representation of the VAB-10A and VAB-10B major isoforms (Gally, Zhang et al. 2016). The hemidesmosomes labelled with *vab-10(Δsh3)::mcherry* do not show any defects in *vab-10(Δsh3)::mcherry* alone. Different time points of development, t=0s after the embryo reaches the 2-fold stage. At t=20s the hemidesmosomes start falling apart and are detaching apico-basally at the turn of the 2-fold embryo. d. t=30s CeHD starts deforming at multiple places.

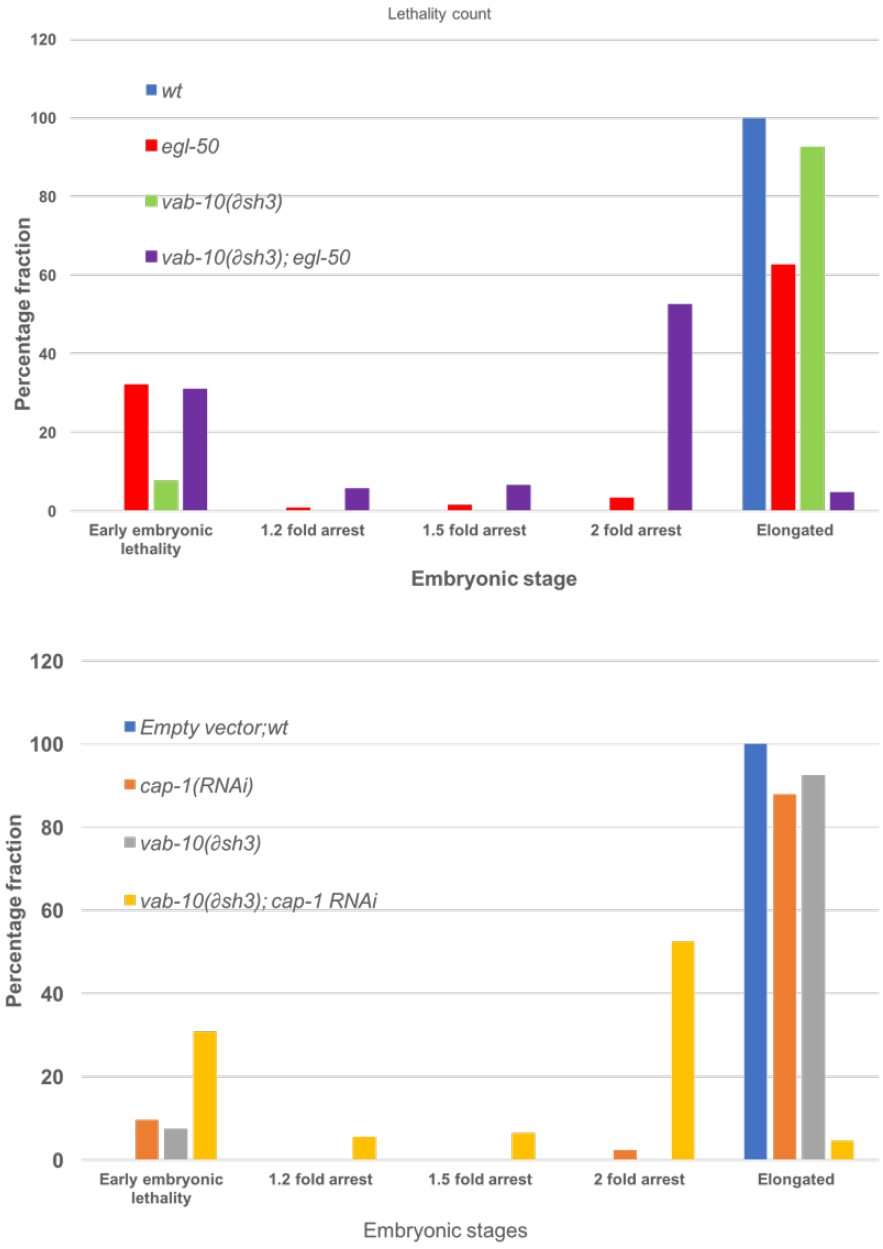

Figure 15. Embryonic lethality quantification. The double mutant *egl-50; vab-10(Δsh3)* arrests at two-fold, whereas either of the single mutants *egl-50(n1086)* (that pass early embryonic arrest) or *vab-10(Δsh3)* do not show arrest at that stage.
Embryonic lethality quantification. The depletion of *cap-1(RNAi)* in *vab-10(Δsh3)* embryos results in arrest at two-fold, whereas depletion of either one of the *cap-1(RNAi)* or *vab-10(Δsh3)* do not show arrest at the two-fold stage.

7. *sma-1(RNAi)* partially rescues the apico-basal detachment of hemidesmosomes in *vab-10(Δsh3); egl-50* double mutants.

To determine the possible cause of the apico-basal detachment of hemidesmosomes we performed a *sma-1(RNAi)* on the double mutant *vab-10(Δsh3); egl-50.* Indeed, it has been reported that loss of the *sma-1/ß$_h$-spectrin* chain can partly bypass the requirement for VAB-19 in elongation. VAB-19::GFP localize with the components of hemidesmosomes. *vab-19* mutants display actin alignment defects and muscle detachment. (Ding, Goncharov et al. 2003).

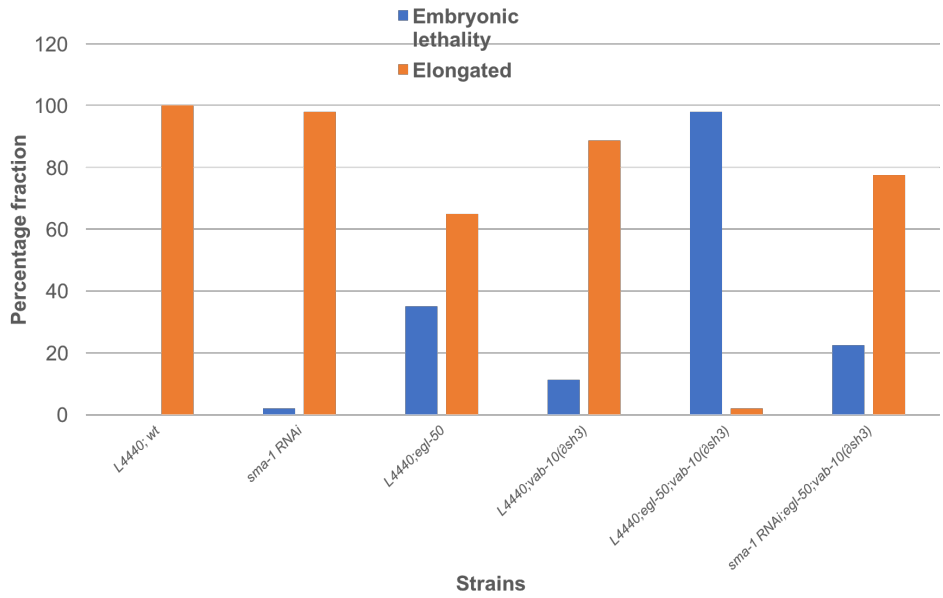

Figure 16. Embryonic lethality quantification (n>100, for all combinations). The double mutant *vab-10(Δsh3); egl-50* arrests at the two-fold stage, whereas neither of the single mutants *egl-50(n1086ts)* nor *vab-10(Δsh3)* show arrest at the two-fold stage. *sma-1* RNAi partially rescued the embryonic lethality of the double mutant *vab-10(Δsh3); egl-50.*

We can think of two reasons why *sma-1(*RNAi) can partially rescue the *vab-10(ΔSH3); egl-50* double mutants (i) either a slower rate of growth and elongation; or it acts antagonistic to *vab-19,* which might have localization defects in the double mutant. To determine which one of this hypothesis is indeed true, we created two further strains. The allele *sb118ts,* the temperature sensitive allele of *let-502* has been introduced in the double mutant. The *let-502(sb118ts)* mutation is known to slow the growth of the animal. A rescue by the *sb118* allele would hint at the slower growth rate as the main cause of the rescue of *vab-10(Δsh3); egl*-50 by *sma-1(RNAi).* On the other hand, we introduced the CRISPR/cas9 tagged *vab-19::mcherry* strain (Shashi et al, unpublished data) in egl-50; git-1 and *vab-10(Δsh3); egl-50* to check the levels of VAB-19 in both the strains (currently ongoing).

8. Genetic interaction of *egl-50(n1086)* with *spc-1* reveals defects in actin pattern.

Spectrin mutants arrest at the two-fold stage (Norman and Moerman 2002). As a continuation to verify if *egl-50* interacts with other known players of elongation, we studied the genetic interaction between *egl-50* and *spc-1*. A separate study from the lab has shown (Pasti and Lardennois, 2017, in preparation) that depletion of *spc-1* in *pak-1(ok448)* background leads to a retraction phenotype. The embryo grows up to the 1.5-fold stage and retracts back to almost the 1.2-fold stage. In continuation of our approach to connect multiple approaches to understand elongation in the lab, *spc-1 (RNAi)* was performed in the *egl-50* background. *egl-50* genetically interacted with *spc-1* in a in the similar fashion as *pak-1* interacts with *spc-1*, though not as strongly. Time lapse analyses revealed two phenotypes - a retraction phenotype as well as a two-fold arrest. The two populations were significantly different. The retracting to non- retracting embryos are present in 6:4 ratio in the population of elongating embryos (Figure 17 and 18). To determine if this interaction is *arp-1*-specific or if it extends to dynactin complex as a whole, we performed *spc-1 (RNAi)* in *dnc-1(or404ts)* background. Time lapse analyses revealed two phenotypes - a retraction phenotype as well as a two-fold arrest in *dnc-1(or404ts); spc-1(RNAi)* background. These results suggest that the dynactin complex as a whole genetically interacts with *spc-1*. *dnc-1* is another major subunit of dynactin and it showed a similar interaction with *spc-1* as that of *egl-50* (*spc-1* like non-retracting and *spc-1(RNAi); pak-1* like retracting), which suggests that interaction of *spc-1* is not *arp-1* subunit specific, instead, it is the dynactin complex that participates in this process as a whole.

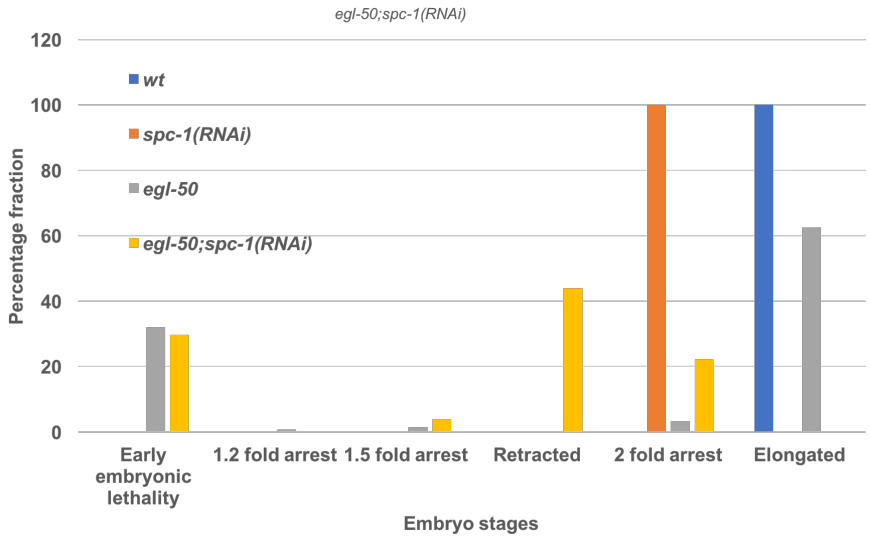

Figure 17. Embryonic lethality quantification. The percentage of retracting embryos increase when *spc-1(RNAi)* was performed in *egl-50* worms.

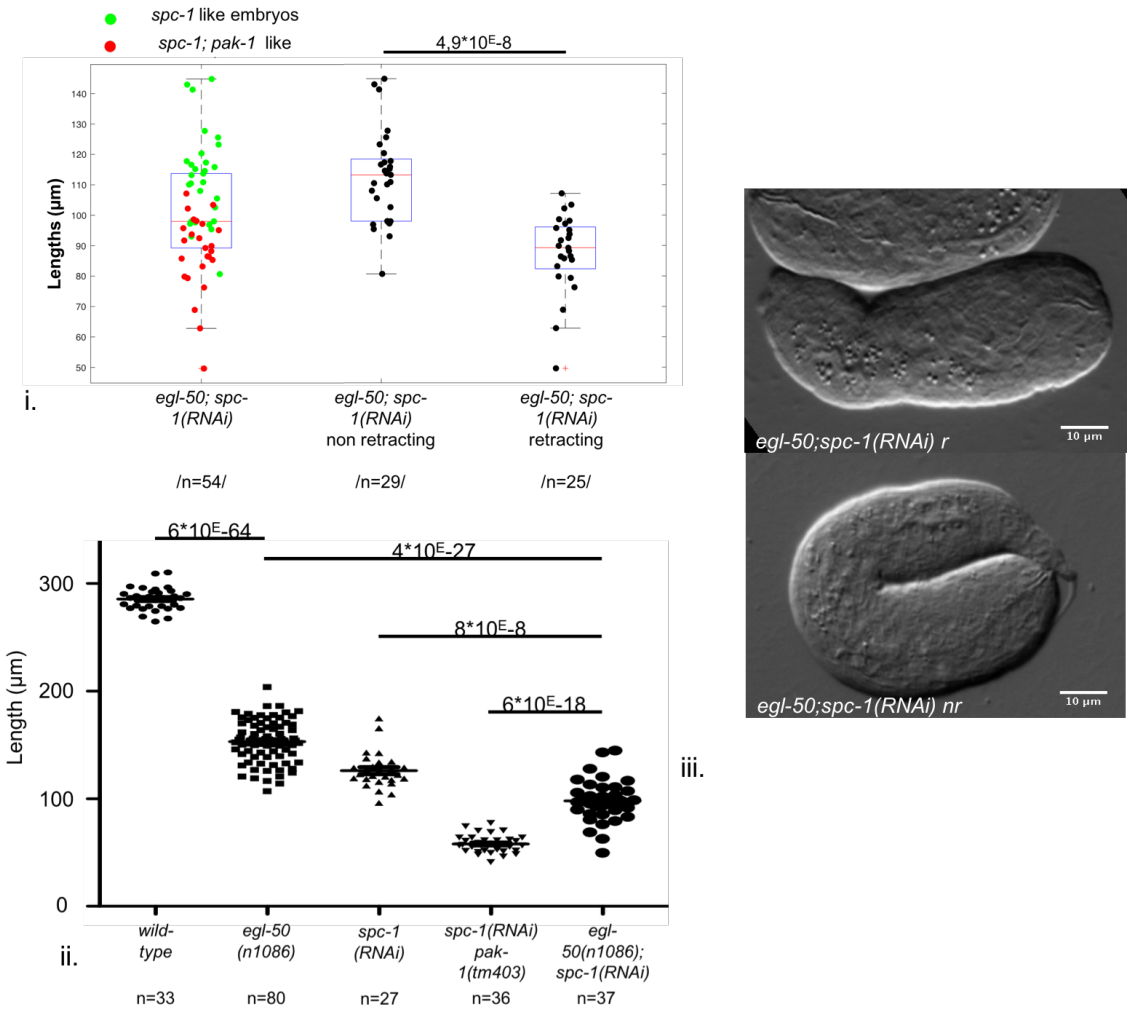

Figure 18. The length of the hatchlings was measured.

i. A closer inspection reveals that *egl-50; spc-1(-)* hatchlings display two populations – *spc-1(-)* like two-fold arrest and *spc-1(-); pak-1(-)* like retracting phenotype.

ii. *egl-50; spc-1(RNAi)* is significantly different from the *spc-1(RNAi)* treated embryos.

iii. The picture on the right (top) shows a hatchling from a retracted embryo (r), while the one below it is a hatchling from a 2-fold arrest non- retracting (nr) embryo.

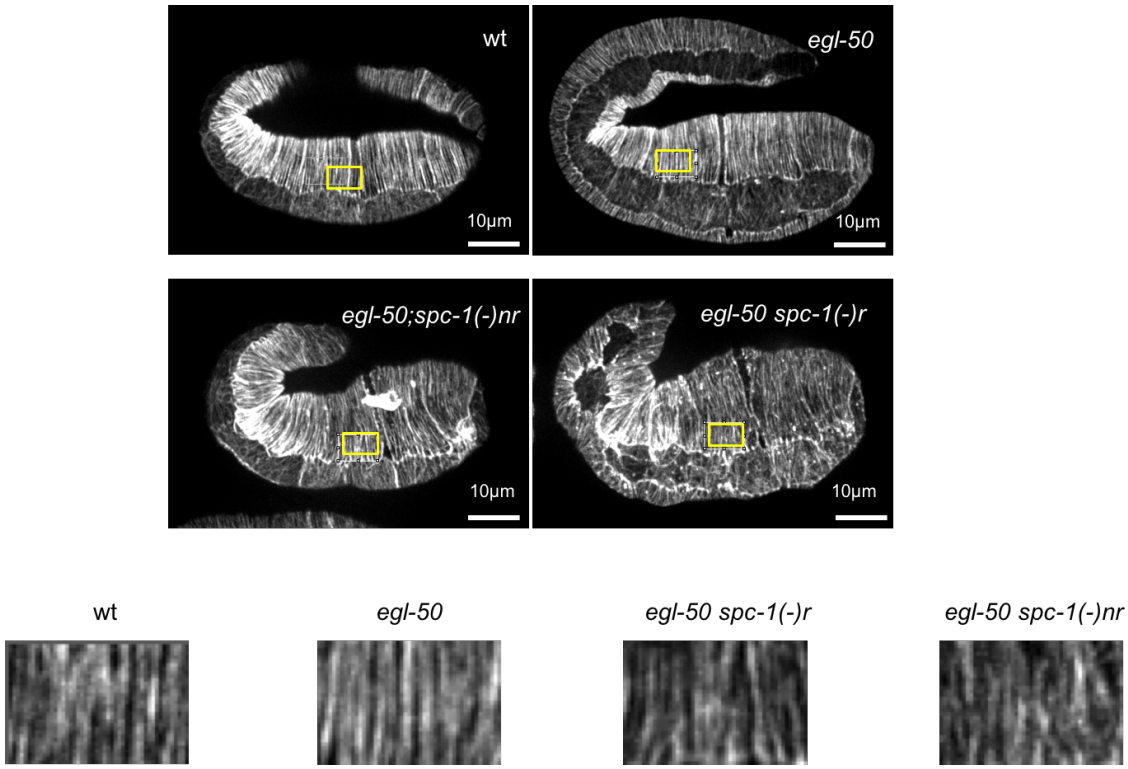

Figure 19. *egl-50; spc-1(-)* embryos. The actin pattern in the epidermis was imaged using *Pdpy-7::LifeAct::GFP*. A region of interest was chosen in dorso-ventral epidermis and both continuity analysis and orientation analysis was performed on this region.

Next, we analyzed the fluorescence signal (*Pdpy-7::LifeAct::GFP*) associated with actin filaments in the dorso-ventral epidermis. Lifeact is a 17-amino-acid peptide, which stains filamentous actin (F-actin) structures in eukaryotic cells and tissues. Lifeact does not interfere with actin dynamics in vitro and in vivo. Depletion of *spc-1* in *pak-1(ok448)* background shows actin orientation and continuity defects. The actin pattern was studied by using sleeping embryos imaged with a spinning-disk Zeiss microscope Axio Observer, using a 100X oil immersion objective (Figure 19). Continuity analysis is based on the distribution of actin segments based on their length, whereas the orientation analysis curves represent the number of the actin filaments oriented perpendicular to the elongation axis (Pasti and Lardennois, manuscript in preparation).

The *spc-1(RNAi); pak-1(-)* like retracted embryos of *egl-50; spc-1(RNAi)* revealed more discontinuity compared to controls and non-retracting *egl-50; spc-1(RNAi)* embryos. The retracting embryos of *egl-50; spc-1(RNAi)* also revealed an abnormal degree of anisotropy relative to the circumferential axis (Figure 20).

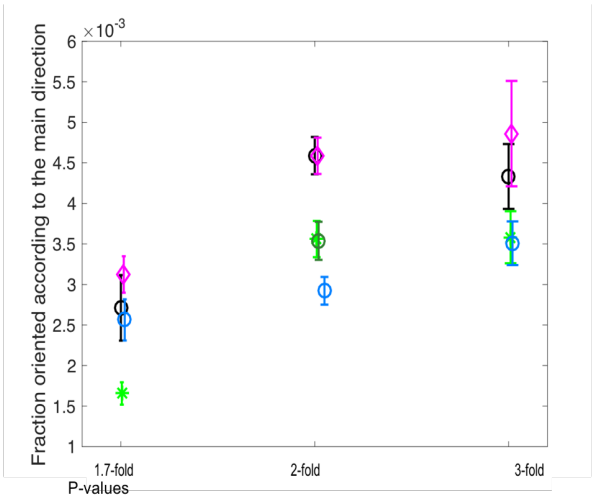

P-values

2f *egl-50; spc-1*r vs *egl-50;spc-1*nr	0.0321471
2f *egl-50;s pc-1r* vs *spc-1*	0.0242933
2f *egl-50; spc-1r* vs wt	2.85757e-07
2f *egl-50; spc-1r* vs *egl-50*	1.33333e-07
2f *egl-50; spc-1*nr vs *spc-1*	0.946822
2f *egl-50; spc-1*nr vs wt	0.0023479
2f *egl-50; spc-1*nr vs *egl-50*	0.00217561

r – retracting
nr – non-retracting

i.

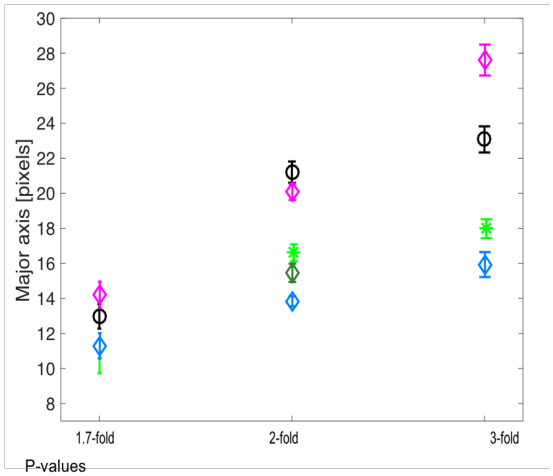

P-values

2f *egl-50r* vs *egl-50*nr	0.0228379
2f *egl-50; spc-1r* vs *spc-1*	0.000166
2f *egl-50; spc-1r* vs *egl-50*	6.69424e-17
2f *egl-50;spc-1r* vs wt	1.09698e-16
2f *egl-50; spc-1*nr vs *spc-1*	0.0686526
2f *egl-50; spc-1*nr vs *egl-50*	4.68848e-10
2f *egl-50; spc-1*nr vs wt	7.62793e-11

ii.

Figure 20. i. The orientation analysis performed on embryos from *egl-50; spc-1(RNAi)* in three stages of embryo development revealed defects in actin orientation at the 2-fold stage. The retracting embryos (blue) are significantly different from wild type (black), individual mutants *spc-1* (light green), *egl-50* (purple) and the non-retracting embryos (dark green). The non-retracting embryos behave the same as *spc-1(RNAi)* embryos. The P-values shown below the graph show that the difference among the wild type and mutants at 2-fold stage (n>10).

ii. The continuity analysis performed on embryos from *egl-50; spc-1(RNAi)* in three stages of embryo development revealed defects in actin continuity at 2-fold stage. The retracting embryos (blue) are significantly different from wild type (black), individual mutants *spc-1* (light green), *egl-50* (purple) and the non-retracting embryos (dark green). The non-retracting embryos behave the same as *spc-1(RNAi)* embryos. The P-values shown below the graph show that the difference among the wild type and mutants at 2-fold stage (n>10).

9. Is the 2-fold arrest of *egl-50; git-1* due to the microtubule dependent function of the Dynein/Dynactin?

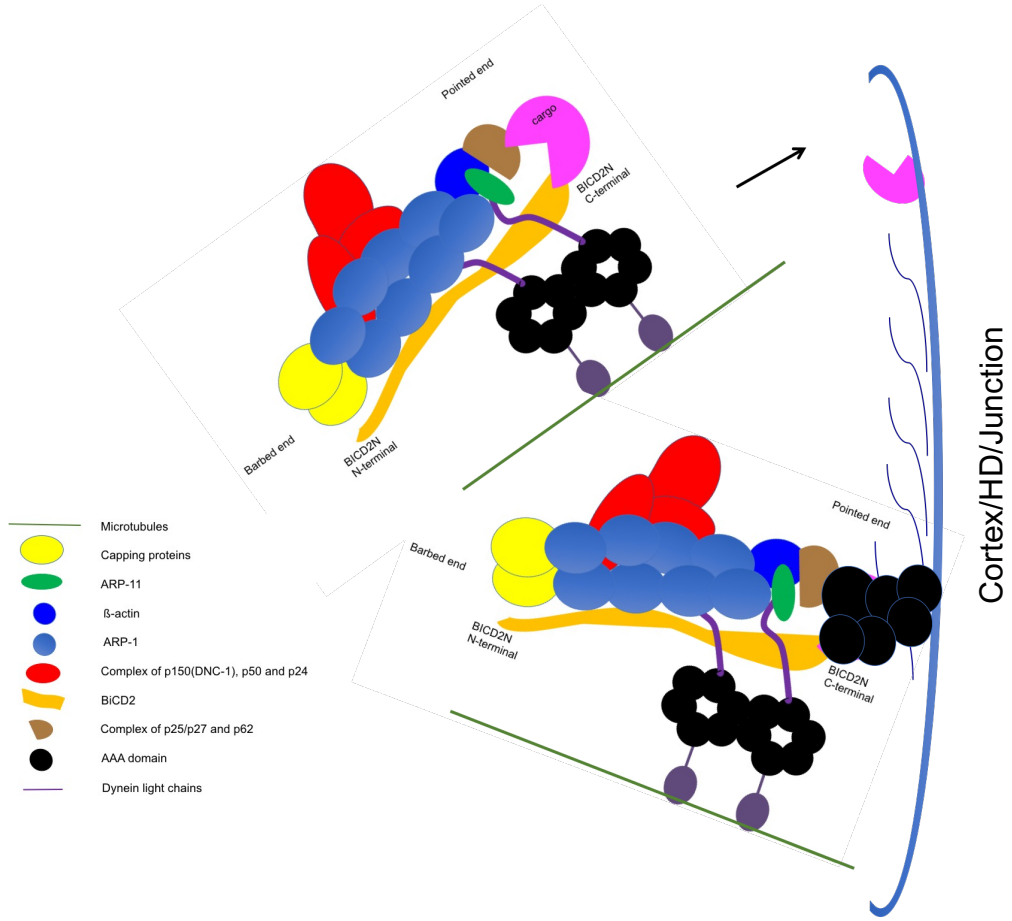

Figure 21. Two roles have widely been attributed to the dynein/dynactin complex as shown here in the cartoon. Transport of important components to structures such as the cortex, junctions and hemidesmosomes is one such role. In another role, the dynein complex can attach to the cortex and pull microtubules towards it, which is important during spindle positioning during the first *C. elegans* cell cycle.

The two potential roles of dynein/dynactin in embryonic elongation can be either transport of essential structural components or as a cortical anchor responsible for pulling and positioning structures such as nucleus and centrosome (introduced extensively in Introduction section of this thesis, Figure 21). Nevertheless, both the cytoplasmic transport and the cortical attachment roles of the dynein/dynactin require microtubules either as tracks or as pulling cables to facilitate the function of this complex. To determine whether microtubules are indispensable for the two-fold arrest phenotype observed in *egl-50; git-1* embryos and other dynactin mutants combined with *git-1/pak-1*

mutants, we disrupted microtubules. Microtubule disruption by use of inhibitors and drugs affected embryonic elongation to a variable extent, though less than actin (Priess and Hirsh 1986). One important shortcoming of using drug administration is that any elongation defect might be a result of disrupting microtubules in multiple tissues. Therefore, we used spastin expressed under *dpy-7* promotor (hereafter referred as spastin) (Quintin, Wang et al. 2016) to disrupt microtubules. Spastin is a microtubule severing protein, which can be used to force the disassembly of microtubules (Matsushita-Ishiodori, Yamanaka et al. 2007). The *dpy-7* promotor is specifically active in the epidermis, thereby ruling out the degradation of microtubules in other tissues (Quintin, Wang et al. 2016). To confirm the expression of spastin, we used an mCherry reporter coupled to spastin expression via an operon linker. Spastin larvae were significantly shorter than their wildtype counterparts (Figure 22) and I observed a synergistic embryonic lethality between spastin and *let-502(sb118ts)* (Figure 22) at 23°C as shown previously (Quintin, Wang et al. 2016). I performed *git-1/pak-1* RNAi in a strain expressing spastin under the *dpy-7* promoter and observed their embryonic lethality and did time lapse analyses. A two-fold arrest by microtubule disruption in *git-1/pak-1*(RNAi) would suggest the importance of dynein/dynactin as either important for transport or cortical tension. However, there was no significant increase in the embryonic lethality by *pak-1(RNAi*) in spastin. The spastin; *pak-1(RNAi)* embryos grew past 2-fold and hatched (Figure 22), thereby suggesting a microtubule independent role of dynactin complex.

To determine if the interaction of dynactin complex with *spc-1* is independent of microtubules, *spc-1 (RNAi)* was performed in Spastin-expressing embryos. Time-lapse analyses revealed that the absence of microtubules, along with *spc-1* depletion did not result in a retraction phenotype as observed for *egl-50; spc-1(RNAi)* (Figure 22).

This experiment suggests that dynactin has a microtubule independent role in embryonic elongation. A microtubule independent role would rule out not only the transport role of dynein/dynactin complex but also the cortical attachment function of this complex as microtubules are essential for both transport and cortical attachment. The microtubule independence of dynactin would imply a motor independent role of dynactin in our system. We decided to check this by using RNA interference of different subunits of dynein complex.

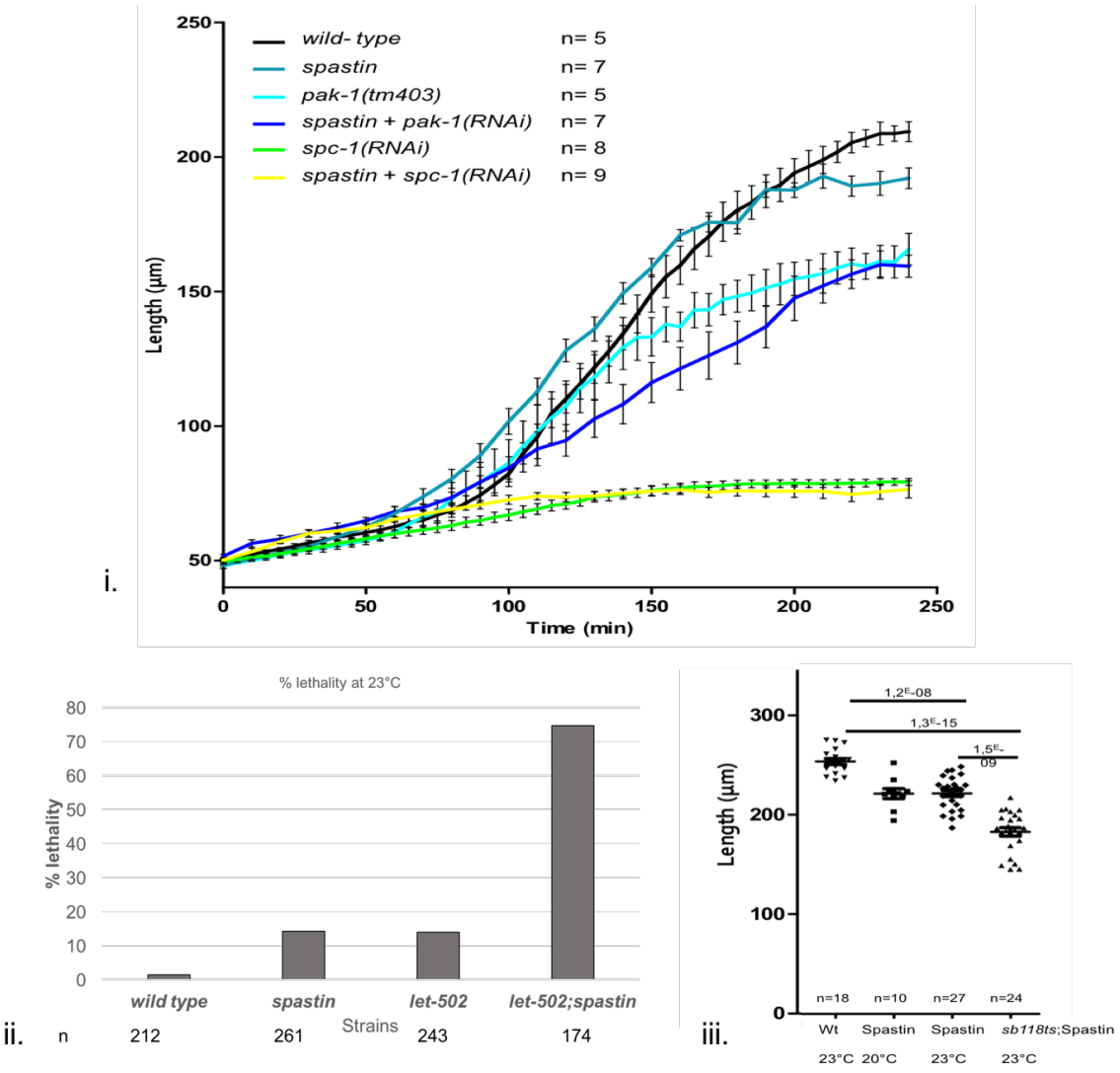

Figure 22. **i.** Growth curves in the absence of microtubules. *pak-1(RNAi)* in Spastin expressing embryos did not cause a 2-fold arrest. *spc-1(RNAi)* in Spastin-expressing embryos did not show a retraction phenotype. It shows only a *spc-1(-)* 2-fold arrest phenotype.

ii. The synthetic lethality increases at semi-permissive temperature of 23°C for *let-502(sb118ts); spastin* embryos as compared to spastin and *let-502(sb118ts).*

iii. Lengths of hatchlings were measured at 23°C (semi-permissive temperature for *sb118ts*). Spastin larvae are significantly shorter than wild type and *let-502(sb118ts)* as shown earlier (Quintin, Wang et al. 2016).

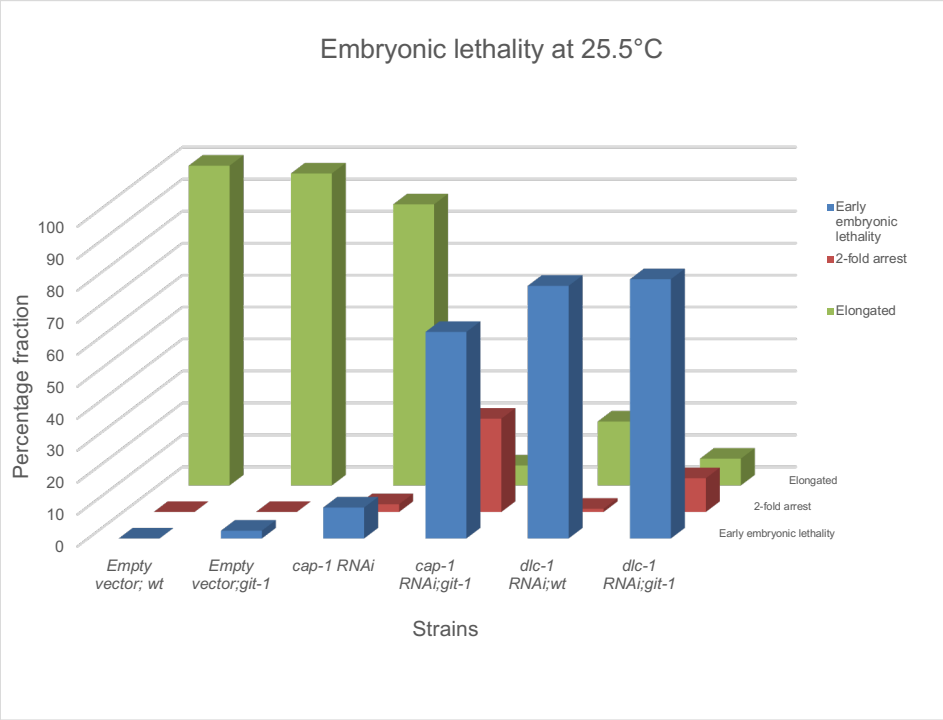

Figure 23. Embryonic lethality quantification (n>100, for all combinations). The depletion of DLC-1 by RNAi in *git-1(tm1962)* background resulted in percentage increase in arrest at two-fold. Although *dlc-1* RNAi alone leads to 80% embryonic lethality. The RNAi of *cap-1* induces an increase in 2-fold arrest in *git-1* background.

The RNAi of *dhc-1, the* dynein heavy chain essentially gives early embryonic lethality. Therefore, we relied on light chains' depletion. RNA interference depletion of *dlc-1*, the dynein light chain in *git-1(tm1962)* background yielded high percentage of early embryonic lethality and a small percentage of 2-fold arrest and elongated embryos (Figure 23). Nevertheless, *dlc-1* has a variety of roles besides being associated with dynein such as DLC-1 directly binds to the translational regulator FBF-2 outside of the RNA-binding domain and promotes FBF-2 localization and function (Wang, Olson et al. 2016). Furthermore, dynein light chains act as dynein heavy chain DHC-1 activators and inhibitors.

10. The expression profile of dynactin subunit cap-1 and dynein heavy chain *dhc-1* reveals differential expression in epidermis.

At this point, it was of our interest to look selectively at the expression of different dynein/dynactin components. The dynein heavy chain *dhc-1* subunit as used to visualize dynein, while dynactin subunit *cap-1* was used to visualize dynactin. CRISPR-Cas9 tagged genome edited strains carrying mCHERRY::DHC-1, dynein heavy chain (Schmidt, Fielmich et al. 2017) and CAP-1::GFP (from lab), were combined and tested for localization (Figure 24).

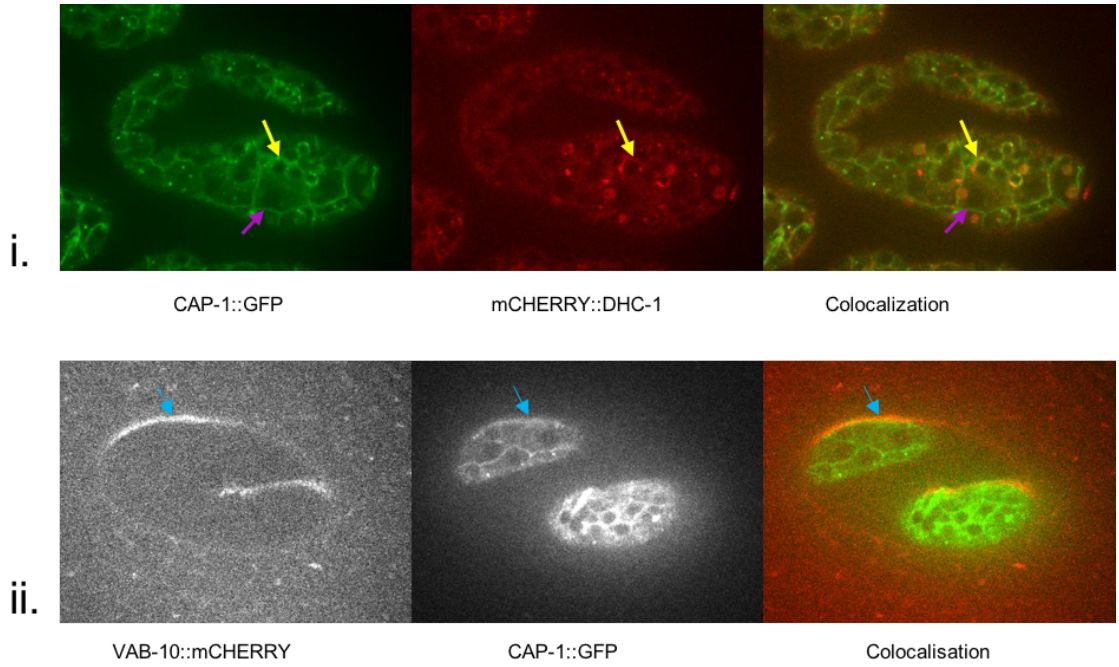

Figure 24. i. From left to right – CAP-1::GFP expression, expression of mCHERRY::DHC-1 and their colocalization. CAP-1 and DHC-1 do not colocalize (pink arrow) in the epidermis, whereas in the tissues underneath, CAP-1 and DHC-1 colocalize (yellow arrow). Z-projection of 5-6 focal planes are shown here. **ii.** From left to right – CAP-1::GFP localize with VAB-10 at the level of hemidesmosomes. Z-projection of 2-3 focal planes are shown here.

DHC-1 and CAP-1 colocalize in the tissues underneath epidermis. Cytoplasmic dynein is ubiquitously present in all the cell and tissue types. It is its association with dynactin which increases its processivity. A colocalization can be seen in the tissues beneath the epidermis. CAP-1 expressed with DHC-1 ubiquitously in all the tissues, but only CAP-1 localized at epidermal structures like junctions. The lateral cells can easily be visualized by CAP-1::GFP, while it was not the case with DHC-1 marker. DHC-1 does not localize with VAB-10 at the level of hemidesmosome, whereas CAP-1 localize with VAB-10 towards the basal side of the hemidesmosome. Tagging more components of dynactin and studying their localization compared to dynein would certainly increase our confidence in claiming that dynactin localization in epidermis is independent of dynein.

11. How do muscle contractions affect the localization of dynein/dynactin subunits?

Do muscle contractions affect the localization of the dynein/dynactin subunits? To investigate this we checked the expression of dynein heavy chain (DHC-1) using eGFP::DHC-1 marker generated by CRISPR-Cas9 method of genome editing (Schmidt, Fielmich et al. 2017) and dynactin capping subunit CAP-1 using CAP-1::GFP marker generated by CRISPR-Cas9 method of genome editing in our lab. To determine the effect of muscle contractions on the expression of dynein/dynactin subunits, *unc-112(RNAi)* was performed on worms expressing *cap-1::gfp* and *dhc-1::gfp* to paralyze the muscles. Accumulation of the CAP-1 and DHC-1 at the levels of muscles is lost in muscle paralyzed *unc-112*(RNAi) embryos (Figure 25).

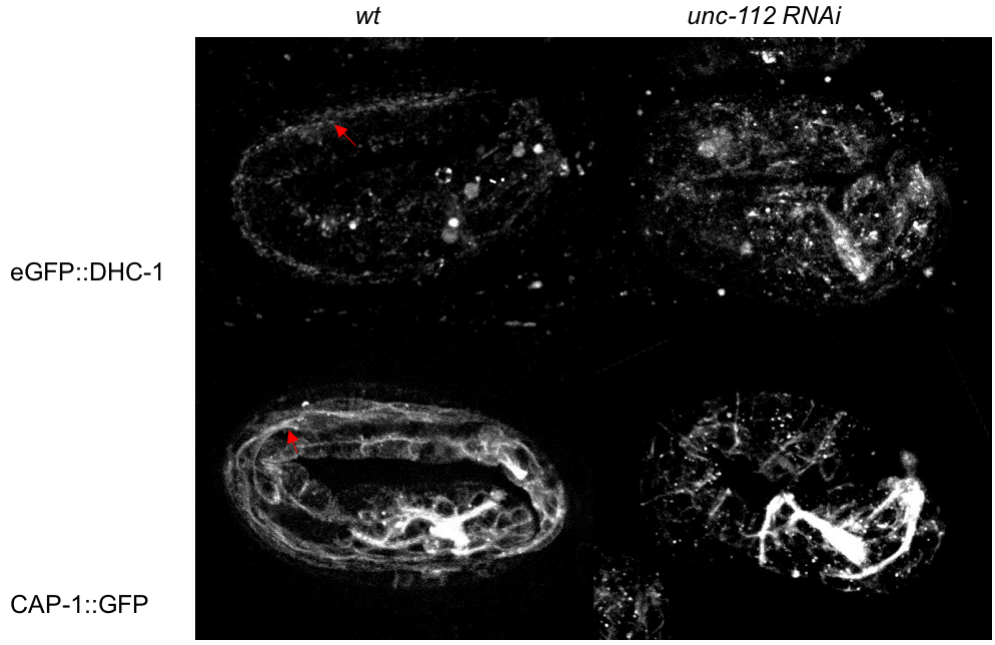

Figure 25. Accumulation of CAP-1 and DHC-1 at the levels of muscles is lost in muscle paralyzed *unc-112(RNAi)* embryos. The images were subtracted for the background intensity to visualize fluorescence intensity at the level of muscles. The red arrows point to the muscle. Note that in *unc-112 RNAi* embryos, the expression at the level of muscles decreases for both CAP-1 and DHC-1.
Top panel – Left. Wild type expression of DHC-1 at the level of muscles. Right. Expression of DHC-1 in *unc-112(RNAi)* treated embryos.
Bottom panel – Left. Wild type expression of CAP-1 at the level of muscles. Right. Expression of CAP-1 in *unc-112(RNAi)* treated embryos.

Since DHC-1 and CAP-1 are expressed everywhere in the embryo being subunits of a major transport complex in all tissue types, the background from the images was subtracted using Image J to see their expression at the level of muscles. This experiment suggests that muscle contractions are necessary to localize dynein/dynactin at the level of muscles.

12. Rescue experiments

To examine the tissue specific requirement of *arp-1* activity in muscles or epidermis, rescue experiments with epidermal and muscle promotors were performed. We cloned the coding part of the *arp-1* gene under the *dpy-7* promotor (Gilleard, Barry et al. 1997) to express it in epidermis and under *myo-3* promotor (Merris, Kraeft et al. 2004) to express it selectively in muscles. The *arp-1* sequence was cloned from genomic DNA and its introns were deleted before inserting under respective promotors. The constructs were injected individually in young adults of *egl-50; git-1* double mutant with injection marker. The transgenic lines with epidermal expression alone, muscle expression alone and both epidermal and muscle expression were created. The lethality count was performed on transgenic *egl-50; git-1* double mutants along with *egl-50; git-1* without any construct as control (Figure 26). The muscle promotor did not rescue the two-fold arrest of the double mutant *egl-50; git-1.*

From this result, we deduce that the 2-fold arrest phenotype is not because of *arp-1* function in muscles. We speculate that its function is essential in epidermis of *C. elegans* embryos (results awaited).

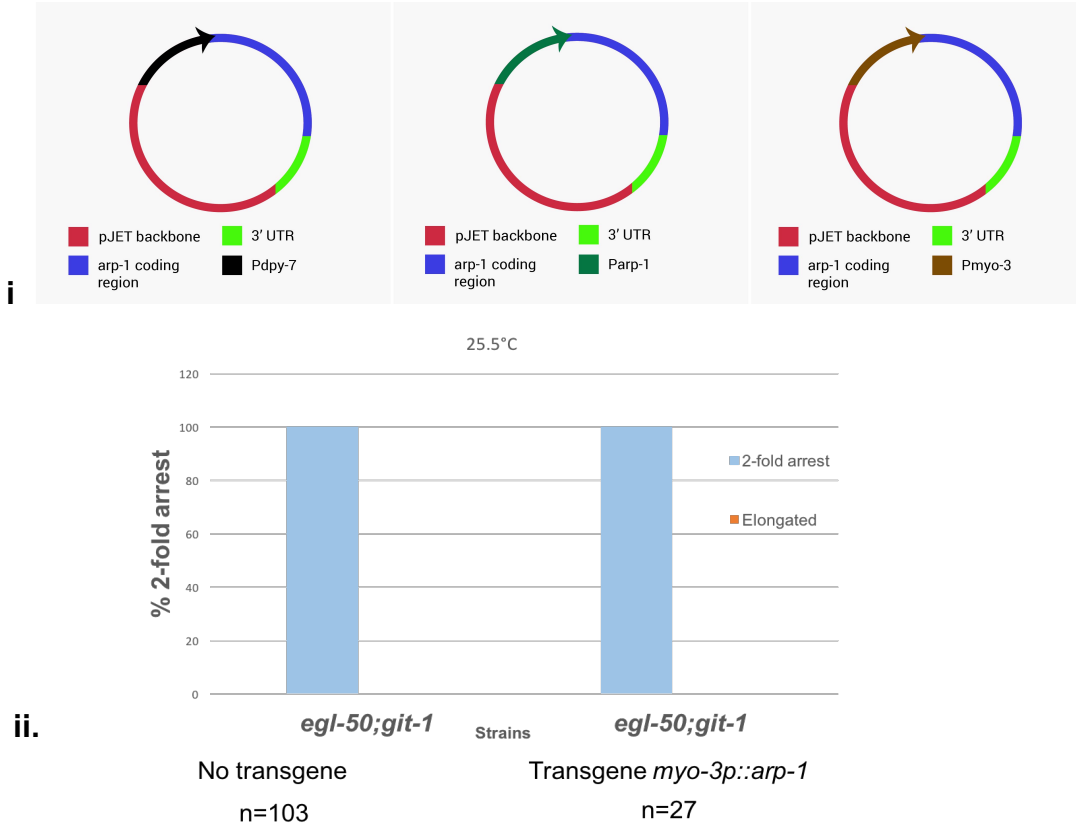

Figure 26. **i**. The schematic of the constructs designed for the rescue experiments.
ii. The transgene *myo-3p::arp-1* did not rescue the double mutant *egl-50; git-1*. None of the embryos that reached 2-fold stage, were able to go beyond this stage and elongate further.

Table 2. List of candidates obtained from Genome wide RNAi screen in *git-1(tm1962)* background

- EEL Early Embryonic Lethality
- BMD Body Morphology defect
- MM Maternal mortality
- NA Not applicable/No result
- LAL Larval lethal
- VLP Very low Progeny
- Nd Not determined
- EGL Egg laying defective

S.no.	Genes	Function	*N2*	*egl-19*	*git-1*
1	*cap-2*	Capping protein	BMD 2-3 fold	10% EEL	100% BMD 2-3 fold
2	*cap-1*	Capping protein	WT	20% EEL	80% BMD 1-3 fold
3	*eps-8*	Capping Protein	WT	WT	20% BMD 2-fold
4	*farl-11*	Cell cycle Suppress DHC lethality	WT	WT	80% BMD 2-fold
5	*F33H1.3*	Collagen and cuticulin-based cuticle development, RNA processing	20% EEL + 20% BMD 2-3-fold	WT	10% EEL + 60% BMD 2-3-fold
6	*dlc-1*	Dynein DLC	10% EEL + 60% BMD 2-fold	40% EEL +20% BMD 2-3 fold	70% BMD 2-fold
7	*paa-1*	Phosphatase 2A	80% EEL + 5 10% BMD 2-fold	90% EEL	VLP + 20% EEL + 60% BMD 2-3-fold
8	*mlt-11*	Serine protease inhibitors	10 20% BMD 2-3-fold	50% EEL + L1 L2 sick	60% BMD 2-3-fold
9	*gei-4*	WAVE/SCAR Intermediate filaments binding protein, forms complex with GEX-2/3	30% EEL	80% EEL + BMD	VLP + 20% EEL + 70% BMD 2-3 fold
10	*wve-1*	WAVE/SCAR Actin nucleation	WT	10% EEL	5 30% BMD 2-3 fold
11	*gex-3*	WAVE/SCAR	WT	WT	WT
12	*mom-5*	Wnt signaling	Egl and	50% EEL	10 50%

			BMD	+ 20% BMD 2-3-fold	BMD 2-3-fold
13	*F54D5.5*	?	WT	WT	30% BMD 2-3 fold
14	*spc-1*	Spectrin alpha	80% (2-fold)	90% arrest +2-fold	100% 1-2 f arrest
15	*sma-1*	Spectrin beta-H	70% Sma (3 fold)	100% Sma	100% arrest at 2-fold
16	*cdc-25.2*	Phosphatase	50% L1 sick	5% EEL + BMD 2-fold	100% L1 court (3-fold)
17	*emb-4*	RNA binding intron-binding spliceosomal	WT	WT	80% BMD 3-fold
18	*xpo-1*	Exportin-1	30% EEL + 30% BMD 2-3-fold	70% EEL	VLP + 20% EEL + 50% BMD 2-fold
19	*sec-24.2*	ER to Golgi vesicle-mediated transport	20% EEL	70% EEL + 20% BMD 2-fold	40% BMD 2-3 fold
20	*hmp-2*	Beta cat Actin anchoring	40% BMD 1-2-fold	60% BMD 1f	60 70% BMD 1-2-fold
21	*let-268*	Collagen Biosynthesis	WT	30% BMD 2-3 fold	30% BMD 2-3 fold
22	*cdk-2*	cell cycle	50% BMD 2-3-fold	WT	50% BMD 2-fold
23	*cye-1*	cell cycle	30% BMD 2-3 fold	70% BMD 2-3 fold	10% EEL + 60 80% BMD 1-2-fold
24	*cdtl-7*	Cell cycle Cyclin-dependent kinase	Egl BMD 2-fold	20% BMD 1-3-fold	5% EEL + 60% BMD 2-3 fold
25	*swsn-7*	Chromatin remodeling	Sick + 20% BMD 2-3-fold + 10% EEL	70% EEL	5% EEL + 95% BMD 2-3-fold
26	*egl-27*	Chromatin remodelling	50% BMD 2-3-fold	70% BMD 2-fold	10% EEL + 80% BMD 1-2-fold
27	*trr-1*	Chromatin	WT	30% EEL	90% BMD

		remodelling		+ 30% BMD 2-fold	2-3 fold
28	*sqt-3*	cuticle collagen	70% BMD 3-fold with big head	100% BMD 3-fold with big head	80% BMD 3-fold (big head)
29	*sex-1*	DNA-binding protein nuclear hormone receptor of transcriptional regulators	WT	5 20% BMD 3-fold	80% BMD 2-3-fold
30	*ima-3*	Importin alpha nuclear transport factors	WT	5 10% EEL + BMD 2-fold	30% BMD 2-3-fold
31	*pat-3*	Integrin beta-	80% EEL	MM + 99% EEL	VLP + 40% BMD 2-3-fold
32	*ifa-3*	Intermediate filament HD components	20% BMD 2-3-fold	50% BMD 2-fold	40% BMD 2-fold
33	*Y19D2B.1*	Microtubules	10% EEL + BMD	60% EEL + BMD	5% EEL + 20% BMD 2-3 fold
34	*sap-49*	RNA binding Splicing factor	VLP + 80% EEL	80% EEL	50% EEL + 30% BMD 2-3-fold
35	*mex-6*	RNA binding Downstream of Par	40% EEL + 20% BMD 2-3-fold	60% EEL	20% EEL + 40% BMD 2-fold
36	*T12A2.7*	RNA binding Splicing factor	30% EEL + 30% BMD 2-3-fold	50% BMD 2-fold	5% EEL + 50% BMD 2-3-fold
37	*C55A6.9*	RNA polymerase II-associated factor 1	30% EEL + 70% 2-fold arrest	60% EEL + 40% BMD 2-3-fold morte	VLP + 70% EEL + 30% BMD 2-3-fold mort
38	*F25B3.6*	RNA polymerase-associated protein	20% BMD 2-3-fold	10% EEL + BMD 2-fold	30 50% BMD 3-fold
39	*pax-3*	Transcription factor DNA binding	10% EEL	20% BMD 2-3-fold	40% BMD 2-3-fold
40	*zyg-12*	HoWT Protein Required for nulear	40 60% EEL + 2	40% EEL + 30%	40 60% EEL + 5%

		and centrosome attachment and recruit DHC to nuclear envelop	15% BMD 3-fold	BMD 1-3-fold	BMD 2-3-fold
41	*pat-4*	Integrin Adhesion complex	30% BMD 2-3 fold	10% EEL + 10% BMD 2-3 fold	10% BMD 2-fold
42	*pat-2*	integrin alpha	70% BMD 2-3 fold	20% BMD 2-fold	40 60% BMD 2-fold
43	*mua-6*	Intermediate filament	NA	NA	NA
44	*knl-3*	Kinetochore formation	WT	60% EEL	10% EEL + 20% BMD 2-3-fold
45	*let-805*	Myotactin HD components	80% BMD 2-3 fold	MM + VLP + 100% BMD 2-fold	95% BMD 2-fold
46	*par-3*	PDZ domain-containing protein	40% EEL	70% EEL	20% EEL + 5% BMD 2-3-fold
47	*rpn-9*	Proteasome	WT	WT	10% BMD 2-3-fold
48	*lov-1*	Protein Binding	30% EEL + 70% BMD 2-fold	80% EEL + 15% BMD 2-3-fold	90% EEL + 10% BMD 1-2-fold
49	*pat-9*	Transcription factor nuclear zinc finger protein	30 50% BMD 2-fold	60 70% BMD 2-fold	70% BMD 2-fold
50	*hlh-1*	Transcription factor Regulation of muscle differentiation	40 60% BMD 2-fold	70% BMD 2-3 fold	60% BMD 1-2-fold
51	*pal-1*	Transcription factor	100% EEL (2-fold)	100% EEL	100% EEL
52	*tbx-33*	Transcription factor	30% EEL + 30% BMD 1-2-fold	70% EEL + BMD	20% EEL + 20% BMD 1-2-fold
53	*sknr-1*	Transcription factor	80% EEL + 20% L2 let	70% EEL + 30% arrest 1,5f rest	VLP + 20% EEL + BMD
54	*hbl-1*	Transcription factor	20% BMD 2-3-fold	10% BMD 2-3-fold	60% BMD 2-3-fold arrest

55	*F28C6.1*	Transcription factor	10 30% EEL + 50% BMD 2-3-fold	70% EEL	40% EEL + 50% BMD 2-3-fold
56	*tni-1*	Troponin	50% BMD 2-fold	50% BMD 2-fold	80% BMD 2-fold
57	*lin-23*	Ubiquitin Complex	10% EEL + 15 20% BMD 2-3-fold	60% EEL + BMD 3-fold	10% EEL + 20 70% BMD 2-3-fold
58	*par-2*	Ubiquitin protein ligase	50% EEL + BMD 3 fold	60% EEL + BMD	40 60% EEL + 10 20% BMD 2-fold
59	*unc-45*	Ubiquitin protein ligase binding	20% BMD 2-fold	5% EEL + 50% BMD 2-fold	10% BMD 2-3 fold
60	*mom-5*	Wnt signaling	5% EEL + 10% BMD 2-fold	50% EEL + 30% BMD 1-3-fold	10% EEL + 5% BMD 1-2-fold
61	*acdh-1*		WT	WT	WT
62	*inx-14*		40% EEL + 5% BMD 2-fold	20% EEL	15 20% EEL + 5% BMD 2-fold
63	*apb-3*	Adaptin Adaptor protein complex 3	BMD in the mothers	WT	BMD
64	*ztf-11*		5% EEL	30% EEL + BMD	5% LPE + 20% BMD 3-fold
65	*aph-2*		Mothers EGL but embryos WT	10% EEL	WT
66	*tct-1*		WT	WT	WT
67	*vab-19*		WT	WT	20% BMD 2-3-fold
68	*cdc-42*		10% BMD 3 fold	WT	5 30% BMD 2-3 fold
69	*mel-11*		40% EEL	WT	10% EEL + BMD
70	*F32A11.4*		60% EEL	70% EEL	VLP + 20% EEL + 20%

					BMD 2-3-fold
71	*tbx-33*		30% EEL + 30% BMD 1-2-fold	40% EEL + BMD	20% EEL + 20% BMD 1-2-fold
72	*emb-4*		WT	WT	5 20% BMD 1-3-fold
73	*C27F2.7*	?	5% EEL + BMD	10% BMD 2-fold	WT
74	*apb-1*	Adaptin Adaptor protein complex 1	50% EEL + L1 sick	70% EEL + 10% BMD 2-3-fold	50% EEL + 30% BMD 2-3-fold+L1 sick
75	*apg-1*	Adaptin AP-1 complex recycling	L1 sick	70% EEL + 20% BMD 2-3-fold	10% EEL + 90% BMD 2-3-fold
76	*ani-1*	Anillins	20% EEL + L1 un peu court 80%	80% EEL + 10% BMD 2-3-fold	20% EEL + L1 70% plus courts (3-fold)

Discussion

Supplementary Results

1. **CRISPR-Cas9 tagging of CeHD component *let-805* with photo convertible marker.**

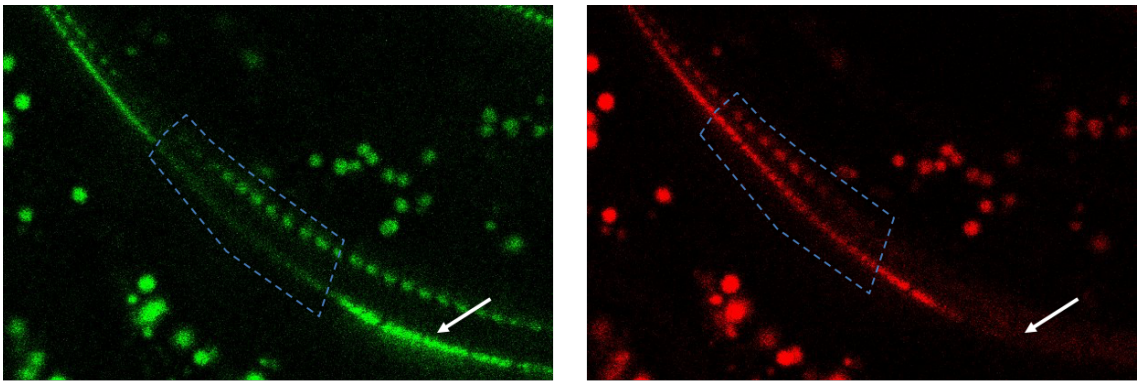

Figure 1. The picture on the left shows the hemidesmosome of a sleeping adult *C. elegans* as seen from a green channel after photo conversion. The dashed box shows the area illuminated by UV light. The picture on the right shows the same area imaged in the red channel. The white arrows show the area not illuminated by the UV light and thus no photo conversion and no signal in the red channel.

The muscles start contracting at 1.7-fold stage in *C. elegans* embryo. It was in our interest to check the dynamics of CeHD proteins under muscle tension. But the muscle contraction is too fast, and therefore the FRAP studies using LET-805::GFP cannot be performed on these moving embryos. Therefore, to probe effect of muscle contraction on dynamics of CeHD protein LET-805, we introduced mMaple3, a photo convertible protein which turns to red from green on being illuminated by UV light (Wang, Moffitt et al. 2014) by using the CRISPR-Cas9 gene editing technique. We codon optimized the mMaple3 sequence according to *C. elegans* genome before inserting it on the C-terminal of LET-805. As is shown here, the protein photo converts quite nicely, nevertheless, in a live wild type embryo, the movements are still too strong to get any meaningful data out of it.

2. CRISPR-Cas9 tagging of CeHD component *ifb-1*.

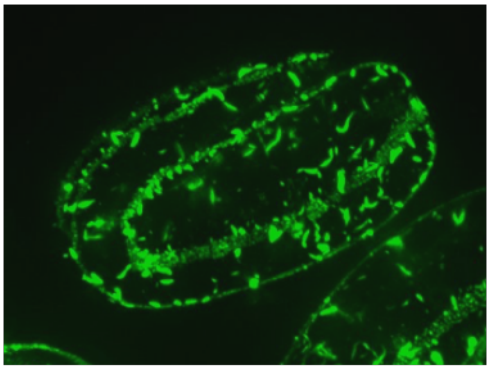

Figure 2. GFP was inserted on the C-terminus of *ifb-1* using the CRISPR-Cas9 gene editing technique. A 2-fold embryo showing IFB-1::GFP

In this study we had the tool to visualize the basal side of the CeHD – LET-805::GFP (created in the lab, before this study), we created the apical side marker –MUP-4::GFP using the CRISPR-Cas9 gene editing technique. Intermediate filaments were the last component to be tagged to visualize all aspects of CeHD. We successfully edited the *ifb-1* locus and inserted the GFP on the C-terminal of IFB-1 using the CRISPR-Cas9 gene editing technique. Though the IFB-1 shows ectopic localization and therefore, we did not use this in our study.

3. Creation of a CeHD marker for actin related protein *arp-1*.

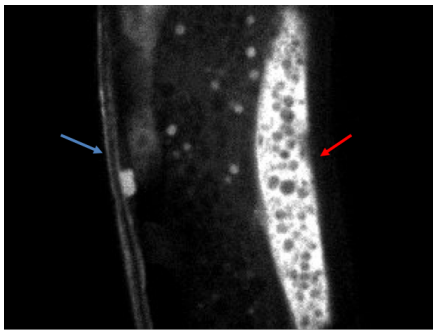

Figure 3. A gonad (red arrow) and CeHD (blue arrow) as seen by GFP::ARP-1 in an adult *C. elegans*.

Arp-1 is actin related protein and its DNA sequence is 55-60% similar to actin genes. Moreover, similarity of its DNA sequence with the sequence of other actin related proteins is also quite high. Therefore, it had been quite tough to clone a repair template for this gene. After multiple unsuccessful attempts at introducing a tag at arp-1 locus using the CRISPR-Cas9 gene editing technique, we finally have a positive hit.

4. The expression level of *farl-11* decreases in *pak-1(ok448)* mutants.

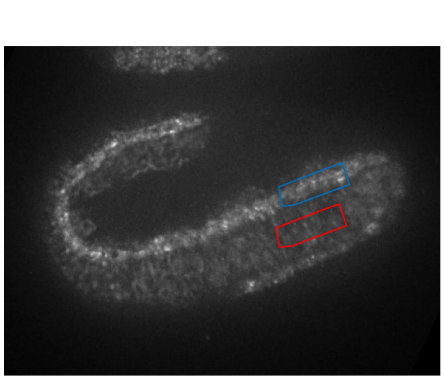

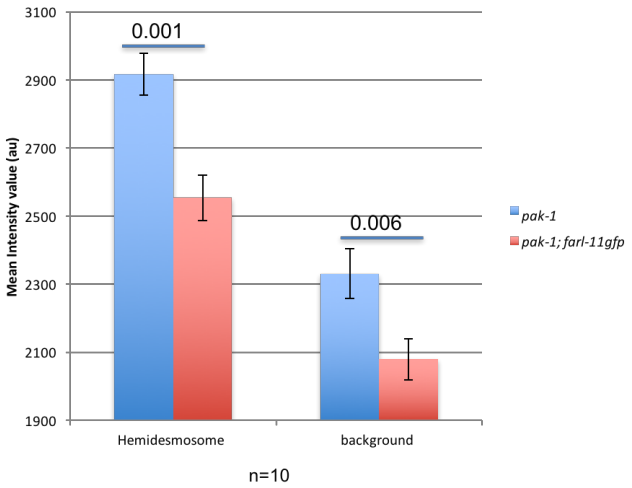

Figure 4. A two-fold embryo with FARL-11::GFP. Intensity measurement both at the level of CeHD and background, show decrease in intensity.

We measured the intensity at the level of hemidesmosomes (blue box) and the background (red box) in *pak-1(ok448)* mutant. The intensity decreases at both the places significantly, which shows that the overall expression of the FARL-11::GFP decreases in *pak-1(ok448)* mutant.

5. The expression level of *ral-1* decreases in *ral-1(RNAi)* worms

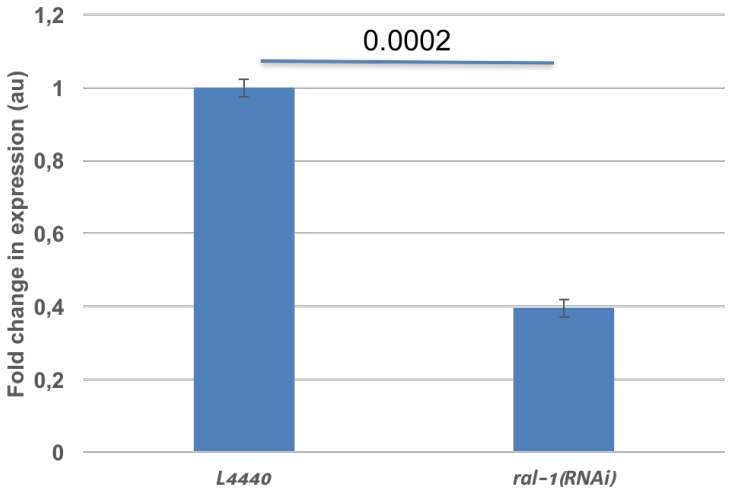

Figure 5. The expression of ral-1 significantly decreases as compared to the control.

I performed the qPCR analysis to verify the authenticity of RNA interference of *ral-1*. (Hyenne, Apaydin et al. 2015). I used *eif-3f* and *act-1* as reference genes for this quantification.

Bibliography

References

Afzelius, B. (1976). "[What happens when the cilia remain immobile?]." Lakartidningen **73**(7): 509-510.

Afzelius, B. A. (1976). "A human syndrome caused by immotile cilia." Science **193**(4250): 317-319.

Afzelius, B. A., R. Eliasson, O. Johnsen and C. Lindholmer (1975). "Lack of dynein arms in immotile human spermatozoa." J Cell Biol **66**(2): 225-232.

Aldaz, H., L. M. Rice, T. Stearns and D. A. Agard (2005). "Insights into microtubule nucleation from the crystal structure of human gamma-tubulin." Nature **435**(7041): 523-527.

Astumian, R. D. (2017). "How molecular motors work - insights from the molecular machinist's toolbox: the Nobel prize in Chemistry 2016." Chem Sci **8**(2): 840-845.

Beck, K. A., J. A. Buchanan, V. Malhotra and W. J. Nelson (1994). "Golgi spectrin: identification of an erythroid beta-spectrin homolog associated with the Golgi complex." J Cell Biol **127**(3): 707-723.

Bennett, V. and D. M. Gilligan (1993). "The spectrin-based membrane skeleton and micron-scale organization of the plasma membrane." Annu Rev Cell Biol **9**: 27-66.

Blum, J. J. (1973). "ATPase activity of Tetrahymena cilia before and after extraction of dynein." Arch Biochem Biophys **156**(1): 310-320.

Bonfanti, P., A. Colombo, M. B. Heintzelman, M. S. Mooseker and M. Camatini (1992). "The molecular architecture of an insect midgut brush border cytoskeleton." Eur J Cell Biol **57**(2): 298-307.

Bosveld, F., I. Bonnet, B. Guirao, S. Tlili, Z. Wang, A. Petitalot, R. Marchand, P. L. Bardet, P. Marcq, F. Graner and Y. Bellaiche (2012). "Mechanical control of morphogenesis by Fat/Dachsous/Four-jointed planar cell polarity pathway." Science **336**(6082): 724-727.

Broadie, K., S. Baumgartner and A. Prokop (2011). "Extracellular matrix and its receptors in Drosophila neural development." Dev Neurobiol **71**(11): 1102-1130.

Burns, R. G. and T. D. Pollard (1974). "A dynein-like protein from brain." FEBS Lett **40**(2): 274-280.

Burns, R. G. and D. Starling (1974). "The in vitro assembly of tubulins from sea-urchin eggs and rat brain: use of heterologous seeds." J Cell Sci **14**(2): 411-419.

Carter, A. P., C. Cho, L. Jin and R. D. Vale (2011). "Crystal structure of the dynein motor domain." Science **331**(6021): 1159-1165.

Cheney, R. E. and M. S. Mooseker (1992). "Unconventional myosins." Curr Opin Cell Biol **4**(1): 27-35.

Cheong, F. K., L. Feng, A. Sarkeshik, J. R. Yates, 3rd and T. A. Schroer (2014). "Dynactin integrity depends upon direct binding of dynamitin to Arp1." Mol Biol Cell **25**(14): 2171-2180.

Chisholm, R. L. and R. A. Firtel (2004). "Insights into morphogenesis from a simple developmental system." Nat Rev Mol Cell Biol **5**(7): 531-541.

Clark, S. W. and D. I. Meyer (1992). "Centractin is an actin homologue associated with the centrosome." Nature **359**(6392): 246-250.

Colombo, K., S. W. Grill, R. J. Kimple, F. S. Willard, D. P. Siderovski and P. Gonczy (2003). "Translation of polarity cues into asymmetric spindle positioning in Caenorhabditis elegans embryos." Science **300**(5627): 1957-1961.

Cooke, R. (2004). "The sliding filament model: 1972-2004." J Gen Physiol **123**(6): 643-656.

Costa, M., W. Raich, C. Agbunag, B. Leung, J. Hardin and J. R. Priess (1998). "A putative catenin-cadherin system mediates morphogenesis of the Caenorhabditis elegans embryo." J Cell Biol **141**(1): 297-308.

Coulombe, P. A., M. E. Hutton, A. Letai, A. Hebert, A. S. Paller and E. Fuchs (1991). "Point mutations in human keratin 14 genes of epidermolysis bullosa simplex patients: genetic and functional analyses." Cell **66**(6): 1301-1311.

Couwenbergs, C., J. C. Labbe, M. Goulding, T. Marty, B. Bowerman and M. Gotta (2007). "Heterotrimeric G protein signaling functions with dynein to promote spindle positioning in C. elegans." J Cell Biol **179**(1): 15-22.

De La Cruz, E. M., A. L. Wells, S. S. Rosenfeld, E. M. Ostap and H. L. Sweeney (1999). "The kinetic mechanism of myosin V." Proc Natl Acad Sci U S A **96**(24): 13726-13731.

De Simone, A., F. Nedelec and P. Gonczy (2016). "Dynein Transmits Polarized Actomyosin Cortical Flows to Promote Centrosome Separation." Cell Rep **14**(9): 2250-2262.

Ding, M., A. Goncharov, Y. Jin and A. D. Chisholm (2003). "C. elegans ankyrin repeat protein VAB-19 is a component of epidermal attachment structures and is essential for epidermal morphogenesis." Development **130**(23): 5791-5801.

Ding, M., W. M. Woo and A. D. Chisholm (2004). "The cytoskeleton and epidermal morphogenesis in C. elegans." Exp Cell Res **301**(1): 84-90.

Diogon, M., F. Wissler, S. Quintin, Y. Nagamatsu, S. Sookhareea, F. Landmann, H. Hutter, N. Vitale and M. Labouesse (2007). "The RhoGAP RGA-2 and LET-502/ROCK achieve a balance of actomyosin-dependent forces in C. elegans epidermis to control morphogenesis." Development **134**(13): 2469-2479.

Doxsey, S., D. McCollum and W. Theurkauf (2005). "Centrosomes in cellular regulation." Annu Rev Cell Dev Biol **21**: 411-434.

DuFort, C. C., M. J. Paszek and V. M. Weaver (2011). "Balancing forces: architectural control of mechanotransduction." Nat Rev Mol Cell Biol **12**(5): 308-319.

Engler, A. J., S. Sen, H. L. Sweeney and D. E. Discher (2006). "Matrix elasticity directs stem cell lineage specification." Cell **126**(4): 677-689.

Farrell, K. B., S. McDonald, A. K. Lamb, C. Worcester, O. B. Peersen and S. M. Di Pietro (2017). "Novel function of a dynein light chain in actin assembly during clathrin-mediated endocytosis." J Cell Biol.(in press)

Fehon, R. G., A. I. McClatchey and A. Bretscher (2010). "Organizing the cell cortex: the role of ERM proteins." Nat Rev Mol Cell Biol **11**(4): 276-287.

Flanagan, L. A., Y. E. Ju, B. Marg, M. Osterfield and P. A. Janmey (2002). "Neurite branching on deformable substrates." Neuroreport **13**(18): 2411-2415.

Frankel, S., M. B. Heintzelman, S. Artavanis-Tsakonas and M. S. Mooseker (1994). "Identification of a divergent actin-related protein in Drosophila." J Mol Biol **235**(4): 1351-1356.

Fyrberg, C., L. Ryan, M. Kenton and E. Fyrberg (1994). "Genes encoding actin-related proteins of Drosophila melanogaster." J Mol Biol **241**(3): 498-503.

Fyrberg, C., L. Ryan, L. McNally, M. Kenton and E. Fyrberg (1994). "The actin protein superfamily." Soc Gen Physiol Ser **49**: 173-178.

Gally, C., F. Wissler, H. Zahreddine, S. Quintin, F. Landmann and M. Labouesse (2009). "Myosin II regulation during C. elegans embryonic elongation: LET-502/ROCK, MRCK-1 and PAK-1, three kinases with different roles." Development **136**(18): 3109-3119.

Gally, C., H. Zhang and M. Labouesse (2016). "Functional and Genetic Analysis of VAB-10 Spectraplakin in Caenorhabditis elegans." Methods Enzymol **569**: 407-430.

Garcia, A. J. and C. D. Reyes (2005). "Bio-adhesive surfaces to promote osteoblast differentiation and bone formation." J Dent Res **84**(5): 407-413.

Gaskin, F., S. B. Kramer, C. R. Cantor, R. Adelstein and M. L. Shelanski (1974). "A dynein-like protein associated with neurotubules." FEBS Lett **40**(2): 281-286.

Gibbons, I. R. (1966). "Studies on the adenosine triphosphatase activity of 14 S and 30 S dynein from cilia of Tetrahymena." J Biol Chem **241**(23): 5590-5596.

Gibbons, I. R. and E. Fronk (1972). "Some properties of bound and soluble dynein from sea urchin sperm flagella." J Cell Biol **54**(2): 365-381.

Gibbons, I. R. and A. J. Rowe (1965). "Dynein: A Protein with Adenosine Triphosphatase Activity from Cilia." Science **149**(3682): 424-426.

Gill, S. R., T. A. Schroer, I. Szilak, E. R. Steuer, M. P. Sheetz and D. W. Cleveland (1991). "Dynactin, a conserved, ubiquitously expressed component of an activator of vesicle motility mediated by cytoplasmic dynein." J Cell Biol **115**(6): 1639-1650.

Gilleard, J. S., J. D. Barry and I. L. Johnstone (1997). "cis regulatory requirements for hypodermal cell-specific expression of the Caenorhabditis elegans cuticle collagen gene dpy-7." Mol Cell Biol **17**(4): 2301-2311.

Gonczy, P., S. Pichler, M. Kirkham and A. A. Hyman (1999). "Cytoplasmic dynein is required for distinct aspects of MTOC positioning, including centrosome separation, in the one cell stage Caenorhabditis elegans embryo." J Cell Biol **147**(1): 135-150.

Gotta, M. and J. Ahringer (2001). "Distinct roles for Galpha and Gbetagamma in regulating spindle position and orientation in Caenorhabditis elegans embryos." Nat Cell Biol **3**(3): 297-300.

Gotta, M., Y. Dong, Y. K. Peterson, S. M. Lanier and J. Ahringer (2003). "Asymmetrically distributed C. elegans homologs of AGS3/PINS control spindle position in the early embryo." Curr Biol **13**(12): 1029-1037.

Hachet, V., C. Canard and P. Gonczy (2007). "Centrosomes promote timely mitotic entry in C. elegans embryos." Dev Cell **12**(4): 531-541.

Harris, T. J. and U. Tepass (2010). "Adherens junctions: from molecules to morphogenesis." Nat Rev Mol Cell Biol **11**(7): 502-514.

Heid, P. J., W. B. Raich, R. Smith, W. A. Mohler, K. Simokat, S. B. Gendreau, J. H. Rothman and J. Hardin (2001). "The zinc finger protein DIE-1 is required for late events during epithelial cell rearrangement in C. elegans." Dev Biol **236**(1): 165-180.

Heisenberg, C. P. and Y. Bellaiche (2013). "Forces in tissue morphogenesis and patterning." Cell **153**(5): 948-962.

Helfand, B. T., L. Chang and R. D. Goldman (2003). "The dynamic and motile properties of intermediate filaments." Annu Rev Cell Dev Biol **19**: 445-467.

Hill, D. P. and S. Strome (1990). "Brief cytochalasin-induced disruption of microfilaments during a critical interval in 1-cell C. elegans embryos alters the partitioning of developmental instructions to the 2-cell embryo." Development **108**(1): 159-172.

Hinck, L., I. S. Nathke, J. Papkoff and W. J. Nelson (1994). "Dynamics of cadherin/catenin complex formation: novel protein interactions and pathways of complex assembly." J Cell Biol **125**(6): 1327-1340.

Holzbaur, E. L., J. A. Hammarback, B. M. Paschal, N. G. Kravit, K. K. Pfister and R. B. Vallee (1991). "Homology of a 150K cytoplasmic dynein-associated polypeptide with the Drosophila gene Glued." Nature **351**(6327): 579-583.

Hong, L., T. Elbl, J. Ward, C. Franzini-Armstrong, K. K. Rybicka, B. K. Gatewood, D. L. Baillie and E. A. Bucher (2001). "MUP-4 is a novel transmembrane protein with functions in epithelial cell adhesion in Caenorhabditis elegans." J Cell Biol **154**(2): 403-414.

Hoogenraad, C. C., P. Wulf, N. Schiefermeier, T. Stepanova, N. Galjart, J. V. Small, F. Grosveld, C. I. de Zeeuw and A. Akhmanova (2003). "Bicaudal D induces selective dynein-mediated microtubule minus end-directed transport." EMBO J **22**(22): 6004-6015.

Howard, J. (1997). "Molecular motors: structural adaptations to cellular functions." Nature **389**(6651): 561-567.

Hresko, M. C., L. A. Schriefer, P. Shrimankar and R. H. Waterston (1999). "Myotactin, a novel hypodermal protein involved in muscle-cell adhesion in Caenorhabditis elegans." J Cell Biol **146**(3): 659-672.

Hug, C., T. M. Miller, M. A. Torres, J. F. Casella and J. A. Cooper (1992). "Identification and characterization of an actin-binding site of CapZ." J Cell Biol **116**(4): 923-931.

Hyenne, V., A. Apaydin, D. Rodriguez, C. Spiegelhalter, S. Hoff-Yoessle, M. Diem, S. Tak, O. Lefebvre, Y. Schwab, J. G. Goetz and M. Labouesse (2015). "RAL-1 controls multivesicular body biogenesis and exosome secretion." J Cell Biol **211**(1): 27-37.

Hyman, A. A. (1989). "Centrosome movement in the early divisions of Caenorhabditis elegans: a cortical site determining centrosome position." J Cell Biol **109**(3): 1185-1193.

Hyman, A. A. and J. G. White (1987). "Determination of cell division axes in the early embryogenesis of Caenorhabditis elegans." J Cell Biol **105**(5): 2123-2135.

Ichii, T. and M. Takeichi (2007). "p120-catenin regulates microtubule dynamics and cell migration in a cadherin-independent manner." Genes Cells **12**(7): 827-839.

Isermann, P. and J. Lammerding (2013). "Nuclear mechanics and mechanotransduction in health and disease." Curr Biol **23**(24): R1113-1121.

Jansen, G., K. L. Thijssen, P. Werner, M. van der Horst, E. Hazendonk and R. H. Plasterk (1999). "The complete family of genes encoding G proteins of Caenorhabditis elegans." Nat Genet **21**(4): 414-419.

Kamath, R. S. and J. Ahringer (2003). "Genome-wide RNAi screening in Caenorhabditis elegans." Methods **30**(4): 313-321.

Keller, R. (2012). "Developmental biology. Physical biology returns to morphogenesis." Science **338**(6104): 201-203.

Kikkawa, M. (2013). "Big steps toward understanding dynein." J Cell Biol **202**(1): 15-23.

Kon, T., T. Mogami, R. Ohkura, M. Nishiura and K. Sutoh (2005). "ATP hydrolysis cycle-dependent tail motions in cytoplasmic dynein." Nat Struct Mol Biol **12**(6): 513-519.

Kuhn, H. (1976). "Model consideration for the origin of life. Environmental structure as stimulus for the evolution of chemical systems." Naturwissenschaften **63**(2): 68-80.

Leckband, D. E., Q. le Duc, N. Wang and J. de Rooij (2011). "Mechanotransduction at cadherin-mediated adhesions." Curr Opin Cell Biol **23**(5): 523-530.

Lecuit, T., P. F. Lenne and E. Munro (2011). "Force generation, transmission, and integration during cell and tissue morphogenesis." Annu Rev Cell Dev Biol **27**: 157-184.

Lees-Miller, J. P., D. M. Helfman and T. A. Schroer (1992). "A vertebrate actin-related protein is a component of a multisubunit complex involved in microtubule-based vesicle motility." Nature **359**(6392): 244-246.

Mabuchi, I., T. Shimizu and Y. Mabuchi (1976). "A biochemical study of flagellar dynein from starfish spermatozoa: protein components of the arm structure." Arch Biochem Biophys **176**(2): 564-576.

Marston, D. J., C. D. Higgins, K. A. Peters, T. D. Cupp, D. J. Dickinson, A. M. Pani, R. P. Moore, A. H. Cox, D. P. Kiehart and B. Goldstein (2016). "MRCK-1 Drives Apical Constriction in C. elegans by Linking Developmental Patterning to Force Generation." Curr Biol **26**(16): 2079-2089.

Martin, A. C., M. Gelbart, R. Fernandez-Gonzalez, M. Kaschube and E. F. Wieschaus (2010). "Integration of contractile forces during tissue invagination." J Cell Biol **188**(5): 735-749.

Matsushita-Ishiodori, Y., K. Yamanaka and T. Ogura (2007). "The C. elegans homologue of the spastic paraplegia protein, spastin, disassembles microtubules." Biochem Biophys Res Commun **359**(1): 157-162.

McKenney, R. J., W. Huynh, M. E. Tanenbaum, G. Bhabha and R. D. Vale (2014). "Activation of cytoplasmic dynein motility by dynactin-cargo adapter complexes." Science **345**(6194): 337-341.

Merris, M., J. Kraeft, G. S. Tint and J. Lenard (2004). "Long-term effects of sterol depletion in C. elegans: sterol content of synchronized wild-type and mutant populations." J Lipid Res **45**(11): 2044-2051.

Mijalkovic, J., B. Prevo, F. Oswald, P. Mangeol and E. J. Peterman (2017). "Ensemble and single-molecule dynamics of IFT dynein in Caenorhabditis elegans cilia." Nat Commun **8**: 14591.

Mullins, R. D., J. A. Heuser and T. D. Pollard (1998). "The interaction of Arp2/3 complex with actin: nucleation, high affinity pointed end capping, and formation of branching networks of filaments." Proc Natl Acad Sci U S A **95**(11): 6181-6186.

Nakamura, K. I. and E. Masuyama (1979). "Studies of dynein from Tetrahymena cilia using agarose polyacrylamide gel electrophoresis." Biochim Biophys Acta **578**(1): 54-60.

Nathke, I. S., L. Hinck, J. R. Swedlow, J. Papkoff and W. J. Nelson (1994). "Defining interactions and distributions of cadherin and catenin complexes in polarized epithelial cells." J Cell Biol **125**(6): 1341-1352.

Neer, E. J. (1995). "Heterotrimeric G proteins: organizers of transmembrane signals." Cell **80**(2): 249-257.

Neuhuber, B., G. Gallo, L. Howard, L. Kostura, A. Mackay and I. Fischer (2004). "Reevaluation of in vitro differentiation protocols for bone marrow stromal cells: disruption of actin cytoskeleton induces rapid morphological changes and mimics neuronal phenotype." J Neurosci Res **77**(2): 192-204.

Nguyen-Ngoc, T., K. Afshar and P. Gonczy (2007). "Coupling of cortical dynein and G alpha proteins mediates spindle positioning in Caenorhabditis elegans." Nat Cell Biol **9**(11): 1294-1302.

Norman, K. R. and D. G. Moerman (2002). "Alpha spectrin is essential for morphogenesis and body wall muscle formation in Caenorhabditis elegans." J Cell Biol **157**(4): 665-677.

O'Rourke, S. M., C. Carter, L. Carter, S. N. Christensen, M. P. Jones, B. Nash, M. H. Price, D. W. Turnbull, A. R. Garner, D. R. Hamill, V. R. Osterberg, R. Lyczak, E. E. Madison, M. H. Nguyen, N. A. Sandberg, N. Sedghi, J. H. Willis, J. Yochem, E. A. Johnson and B. Bowerman (2011). "A survey of new temperature-sensitive, embryonic-lethal mutations in C. elegans: 24 alleles of thirteen genes." PLoS One **6**(3): e16644.

O'Rourke, S. M., M. D. Dorfman, J. C. Carter and B. Bowerman (2007). "Dynein modifiers in C. elegans: light chains suppress conditional heavy chain mutants." PLoS Genet **3**(8): e128.

Ogawa, K., M. Okuno and H. Mohri (1975). "Amino acid composition of dynein and comparison with myosin." J Biochem **78**(4): 729-737.

Otokawa, M. (1972). "Stimulation of ATPase activity of 30-S dynein with microtubular protein." Biochim Biophys Acta **275**(3): 464-466.

Petzelt, C. (1979). "Biochemistry of the mitotic spindle." Int Rev Cytol **60**: 53-92.

Piekny, A. J., J. L. Johnson, G. D. Cham and P. E. Mains (2003). "The Caenorhabditis elegans nonmuscle myosin genes nmy-1 and nmy-2 function as redundant components of the let-502/Rho-binding kinase and mel-11/myosin phosphatase pathway during embryonic morphogenesis." Development **130**(23): 5695-5704.

Praitis, V., E. Ciccone and J. Austin (2005). "SMA-1 spectrin has essential roles in epithelial cell sheet morphogenesis in C. elegans." Dev Biol **283**(1): 157-170.

Priess, J. R. and D. I. Hirsh (1986). "Caenorhabditis elegans morphogenesis: the role of the cytoskeleton in elongation of the embryo." Dev Biol **117**(1): 156-173.

Quintin, S., S. Wang, J. Pontabry, A. Bender, F. Robin, V. Hyenne, F. Landmann, C. Gally, K. Oegema and M. Labouesse (2016). "Non-centrosomal epidermal microtubules act in parallel to LET-502/ROCK to promote C. elegans elongation." Development **143**(1): 160-173.

Reck-Peterson, S. L., A. Yildiz, A. P. Carter, A. Gennerich, N. Zhang and R. D. Vale (2006). "Single-molecule analysis of dynein processivity and stepping behavior." Cell **126**(2): 335-348.

Roberts, A. J., N. Numata, M. L. Walker, Y. S. Kato, B. Malkova, T. Kon, R. Ohkura, F. Arisaka, P. J. Knight, K. Sutoh and S. A. Burgess (2009). "AAA+ Ring and linker swing mechanism in the dynein motor." Cell **136**(3): 485-495.

Roberts, M. N., J. K. Nagle, J. G. Finden, N. R. Branda and M. O. Wolf (2009). "Linker-dependent metal-sensitized photoswitching of dithienylethenes." Inorg Chem **48**(1): 19-21.

Samso, M. and M. P. Koonce (2004). "25 Angstrom resolution structure of a cytoplasmic dynein motor reveals a seven-member planar ring." J Mol Biol **340**(5): 1059-1072.

Satterwhite, L. L. and T. D. Pollard (1992). "Cytokinesis." Curr Opin Cell Biol **4**(1): 43-52.

Schafer, D. A., S. R. Gill, J. A. Cooper, J. E. Heuser and T. A. Schroer (1994). "Ultrastructural analysis of the dynactin complex: an actin-related protein is a component of a filament that resembles F-actin." J Cell Biol **126**(2): 403-412.

Schmidt, R., L. E. Fielmich, I. Grigoriev, E. A. Katrukha, A. Akhmanova and S. van den Heuvel (2017). "Two populations of cytoplasmic dynein contribute to spindle positioning in C. elegans embryos." J Cell Biol.(in press)

Schroer, T. A., E. Fyrberg, J. A. Cooper, R. H. Waterston, D. Helfman, T. D. Pollard and D. I. Meyer (1994). "Actin-related protein nomenclature and classification." J Cell Biol **127**(6 Pt 2): 1777-1778.

Schweizer, J., P. E. Bowden, P. A. Coulombe, L. Langbein, E. B. Lane, T. M. Magin, L. Maltais, M. B. Omary, D. A. Parry, M. A. Rogers and M. W. Wright (2006). "New consensus nomenclature for mammalian keratins." J Cell Biol **174**(2): 169-174.

Shelton, C. A., J. C. Carter, G. C. Ellis and B. Bowerman (1999). "The nonmuscle myosin regulatory light chain gene mlc-4 is required for cytokinesis, anterior-posterior polarity, and body morphology during Caenorhabditis elegans embryogenesis." J Cell Biol **146**(2): 439-451.

Skop, A. R. and J. G. White (1998). "The dynactin complex is required for cleavage plane specification in early Caenorhabditis elegans embryos." Curr Biol **8**(20): 1110-1116.

Srinivasan, D. G., R. M. Fisk, H. Xu and S. van den Heuvel (2003). "A complex of LIN-5 and GPR proteins regulates G protein signaling and spindle function in C elegans." Genes Dev **17**(10): 1225-1239.

Sulston, J. E., E. Schierenberg, J. G. White and J. N. Thomson (1983). "The embryonic cell lineage of the nematode Caenorhabditis elegans." Dev Biol **100**(1): 64-119.

Summers, K. E. and I. R. Gibbons (1973). "Effects of trypsin digestion on flagellar structures and their relationship to motility." J Cell Biol **58**(3): 618-629.

Tucker, P. A. and L. Sallai (2007). "The AAA+ superfamily--a myriad of motions." Curr Opin Struct Biol **17**(6): 641-652.

Urnavicius, L., K. Zhang, A. G. Diamant, C. Motz, M. A. Schlager, M. Yu, N. A. Patel, C. V. Robinson and A. P. Carter (2015). "The structure of the dynactin complex and its interaction with dynein." Science **347**(6229): 1441-1446.

Vale, R. D. and L. S. Goldstein (1990). "One motor, many tails: an expanding repertoire of force-generating enzymes." Cell **60**(6): 883-885.

Vale, R. D., T. S. Reese and M. P. Sheetz (1985). "Identification of a novel force-generating protein, kinesin, involved in microtubule-based motility." Cell **42**(1): 39-50.

van der Voet, M., C. W. Berends, A. Perreault, T. Nguyen-Ngoc, P. Gonczy, M. Vidal, M. Boxem and S. van den Heuvel (2009). "NuMA-related LIN-5, ASPM-1, calmodulin and dynein promote meiotic spindle rotation independently of cortical LIN-5/GPR/Galpha." Nat Cell Biol **11**(3): 269-277.

Vogel, V. and M. Sheetz (2006). "Local force and geometry sensing regulate cell functions." Nat Rev Mol Cell Biol **7**(4): 265-275.

Vuong-Brender, T. T. K., S. K. Suman and M. Labouesse (2017). "The apical ECM preserves embryonic integrity and distributes mechanical stress during morphogenesis." Development (in press).

Wang, X., J. R. Olson, D. Rasoloson, M. Ellenbecker, J. Bailey and E. Voronina (2016). "Dynein light chain DLC-1 promotes localization and function of the PUF protein FBF-2 in germline progenitor cells." Development **143**(24): 4643-4653.

Wang, S., J. R. Moffitt, G. T. Dempsey, X. S. Xie and X. Zhuang (2014). "Characterization and development of photoactivatable fluorescent proteins for single-molecule-based superresolution imaging." Proc Natl Acad Sci U S A 111(23): 8452-8457.

Wells, A. L., A. W. Lin, L. Q. Chen, D. Safer, S. M. Cain, T. Hasson, B. O. Carragher, R. A. Milligan and H. L. Sweeney (1999). "Myosin VI is an actin-based motor that moves backwards." Nature **401**(6752): 505-508.

Williams, B. D. and R. H. Waterston (1994). "Genes critical for muscle development and function in Caenorhabditis elegans identified through lethal mutations." J Cell Biol **124**(4): 475-490.

Witman, G. B., J. Plummer and G. Sander (1978). "Chlamydomonas flagellar mutants lacking radial spokes and central tubules. Structure, composition, and function of specific axonemal components." J Cell Biol **76**(3): 729-747.

Woo, W. M., A. Goncharov, Y. Jin and A. D. Chisholm (2004). "Intermediate filaments are required for C. elegans epidermal elongation." Dev Biol **267**(1): 216-229.

Yan, Y., E. Winograd, A. Viel, T. Cronin, S. C. Harrison and D. Branton (1993). "Crystal structure of the repetitive segments of spectrin." Science **262**(5142): 2027-2030.

Yildiz, A., J. N. Forkey, S. A. McKinney, T. Ha, Y. E. Goldman and P. R. Selvin (2003). "Myosin V walks hand-over-hand: single fluorophore imaging with 1.5-nm localization." Science **300**(5628): 2061-2065.

Zhang, H., F. Landmann, H. Zahreddine, D. Rodriguez, M. Koch and M. Labouesse (2011). "A tension-induced mechanotransduction pathway promotes epithelial morphogenesis." Nature **471**(7336): 99-103.

Zhang, K., H. E. Foster, A. Rondelet, S. E. Lacey, N. Bahi-Buisson, A. W. Bird and A. P. Carter (2017). "Cryo-EM Reveals How Human Cytoplasmic Dynein Is Auto-inhibited and Activated." Cell **169**(7): 1303-1314 e1318.

Zigmond, S. H. (2004). "Beginning and ending an actin filament: control at the barbed end." Curr Top Dev Biol **63**: 145-188.

Zwaal, R. R., J. Ahringer, H. G. van Luenen, A. Rushforth, P. Anderson and R. H. Plasterk (1996). "G proteins are required for spatial orientation of early cell cleavages in C. elegans embryos." Cell **86**(4): 619-629.

Saurabh Tak

Les voies de mécanotransduction entre muscles et épiderme impliquées dans l'élongation embryonnaire de C. elegans

Résumé en français suivi des mots-clés en français

L'élongation embryonnaire de *C. elegans* a lieu en deux étapes. La première phase est permise par les contractions d'actomyosine et régulée par les kinases *let-502* et *pak-1*. La seconde dépend des contractions musculaires (après le stade 1,7-fold). La tension fournie par ces contractions permet le recrutement de GIT-1 aux hémidesmosomes, facilitant la poursuite de l'élongation via l'activation de PAK-1 (Nature, 2011). Étonnamment, en l'absence de *git-1* ou *pak-1*, l'élongation se poursuit, nous conduisant à émettre l'hypothèse de voies de régulation parallèles. Un crible ARNi a été réalisé pour rechercher les candidats impliqués. La majorité des candidats interagissant fortement avec *git-1* appartenait au complexe dynéine-dynactine. En utilisant des allèles sensibles à la température et des protéines affectant les microtubules, nous avons décrit un rôle de la dynactine indépendant des microtubules dans l'épiderme ainsi que son interaction avec la spectraplakine *vab-10* et la spectrine *spc-1.*

Mots clés : L'élongation embryonnaire, PAK-1, dynéine-dynactine, spectraplakine, spectrine

Résumé en anglais suivi des mots-clés en anglais

C. elegans embryonic elongation is driven by 2 forces: Actomyosin contractility and Muscle contraction (after 1.7-fold). Actomyosin contraction is regulated by the Rho kinase and the serine/threonine p21 activated kinase *pak-1*. Tension provided by muscle contraction recruits GIT-1 to hemidesmosomes (HD), which in turn facilitates further elongation by activating proteins such as PAK-1 (Nature 2011). Surprisingly in absence of *git-1*/*pak-1*, elongation still continues, which led us to hypothesize parallel pathways. An RNAi screen was performed to get the candidates in the parallel pathway/s. Candidates interacting strongly with *git-1* belonged to the Dynein Dynactin complex. By use of temperature sensitive alleles and microtubule severing proteins, we found a microtubule independent role of Dynactin in epidermis and that dynactin functionally interacts with spectraplakin *vab-10* and spectrin *spc-1*, which allows us to portray the role of Dynein Dynactin complex during embryonic elongation.

Keywords : *C. elegans* embryo elongation, Dynein Dynactin, Spectraplakin, Spectrin, PAK-1